UNCLASSIFIED

AD NUMBER
AD920000
NEW LIMITATION CHANGE

TO
Approved for public release, distribution unlimited

FROM
Distribution authorized to U.S. Gov't. agencies and their contractors; Specific authority; May 1974. Other requests shall be referred to Director, Naval Research Laboratory, Washington, DC, 20375.

AUTHORITY

NRL ltr, 3 Mar 2004

THIS PAGE IS UNCLASSIFIED

UNCLASSIFIED

AD NUMBER

AD920000

NEW LIMITATION CHANGE

TO
Distribution authorized to U.S. Gov't. agencies and their contractors; Specific authority; May 1974. Other requests shall be referred to Director, Naval Research Laboratory, Washington, DC, 20375.

FROM
Distribution authorized to U.S. Gov't. agencies only; Test and evaluation; May 1974. Other requests shall be referred to Director, Naval Research Laboratory, Washington, DC, 20375.
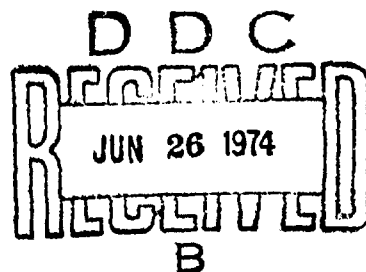
AUTHORITY

NRL, per DTIC Form 55

Optimal Radar Doppler Processors

G. A. Andrews, Jr.

Airborne Radar Branch
Radar Division

May 29, 1974

D D C

JUN 26 1974

B

NAVAL RESEARCH LABORATORY
Washington, D.C.

BEST AVAILABLE COPY

REPORT DOCUMENTATION PAGE		READ INSTRUCTIONS BEFORE COMPLETING FORM
1. REPORT NUMBER NRL Report 7727	2. GOVT ACCESSION NO.	3. RECIPIENT'S CATALOG NUMBER
4. TITLE (and Subtitle) OPTIMUM RADAR DOPPLER PROCESSORS		5. TYPE OF REPORT & PERIOD COVERED
		6. PERFORMING ORG. REPORT NUMBER
7. AUTHOR(s) G. A. Andrews, Jr.		8. CONTRACT OR GRANT NUMBER(s)
9. PERFORMING ORGANIZATION NAME AND ADDRESS Naval Research Laboratory Washington, D.C. 20375		10. PROGRAM ELEMENT, PROJECT, TASK AREA & WORK UNIT NUMBERS 53R02-29 A360-5333/652B/2F00-141-601
11. CONTROLLING OFFICE NAME AND ADDRESS Department of the Navy Naval Air Systems Command Washington, D.C. 20361		12. REPORT DATE May 29, 1974
		13. NUMBER OF PAGES 83
14. MONITORING AGENCY NAME & ADDRESS(if different from Controlling Office)		15. SECURITY CLASS. (of this report) Unclassified
		15a. DECLASSIFICATION/DOWNGRADING SCHEDULE

16. DISTRIBUTION STATEMENT (of this Report)

Distribution limited to U.S. Government Agencies only; test and evaluation; May 1974. Other requests for this document must be referred to the Director, Naval Research Laboratory, Washington, D.C. 20375.

17. DISTRIBUTION STATEMENT (of the abstract entered in Block 20, if different from Report)

An interim report on a continuing NRL Problem

18. SUPPLEMENTARY NOTES

19. KEY WORDS (Continue on reverse side if necessary and identify by block number)

Radar	Moving target indicator
Doppler	MTI
Processing	Pulse doppler

20. ABSTRACT (Continue on reverse side if necessary and identify by block number)

A procedure was developed for maximizing the signal-to-clutter ratio, of transversal filters used for moving-target-detection filters, when the frequency or the doppler shift of the signal is unknown and the noise is nonwhite. First the optimization equations were developed, using the maximum-likelihood-ratio test. Then the optimization procedure, which depends on the covariance functions of the signal and the noise, was applied to the radar MTI problem to illustrate its improvement over conventional MTI. A generalized radar doppler processor was developed by dividing the doppler space into regions and optimizing a filter for each region. The results of this process are compared with those of using conventional coherent integration filters.

DD FORM 1473 EDITION OF 1 NOV 65 IS OBSOLETE
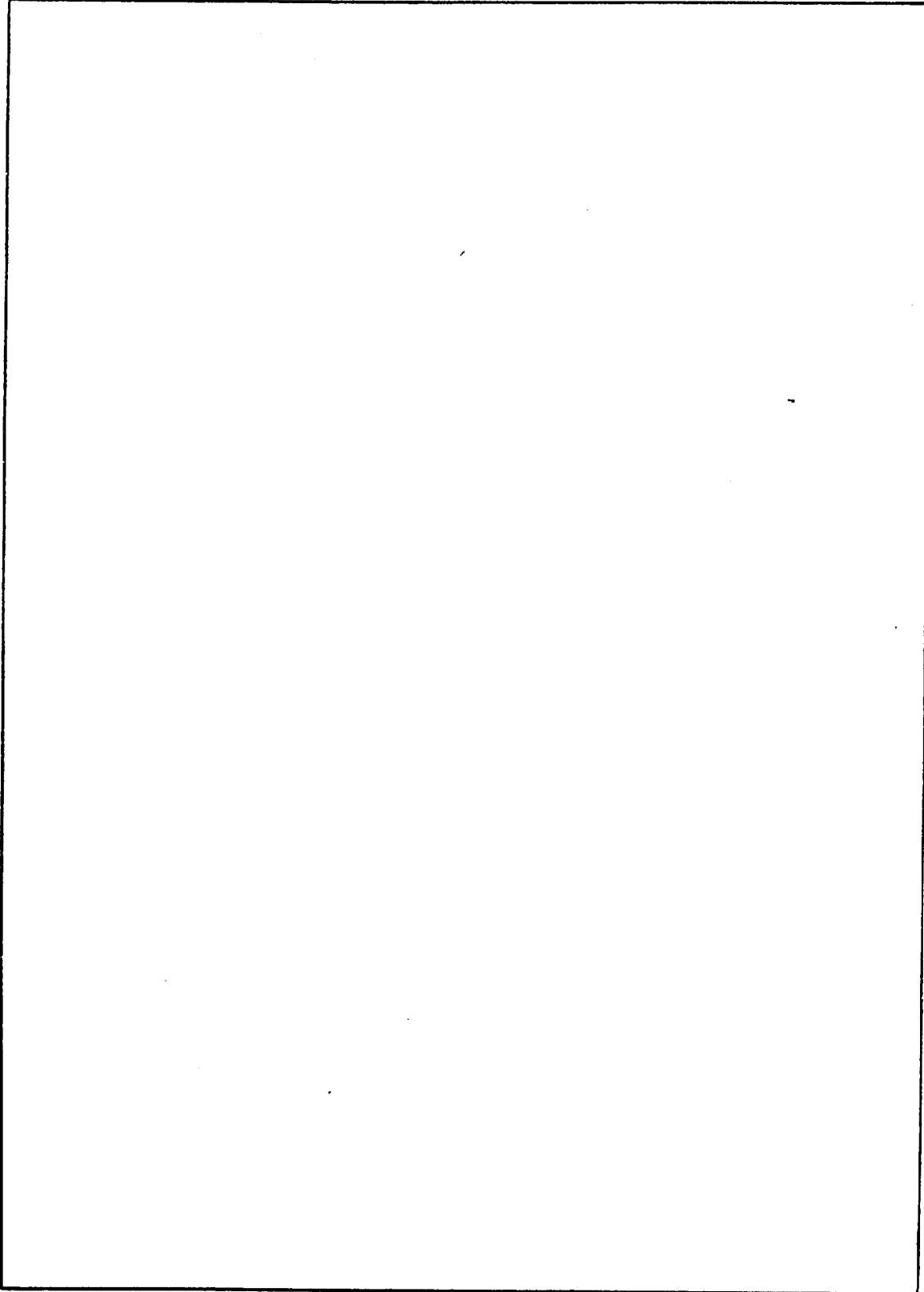S/N 0102-014-6601

i

REPRODUCTION QUALITY NOTICE

This document is the best quality available. The copy furnished to DTIC contained pages that may have the following quality problems:

- Pages smaller or larger than normal.

- Pages with background color or light colored printing.

- Pages with small type or poor printing; and or

- Pages with continuous tone material or color photographs.

Due to various output media available these conditions may or may not cause poor legibility in the microfiche or hardcopy output you receive.

☐ If this block is checked, the copy furnished to DTIC contained pages with color printing, that when reproduced in Black and White, may change detail of the original copy.

CONTENTS

OPTIMAL RADAR DOPPLER PROCESSORS

1. INTRODUCTION

Many receivers in communications, radar, and sonar are essentially finite-memory digital filters. In its canonical form, a finite-memory linear filter is equivalent to a transversal filter, which is a tapped delay line whose tap outputs are weighted and summed. Therefore, optimization procedures for transversal filters would have wide use in communications and detection systems.

One such application of the transversal filter is detection of moving targets by radar systems in ground-clutter or sea-clutter backgrounds (Radar returns from stationary objects are commonly referred to as clutter). This function is usually performed by the moving-target indicator (MTI). The MTI, which is a special transversal filter, detects moving targets by sampling the doppler shifts of returns from fixed objects and moving targets (1). The moving targets produce a doppler shift and are passed by the MTI; returns from fixed objects are filtered out. Theoretically the doppler filters used by MTI radars are relatively simple in that they process a small number of returns, typically two to four. If modern digital filtering technology (2) is used many more returns can be processed. Optimization procedures for these more complex filters are needed to account for the effects of unknown signal and clutter parameters. Because of the random nature of many types of clutter returns, in this research clutter is treated as nonwhite noise.

Most of the work to date involving moving-target detection has been concerned with developing a theoretical optimum and then showing that the performance of the simple doppler filters in use is very close to the optimum. R. C. Emerson (3) has developed a method for minimizing the response of a filter to clutter. An optimization procedure developed by S. P. Applebaum (4) maximizes the signal-to-clutter ratio at the output of such a filter when the doppler shift of the signal is known.

The method introduced in this report is based on an extension of the Applebaum procedure and maximizes the signal-to-clutter ratio at the output of the filter when the frequency or the doppler shift of the signal is unknown and the noise is nonwhite. The investigation starts with a mathematical development of the optimization equations, using the maximum-likelihood-ratio test. The optimal receiver structure depends on the covariance functions of the signal and the noise, which are not usually known a priori. In the second part of the investigation, this optimization procedure is applied to the MTI problem to illustrate the improvements over conventional MTI. A generalized doppler processor is developed by dividing the doppler space into regions and optimizing a processor for each region. The results of these processors are compared with those of conventional coherent integration filters (5).

2. OPTIMIZATION CRITERION

The maximum-likelihood-ratio receiver processes the received data in such a way that ratio

$$\Lambda = \frac{P(x|x = s + n)}{P(x|x = n)}$$

is maximum. Where the received data vector is

$$x = \begin{bmatrix} x_1 \\ x_2 \\ \cdot \\ \cdot \\ \cdot \\ x_N \end{bmatrix} \quad s = \begin{bmatrix} s_1 \\ s_2 \\ \cdot \\ \cdot \\ \cdot \\ s_N \end{bmatrix}, \quad \text{and } n = \begin{bmatrix} n_1 \\ n_2 \\ \cdot \\ \cdot \\ \cdot \\ n_N \end{bmatrix},$$

$P(x|x = s + n)$ is the conditional probability of receiving vector x when signal s is transmitted. $P(x|x = n)$ is the conditional probability of receiving vector x when no signal is present. When these probability distributions are Gaussian (that is when noise n has a Gaussian distribution), maximizing the likelihood ratio corresponds to maximizing the signal-to-noise ratio.

The optimal transversal filter is one that maximizes the output signal-to-noise ratio. The output signal and output noise refer to the squares at the absolute values of the signal and the noise respectively. The expected value of the output signal is

$$\overline{P}_S = a_T M_S a^*, \tag{1}$$

where

M_S is the signal covariance matrix

a is the weight vector

T indicates the transpose of the vector

(*) indicates the complex conjugate of the vector.

The expected value of the output noise is

$$\overline{P}_N = a_T M_N a^*$$

where M_N is the noise covariance matrix. When the expected value of the input signal and the expected value of the input noise are normalized to unity, the improvement in signal-to-noise ratio for a transversal filter can be defined as

$$I_{s/n} = \frac{a_T M_S a^*}{a_T M_N a^*} . \tag{2}$$

The goal of this research was to find weight vectors a that maximize the improvement factor $I_{s/n}$ when received signal s has an unknown doppler shift.

2.1. Single Filter (MTI)

The conventional MTI is designed to detect moving targets with no a priori knowledge of the doppler shift of the target return. A single output is used to detect all such targets.

If no prior knowledge of the signal doppler shift can be assumed, this uncertainty is maximized by giving the doppler shift equal probability of having any value within the analyzing bandwidth. The analyzing bandwidth for a transversal filter is shown in Appendix A to be (0, 1/T), where T is the delay of each delay line (Fig. 1). Therefore, the probability density function for doppler frequency f_d is

$$P(f_d) = \begin{cases} T, & 0 < f_d < \frac{1}{T} \\ 0, & \text{otherwise.} \end{cases}$$
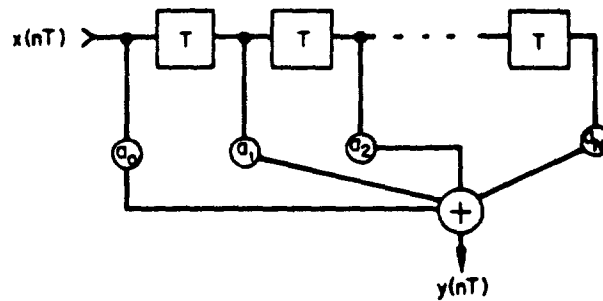

Fig. 1 — An n-stage, or n-canceler, MTI

The signal covariance matrix for this class of signals can be found by using*

$$x(t) = e^{j2\pi f_d(t-t_d)} \sum_{n=0}^{N} \delta(t - nt - t_d)$$

which can be written as a column vector,

---

*As derived in Appendix A (Eq. (A17)).

3

$$\mathbf{x} = \begin{bmatrix} x_1 \\ x_2 \\ x_3 \\ \cdot \\ \cdot \\ \cdot \\ x_n \end{bmatrix},$$

where

$$x_i = \exp \left[j2\pi f_d(i-1)T \right]. \tag{3}$$

Equation (3) is the ith sample of the input function of time defined by Eq. (A17). It is complex because Eq. (A17) is complex *i.e.*, it is a function not of a real frequency but of a frequency shift. With the demodulation procedure outlined in Appendix A, negative as well as positive frequency shifts can be detected. Therefore, if the carrier frequency is removed and the doppler shift is considered as a real frequency, complex signals and complex autocorrelation functions will result in practical applications. A further result of this is that if the mean square of the absolute value of this signal is considered as the power spectrum this "power spectrum" may not be symmetrical with respect to the "zero-frequency" axis.

Assuming stationarity and ergodicity, we find the element (i, k) of the covariance matrix by taking the expected value with respect to the unknown doppler shift,

$$E\left\{ x_i x_k^* \right\} = \int_{-\infty}^{\infty} \exp \left[2j\pi f_d(i-k)T \right] P(f_d) df_d$$

where $P(f_d)$ is given above.

It follows that

$$m_{i,k} = \exp \left[j\pi(i-k) \right] \frac{\sin \pi(i-k)}{\pi(i-k)} \tag{4}$$

for $i = 1, 2, ..., N$ and $k = 1, 2, ..., N$.

From Eq. (4),

$$m_{i,k} = \begin{cases} 1, & i = k \\ 0, & i \neq k. \end{cases}$$

Therefore, the signal covariance matrix for unknown doppler shift is

$$M_S = I \tag{5}$$

4

where I is the identity matrix. The improvement factor is found by substituting Eq. (5) into Eq. (2):

$$I_{s/n} = \frac{a_T a^*}{a_T M_N a^*} . \tag{6}$$

Maximizing Eq. (6) is equivalent to minimizing

$$P_N = a_T M_N a^*,$$

where P_N is the output noise power. This has been shown (3) to be minimum when weight vector a is chosen to be the eigenvector that results in the smallest eigenvalue of M_N. The improvement in signal-to-noise ratio is given by the reciprocal of this eigenvalue.

2.2. Multiple Filters

It has been shown (5) that N independent filters can be generated with N samples of the input data. By dividing the analyzing bandwidth $(0, 1/T)$ into N equal intervals, a filter can be designed to detect optimally a signal in each interval. In this way, the entire analyzing bandwidth can be covered, but the signal for a particular filter can be assumed to have equal probability of occurring anywhere within the interval covered by that filter instead of anywhere within the analyzing bandwidth. This additional information on the signal can be used to improve the detectability of the signal. The goal is to find the weight vector to maximize Eq. (2) for a signal whose doppler shift is known to fall into an interval $((2m - 1)/2NT, (2m + 1)/2NT)$, $m = 0, 1, \ldots, N - 1$.

Derivation of Optimal Weight Vector—The optimal weights are given by the vector A that maximizes Eq. (2):

$$I_{s/n} = \frac{a_T M_S a^*}{a_T M_N a^*} .$$

To find the desired vector, the following definitions will be used:

$$M'_S = W_T M_S W^* \tag{7}$$

$$M'_N = W_T M_N W^* . \tag{8}$$

Further, matrix W will be defined in such a way that

$$M'_N = I. \tag{9}$$

Rewriting Eq. (7) yields

$$M_S = (W_T)^{-1} M'_S (W^*)^{-1}. \tag{10}$$

Rewriting Eq. (8) and making use of Eq. (9) results is

$$M_N = (W_T)^{-1} (W^*)^{-1}. \tag{11}$$

5

Substituting Ews. (10) and (11) into Eq. (2), we have

$$I_{s/n} = \frac{a_T(W_T)^{-1}M'_S(W^*)^{-1}a^*}{a_T(W_T)^{-1}(W^*)^{-1}a^*}$$

Define a vector f as

$$f = W^{-1}a. \tag{12}$$

Then

$$I_{s/n} = \frac{f_T M'_S f^*}{f_T f^*} \quad,$$

which can be written as

$$I_{s/n} = f_T M'_S f^* \tag{13}$$

$$\|f\|^2 = f_T f^* = 1. \tag{14}$$

Equation (13) is maximized when f is chosen to be the eigenvector that results in the largest eigenvalue of M'_S.

Thus, it has been shown that the optimum weight, when the doppler shift is known to be within some interval of values, is

$$a_{opt} = wf \tag{15}$$

where w is defined by

$$w^* w_T = M_N^{-1} \tag{16}$$

and f is the eigenvector that produces the largest eigenvalue of $w_T M_S w^*$.

Signal Covariance Matrix—The signal covariance matrix can be derived in a way similar to that used when the doppler shift is assumed to be completely unknown. The difference is that for this case the signal is assumed to have equal probability of occurring anywhere within a region $((2n - 1)/2NT, (2n + 1)/2NT)$, $n = 0, 1, .., N - 1$, where T is the delay of each delay line and n is an index used to select the region of the analyzing bandwidth $(0, 1/T)$ for this filter. Therefore, the probability density function for the doppler frequency f_d is

$$P_n(f_d) = \begin{cases} NT, & \dfrac{2n-1}{2NT} \leqslant f_d \leqslant \dfrac{2n+1}{2NT} \\ 0, & \text{otherwise.} \end{cases}$$

6

This leads to the element (i, k) of the signal covariance matrix,

$$m_{i,k} = \exp\left[\frac{j2\pi n(i-k)}{N}\right] \frac{\sin\left[\dfrac{\pi(i-k)}{NT}\right]}{\left[\dfrac{\pi(i-k)}{NT}\right]} \tag{17}$$

for $i = 1, 2, ..., N$

$\quad k = 1, 2, ..., N$

$\quad n = 0, 1, ..., N - 1.$

If Eq. (17) is used, the signal covariance matrix for a signal whose doppler shift is known to be within the interval $((2n - 1)/2NT, (2n + 1)/2NT)$ can be generated. Then, Eqs. (15) and (16), we can compute the optimal weight vector. For the case where M_N^{-1} does not exist, the determinant of M_N is zero, which implies that at least one eigenvalue of M_N is zero. The optimum weight vector for this case is the eigenvector that produces one of the zero eigenvalues of M_N.

3.   OPTIMAL RADAR MTI PROCESSORS

The optimization procedures developed in the preceding section can be applied to the detection of moving targets by a radar system. The doppler shift of the returns from moving targets are unknown in general. Therefore, they are usually assumed to have equal probability of occurring anywhere. For this reason, the detection system must be optimized to detect a target that has any doppler shift within the analyzing bandwidth of the radar $(0, 1/T)$, where $1/T$ is the pulse repetition frequency (PRF).

3.1. Conventional MTI

The conventional MTI canceler delays the returns of a given transmitted pulse and subtracts them from the returns of the next transmitted pulse. A number of cancelers n cascaded as shown in Fig. 2 are equivalent to an $(n + 1)$-sample transversal filter with weights corresponding to the nth-degree binomial coefficients with alternating signs. The power transfer functions for these filters can be computed using $\bar{P} = \mathbf{a}M\mathbf{a}^*$ with weight vector $\mathbf{a}$ given by the binomial coefficients with alternating signs and the covariance matrix given by

$$m_{i,k} = \cos 2\pi f_0(k - i)T.$$

The results are shown in Fig. 3 for $n = 1$ through $n = 7$. These curves are normalized by dividing the gain by the maximum gain

$$G_{max} = \left[\sum_{i=1}^{n+1} |\mathbf{a}_i|\right]^2. \tag{18}$$

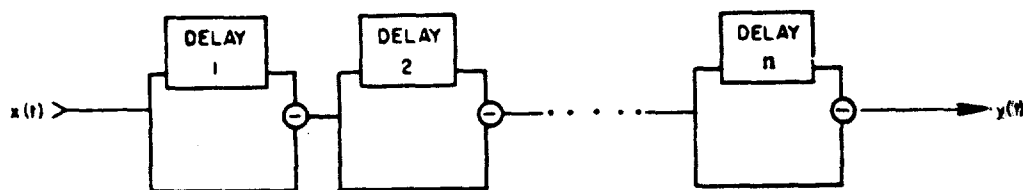where $\mathbf{a}_i$ are the binomial weights.
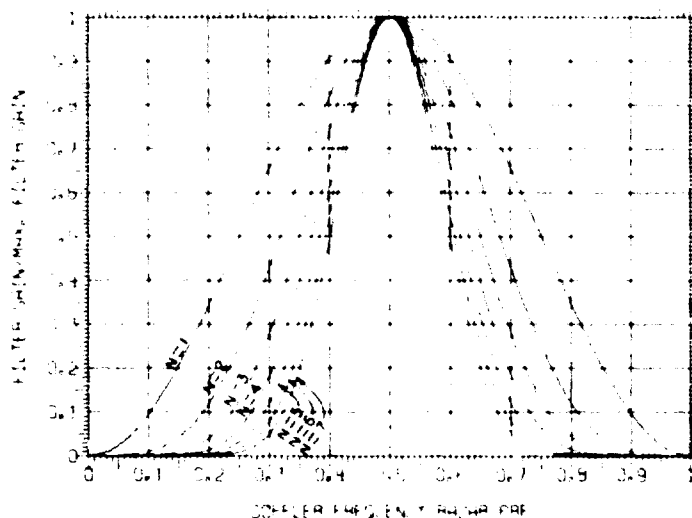
Fig. 2 — An n-stage, or n-canceler, MTI

Fig. 3 — Normalized power transfer function P_s for an MTI having the
indicated number of cancelers

The improvement in signal-to-noise ratio can be computed using Eq. (2). Weight vector a represents the binomial weights. Since the doppler shift is considered to have equal probability of assuming any value, signal covariance matrix M_S was shown to be the indentity matrix. It remains only to define the clutter (noise) covariance matrix M_N in order to evaluate Eq. (2).

In a typical clutter environment, the clutter energy received by the radar is made up of the returns from a large number of scatterers within a resolution cell of the radar. This resolution cell is determined by the antenna pattern and the transmitted pulse width. The scatterers are randomly distributed within the resolution cell, and they generally have random internal motion such as the fluttering of leaves on trees or falling raindrops. Therefore, the clutter must be described as a random variable.

To design an optimum detection system, both the probability distribution of the clutter amplitude statistics and the clutter spectral shape must be known. Nathanson and Reilly (6) have considered the effects of clutter statistics on radar performance and have shown that current knowledge does not allow an optimal detection criterion to be specified a priori. With this dilemma, one is naturally led to adaptive techniques in which critical clutter parameters are estimated and the receiver characteristics are adjusted accordingly.

When the clutter return in each resolution cell is due to many statistically independent scatterers, it follows from the central limit theorem that this clutter can be described by a Gaussian amplitude distribution. This model is representative of many types of clutter, such as rain, forests, and sea returns, and is assumed to apply for this optimization. The distribution of the doppler shift of clutter has been found to be highly dependent on the type of clutter and on weather conditions, particularly wind.

In prior analyses of MTI systems, a Gaussian distribution of the clutter doppler shift was used to evaluate the performance of the MTI system. For this reason, a Gaussian distribution will be used to compare the performance of MTI systems using prior theory with the performance of the optimal processor developed as a part of this research. The model for this doppler shift is

$$P_c(f_d) = C_0 \exp\left[\frac{-(f_d - \mu_c)^2}{2\sigma_c^2}\right] \tag{19}$$

where μ_c and σ_c represent the mean and variance of this distribution and C_0 is the energy level. The Fourier transform of Eq. (19) is

$$\psi(\tau) = \sigma_c C_0 \sqrt{2\pi} \exp(-2\pi^2 \sigma_c^2 \tau^2 - j2\pi\mu_c \tau). \tag{20}$$

Since the receiver design is not affected by C_0, let

$$C_0 = \frac{1}{\sigma_c\sqrt{2\pi}}.$$

Therefore, element (i, k) of M_c is

$$m_{i,k} = \exp[-2\pi^2 \sigma_c^2 (i-k)^2 T^2 - j2\pi\mu_c (i-k)T]. \tag{21}$$

With Eq. (21), all the terms of Eq. (2) are defined, and the improvement factor for a conventional MTI with binomial weights can be computed. The results are shown in Fig. 4 for $\mu_c = 0$ and $0.001 < \sigma_c T < 0.1$ where $1/T$ is the PRF. The mean has been set equal to zero for this comparison, although many types of clutter do not have a zero-mean doppler shift, in particular clutter from clouds and rainfall or that received when the radar is on a moving platform. If this nonzero mean is not taken into account, a smaller improvement factor results. These effects will be considered further in a later report.

3.2. Optimal MTI

The procedure for deriving the optimal MTI weights was developed in Sec. 2. It was shown that when any value for the doppler shift is equally probably, the optimum weights are given by the eigenvector that produces the smallest eigenvalue of M_N. The improvement factor is the reciprocal of that eigenvalue.

If Eq. (21) is used to generate M_N, the improvement factor for the optimal MTI is shown in Fig. 5 for $N = 1$ through $N = 4$, where N is the number of cancelers. For
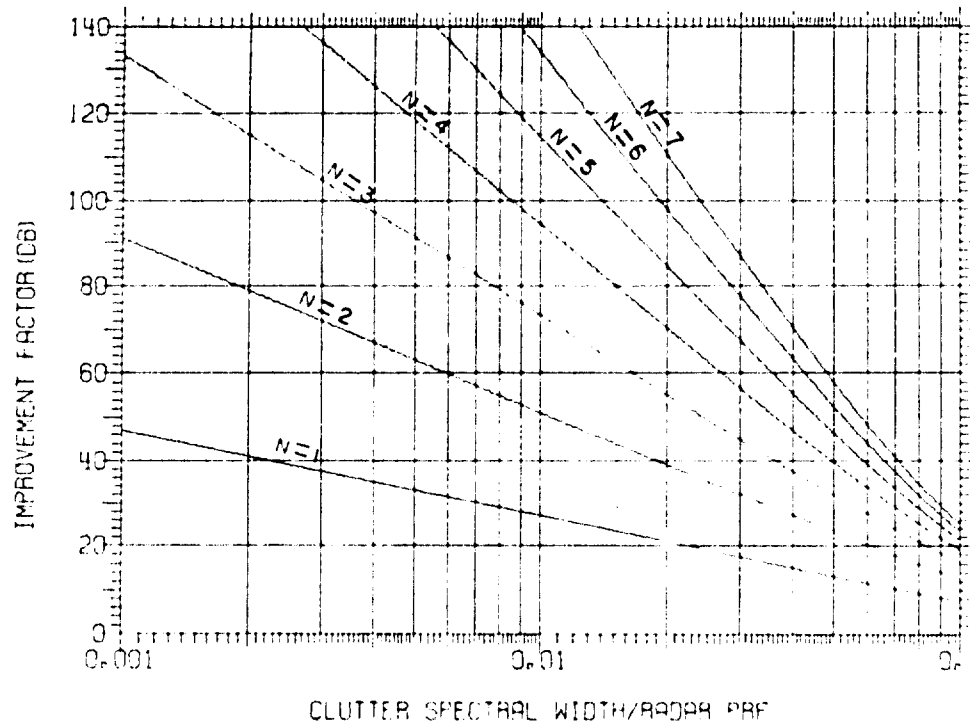
Fig. 4 — MTI improvement factor, binomial weights. N = number of cancelers.
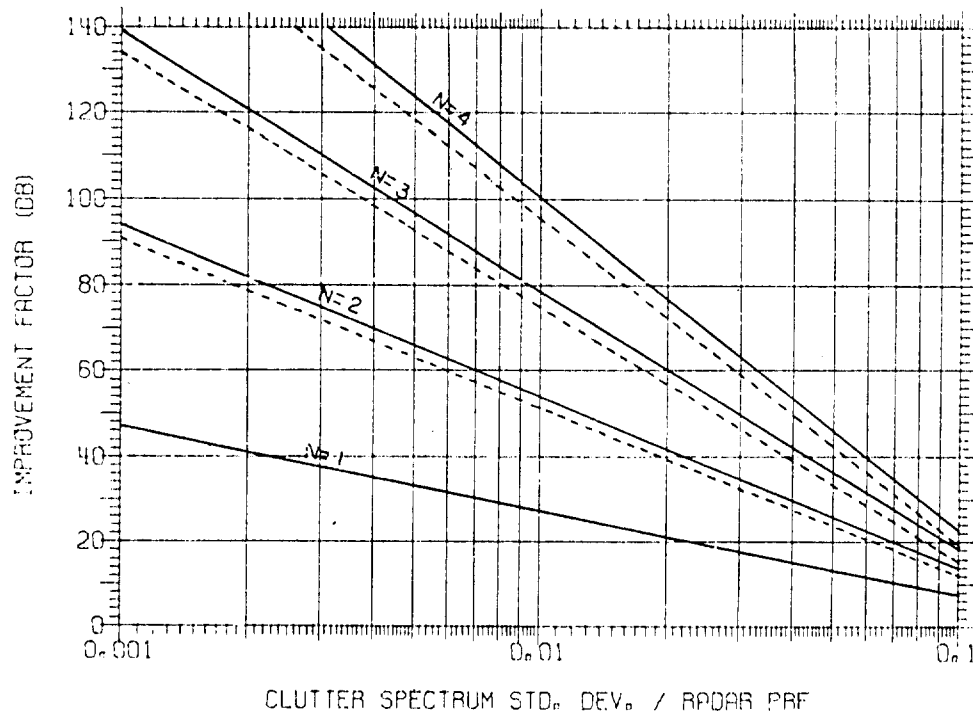

Fig. 5 — MTI improvement factor, optimum weights solid curves, binomial weights broken curves. N = number of cancelers.

comparison, the dotted curves represent the improvement factor for the conventional binomial MTI. The corresponding eigenvectors (optimum weights) are tabulated in Appendix B for $N = 2$ through 4. A single canceler ($N = 1$) is optimized with weights (1, -1) for all values of $\sigma_c T$. These are the binomial coefficients with alternating signs for $N = 1$. In general, the binomial weights are

$$a_i = (-1)^i \binom{N}{i}, \quad i = 0, 1, ..., N. \tag{22}$$

For a double canceler ($N = 2$), the binomial weights can be normalized to

$$\mathbf{a} = (-0.5, 1.0, -0.5) = \frac{1}{2} (-1, 2, -1).$$

The normalized binomial weights for $N = 3$ and 4 are

$$\mathbf{a} = (-.333, 1.0, -1.0, 0.333) = \frac{1}{3} (-1, 3, -3, 1)$$

and

$$\mathbf{a} = (0.1667, -0.6667, 1.0, -0.6667, 0.1667) = \frac{1}{6} (1, -4, 6, -4, 1).$$

If the clutter spectrum is very narrow (i.e., $\sigma_c T \to 0$), the optimum weights are very nearly equal to the binomial weights.* However, the small differences between these optimum weights and the binomial weights result in an appreciable increase of the improvement factor. From this it can be concluded that the accuracy of the weights becomes very critical if the achievable improvement factor is large.

The transition of the optimum weights as the spectral width of the clutter doppler shift increases is shown in Fig. 6 for $N = 3$. This is typical of the results for other values of N. The absolute value of the weights toward the end of the transversal filter (a_1 and a_N), in general, increases as the width of the clutter spectrum increases. This results in a filter transfer characteristic that has a narrower main lobe and higher side lobes, as shown in Fig. 7. The dotted curve is the binomial weighted filter with no sidelobes, which is shown for comparison with the optimal filter for a wide clutter spectrum ($\sigma_c T = 0.5$). The appearance of side lobes for these filters is revealed by careful examination of the filter characteristics near zero doppler shift.

When the signal doppler shift is considered to have equal probability of any value, it has been shown that the signal covariance matrix is the identity matrix. As the clutter spectrum width σ_c is increased, the clutter approaches the characteristics of white noise in that the clutter covariance matrix approaches the identify matrix. For this case, it is seen from Eq. (2) that the improvement factor approaches unity (0 dB) regardless of the weights. Therefore, the accuracy of the optimum weight is less critical for a very wide clutter spectrum and a small maximum achievable improvement factor. This is shown in Fig. 8, where the clutter spectral width $\sigma_c T$ is increased to 0.5.

In summary, this optimization procedure results in a significant additional improvement in signal-to-clutter ratio when (a) more than two pulses ($N > 1$) are processed, (b) the clutter spectrum is narrow, and (c) the filter weights are accurate, as tabulated in

---

*This can be seen in Appendix B, tables B1, B2, and B3, for small values of $\sigma_c T$.
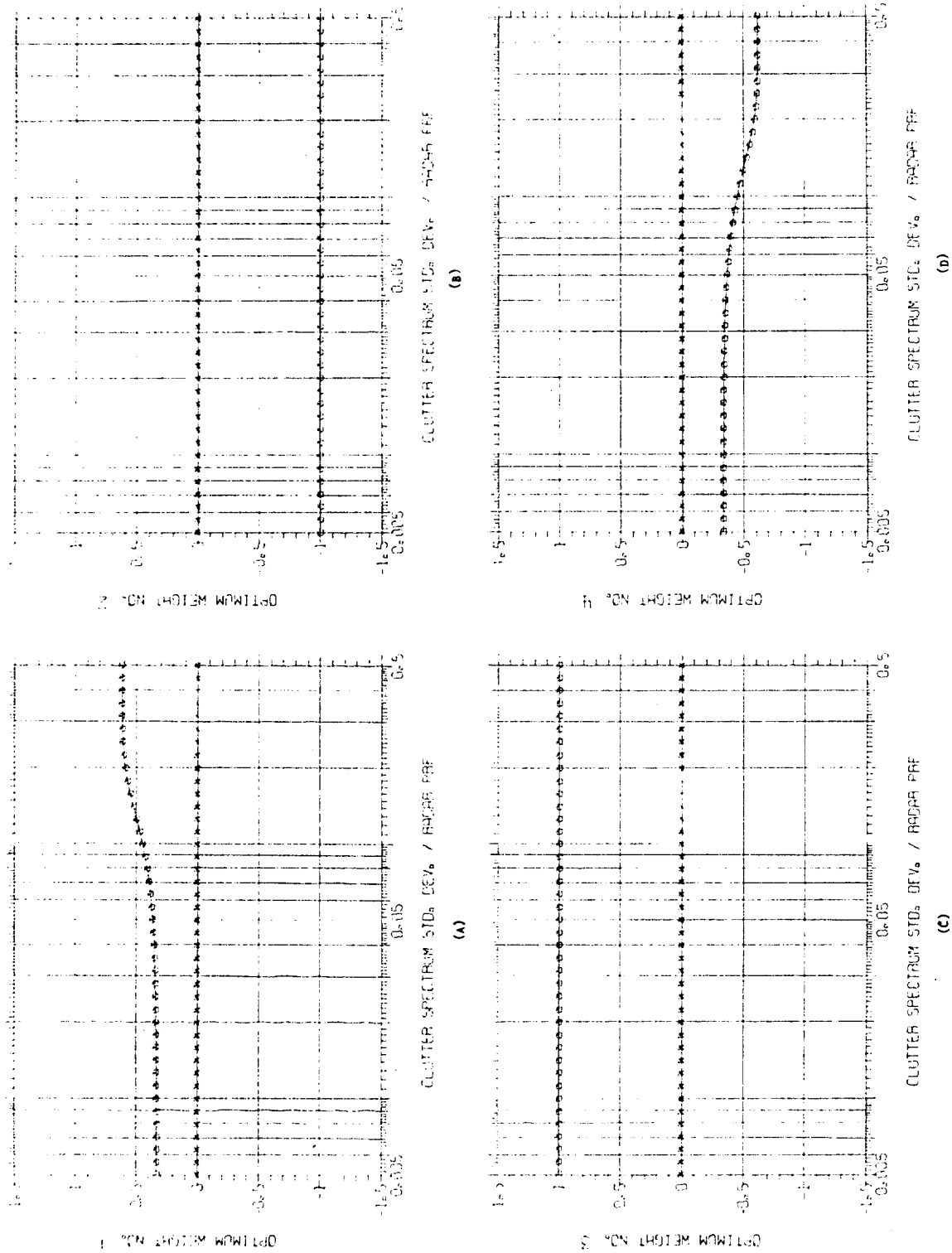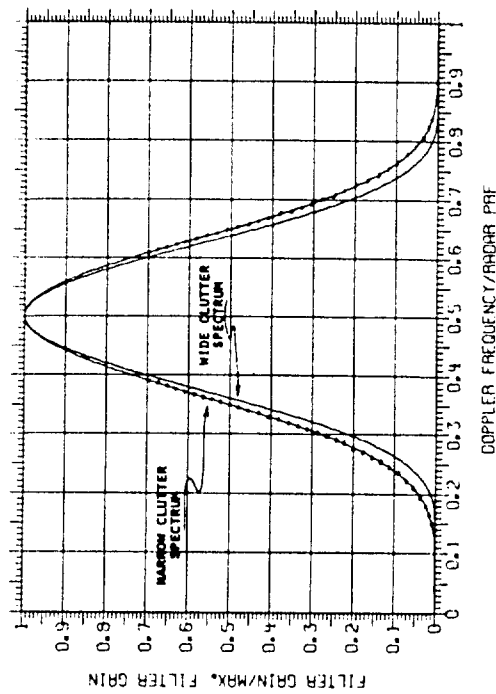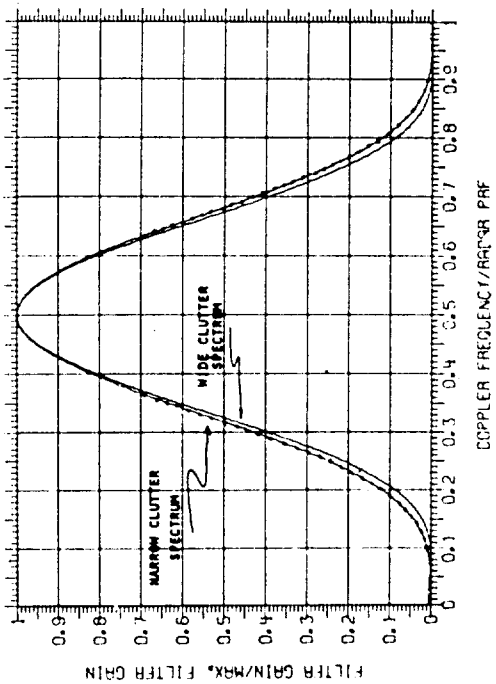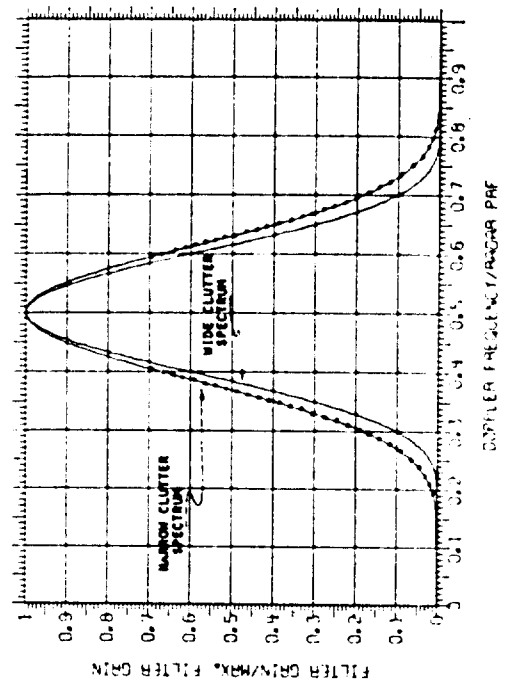
Fig. 6—Optimum weights for a triple-canceler MTI. □ represents the real part of the complex weights.
X represents the imaginary part.

(b)

(a)

(c)

Fig. 7 — Transfer characteristics of optimum MTI. (a) Single canceler. (b) Double canceler. (c) Triple canceler. The curves for clutter with a narrow spectrum correspond to $\sigma_c T = 0.005$, and those for clutter with a wide spectrum, $\sigma_c T = 0.1$.
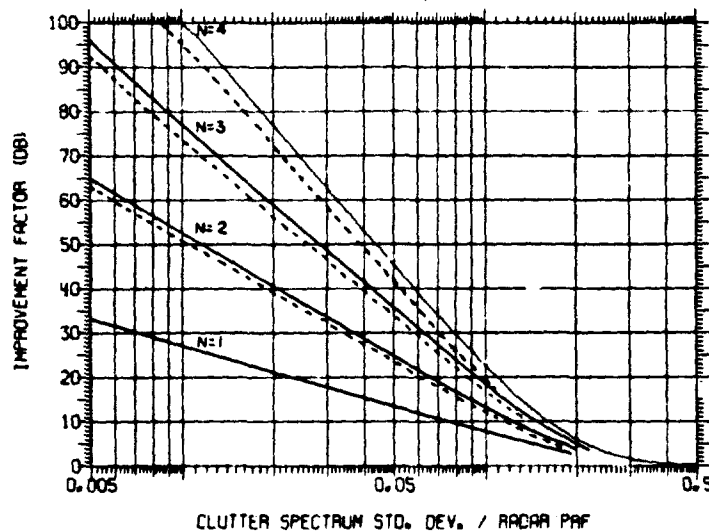
Fig. 8 — MTI improvement factor, optimum weights solid curves,
binomial weights broken curves. N = number of cancelers.

Appendix B. If the standard deviation of the clutter spectrum is 0.01 times the PRF, Fig. 5 shows that the additional improvement factor achievable with optimum weights is about 2 dB for a double canceler ($N = 2$), 3.5 dB for $N = 3$, and 5 dB for $N = 4$. Although the weights must be accurate, Fig. 6 shows that they change very slowly as the width of the clutter spectrum is changed. Therefore, if the approximate width of the clutter spectrum is known for a given application, the optimum weights can be computed and adaptation can be avoided.

4. GENERALIZED N-PORT DOPPLER PROCESSORS

In the preceding section an MTI was optimized for detecting a signal whose doppler shift is given equal probability of having any value. It was shown (Fig. 8) that using the "best" weights gives significantly better results than using binomial weights if the returns from a large number of pulses are processed. However, when the clutter spectrum becomes very wide, the improvement in signal-to-clutter ratio of the optimal MTI, as well as the binomial MTI, approaches 0 dB, as shown in Fig. 8.

The improvement in signal-to-noise ratio of both the optimal and the binomial MTI filters with a signal-plus-white-noise input is also 0 dB. This can be seen by referring to Eq. (2) and remembering that the covariance matrix of white noise is the identity matrix, and the covariance matrix of a signal whose doppler shift is unknown is also the identity matrix. Therefore, the improvement factor is unity (0 dB) regardless of the weights used.

In a realistic radar system, the receiver must contend with both clutter and white noise produced in the input stage of the receiver. To cope with clutter-plus-noise interference, the doppler filters are generalized to form N independent doppler filters from N samples of the input data. Each filter covers a fraction ($1/NT$) of the analyzing bandwidth

14

(0, 1/T). In this way the entire spectrum is covered, but each filter is optimized only for the region to which it is assigned.

4.1. Interference Model for Clutter Plus Noise

To derive a model for clutter plus noise, it is assumed that (a) the total energy of the interference, which includes clutter plus noise, is normalized to unity, (b) the clutter has a Gaussian spectrum, (c) the noise has a "white" frequency spectrum, and (d) the clutter and noise both have Gaussian amplitude probability density functions.

Let E_G represent the power of the Gaussian spectrum and E_W represent the power of the "white" spectrum. Then

$$E_G + E_W = 1$$

and the total interference spectral density is

$$P_I(f) = \frac{1 - E_W}{\sigma_c \sqrt{2\pi}} \exp\left\{-\left[\frac{(f - \mu_c)^2}{2\sigma_c^2}\right]\right\} + E_W T \left[u(f) - u\left(f - \frac{1}{T}\right)\right] \tag{23}$$

where μ_c and σ_c are the mean and variance of the Gaussian spectrum and

$$u(f) = \begin{cases} 0, f < 0 \\ 1, f > 0. \end{cases}$$

The total energy of the interference is found by integrating Eq. (23):

$$\int_{-\infty}^{\infty} P_I(f)df = 1.$$

The Fourier transform of Eq. (23) is

$$\psi(\tau) = (1 - E_W) \exp(-2\pi^2 \sigma_c^2 \tau^2 - j2\pi\mu_c\tau) + E_W \frac{\sin\left(\frac{\pi\tau}{T}\right)}{\left(\frac{\pi\tau}{T}\right)} \exp\left(\frac{j\pi\tau}{T}\right) \tag{24}$$

The element (i, k) of the covariance matrix is

$$m_{i,k} = (1 - E_W) \exp[-2\pi^2 \sigma_c^2 (i - k)^2 T^2 - j2\pi\mu_c(i - k)T]$$

$$+ E_W \frac{\sin \pi(i - k)}{\pi(i - k)} \exp[j\pi(i - k)],$$

15

which can be rewritten as

$$m_{i,k} = (1 - E_W) \exp[- 2\pi^2 \sigma_c^2 (i - k)^2 T^2 - j2\pi\mu_c(i - k)T] + E_W \delta(i - k) \tag{25}$$

where

$$\delta(i - k) = \begin{cases} 1, & i = k \\ 0, & i \neq k. \end{cases}$$

4.2. Effect of White Noise on Optimal MTI

If Eq. (25) is used, the interference covariance matrix M_I can be generated. If Eq. (25) is compared with Eq. (21), it can be seen that M_I is

$$M_I = (1 - E_W)M_C + E_W I \tag{26}$$

where M_C is the covariance matrix of the Gaussian clutter spectrum. Identity matrix I is the covariance matrix of the white spectrum. It has been shown that the optimum weight vector for an MTI is the eigenvector that gives the smallest eigenvalue of M_I. To find this weight vector, the eigenvalues and eigenvectors of M_I will be calculated from the eigenvalues and eigenvectors of M_C.

The eigenvalue equation for M_I is

$$M_I u = \lambda_I u \tag{27}$$

where u is an eigenvector of M_I and λ_I is an eigenvalue. If Eq. (26) is used,

$$[(1 - E_W)M_C + E_W I]u = \lambda_I u,$$

which can be rewritten as

$$M_C u = \frac{\lambda_I - E_W}{1 - E_W} u = \lambda_C u \tag{28}$$

where

$$\lambda_C = \frac{\lambda_I - E_W}{1 - E_W} . \tag{29}$$

Since Eq. (28) is the eigenvalue equation for M_C, it follows that M_C and M_I have the same eigenvectors. The eigenvalues are related by Eq. (29).

The eigenvalues of M_I are found by rewriting Eq. (29) as

$$\lambda_I = (1 - E_W)\lambda_C + E_W . \tag{30}$$

When λ_C is a minimum, λ_I is also a minimum. Therefore, the eigenvector that produces the minimum eigenvalue of M_C also produces the minimum eigenvalue of M_I.

In summary, the optimum weight vector for a Gaussian clutter spectrum is also the optimum weight vector when a white spectrum is added to the Gaussian spectrum. The improvement in signal-to-noise ratio for the optimal MTI is given by the reciprocal of the minimum eigenvalue of the interference covariance matrix,

$$I'_{s/n} = \frac{1}{(\lambda_I)_{min}},$$

where $I'_{s n}$ is the improvement factor for a Gaussian spectrum plus a white spectrum. If Eq. (30) is used,

$$\frac{1}{I'_{s/n}} = \frac{(1 - E_W)}{I_{s/n}} + E_W,\tag{31}$$

where $I_{s/n}$ is the improvement factor for a Gaussian spectrum only. Equation (31) shows that the improvement factor for the optimal MTI when white noise is added is related only to the amount of white noise E_W and the improvement factor for a Gaussian spectrum $I_{s/n}$. The eigenvectors, or optimum weights, are not affected. This means that the degradation of both the conventional and optimal MTI by white noise can be expressed by Eq. (31), which is plotted in Fig. 9.
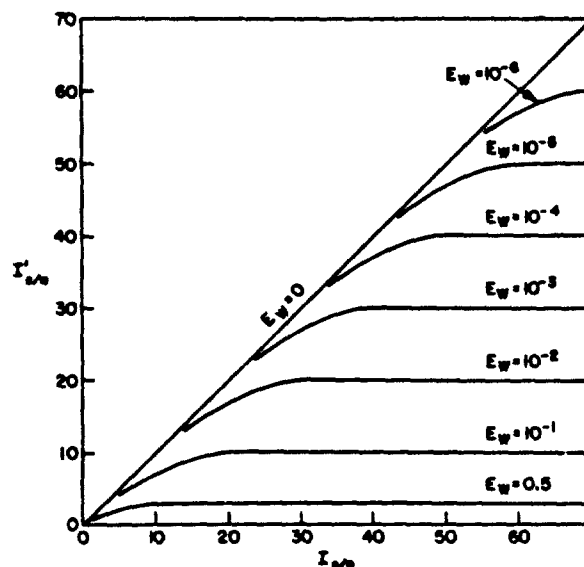
Fig. 9 — Effect of white noise on the improvement factor of both the optimum and the binomial MTI. $I_{s/n}$ is the improvement factor if the interference is clutter alone. $I'_{s/n}$ is the improvement factor for clutter plus noise. E_W is the fraction of the interference that is white noise.

17

Figure 9 shows that when $I_{s/n}$ becomes very large, $I'_{s/n}$ is determined (and limited) by E_W. Under this condition, the achievable improvement in signal-to-noise ratio cannot be increased by processing more samples (increasing N), which would increase $I_{s/n}$ but would not increase $I'_{s/n}$.

$I_{s/n}$ is also increased by decreasing clutter spectrum width σ_c. However, when $I_{s/n}$ becomes very large, $I'_{s/n}$ is limited by the white noise energy E_W. This is shown in Fig. 10 for $N = 2$ through $N = 4$.

4.3. Optimization of the N-Port Doppler Processor

To improve the performance for wide clutter spectra and white noise, a contiguous bank of N filters is formed by applying N independent weight vectors to the N sample input. Each filter is optimized to cover a portion of the analyzing bandwidth. The optimum weights are specified in this section and the performance of these filters are illustrated.

The optimum weight vectors for signals whose doppler shift is known to be within a bounded region was considered in the second section, where the optimum weights are

$$a_{opt} = Wf. \tag{32}$$

The Matrix W is defined by

$$WW_T^* = M_N^{-1}. \tag{33}$$

Vector f is the eigenvector associated with the largest eigenvalue of M'_s,

where

$$M'_S = W_T^* M_S W. \tag{34}$$

Performance Against Clutter With Gaussian Spectrum—As shown above, the optimum weights and the improvement factor can be found if the covariance matrix of clutter M_c and the covariance matrix of the signal M_s are known. Equation (21) can be used to generate the covariance matrix for a Gaussian clutter spectrum. Equation (17) can be used to generate the covariance matrix for a signal whose doppler has a uniform probability distribution within the region $((2n - 1)/2NT, (2n + 1)/2NT)$, $n = 0, 1, ..., N$.

If Eqs. (17) and (21) are used to generate M_s and M_c, the optimum weights and the improvement factor are found for $N = 2$ through $N = 5$. The results are shown in Fig. 11 for $\mu_c = 0$ and $0.005 < \sigma_c T < 0.5$. The N filters are shown by the solid curves graph, the filters are numbered starting with the one at zero frequency. The average improvement factor for all N filters are shown by the dotted curves. Since the solid curves represent the average improvement factor for a doppler shift with uniform probability distribution within the region of the filter, and since the entire analyzing bandwidth $(0, 1/T)$ is covered by the N filters, the dotted curves represent the average improvement factor for a doppler shift with a uniform distribution over the analyzing bandwidth.
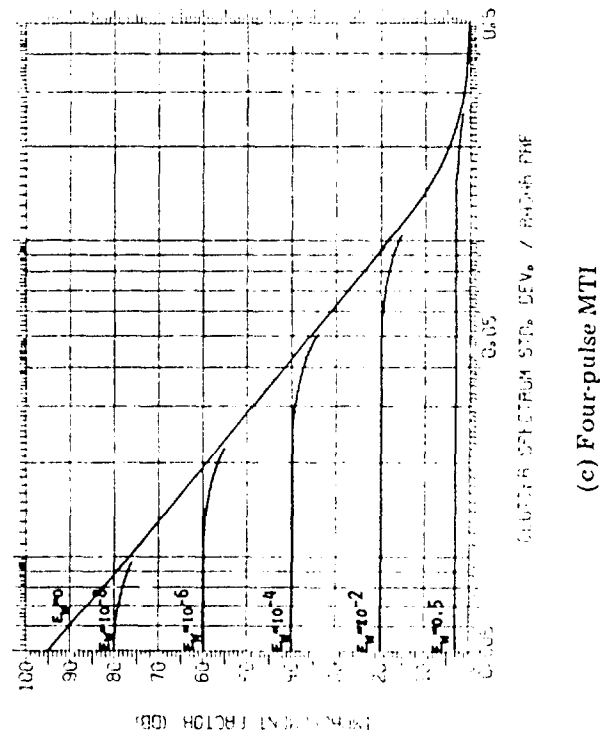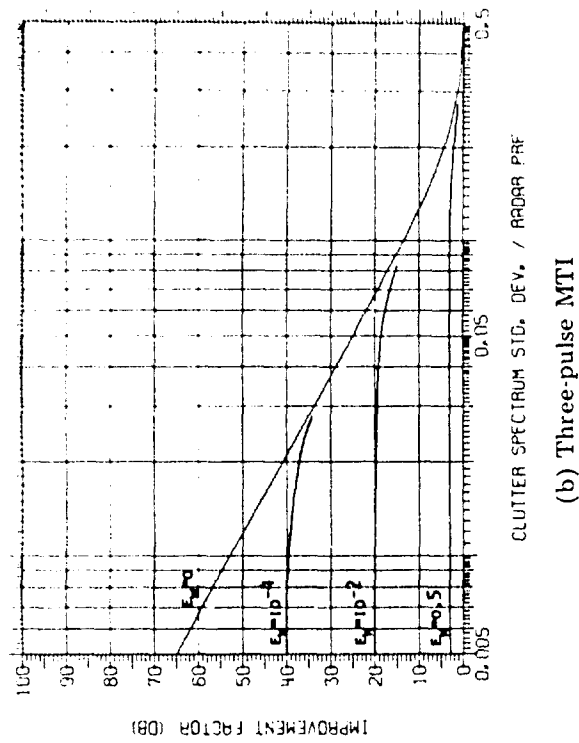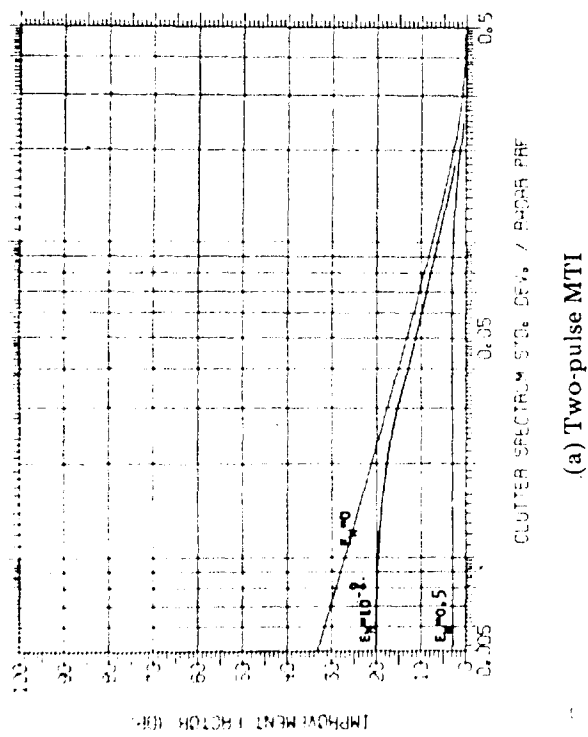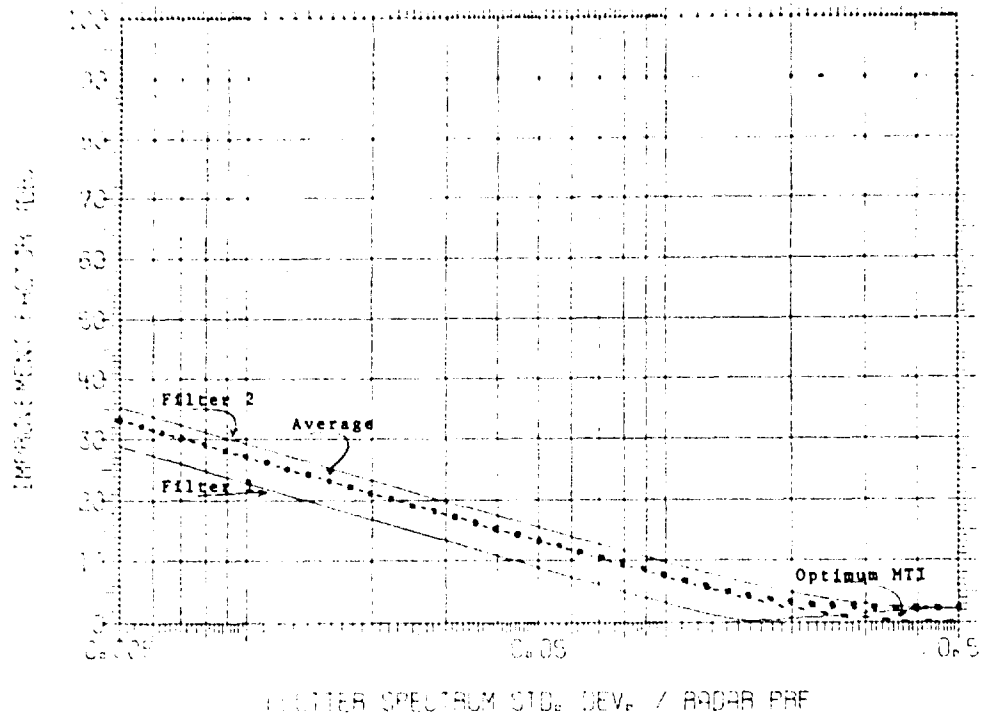
18

(b) Three-pulse MTI

(a) Two-pulse MTI
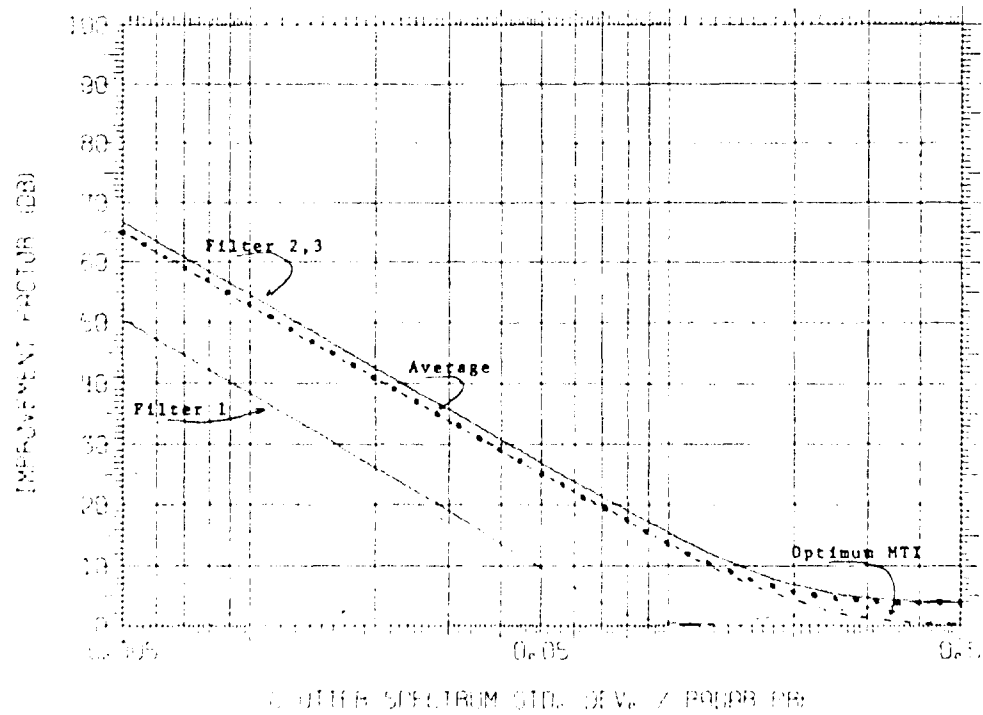
(c) Four-pulse MTI

Fig. 10 — Effect of white noise on the improvement factor of an N-pulse optimum MTI. E_W is the fraction of the total interference energy that is white noise.
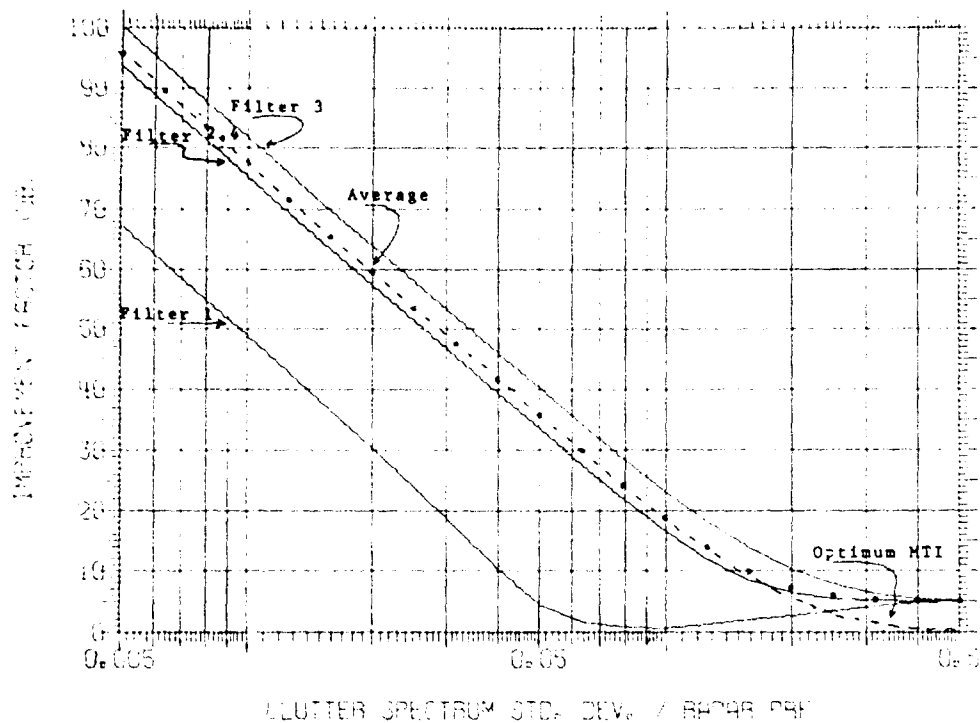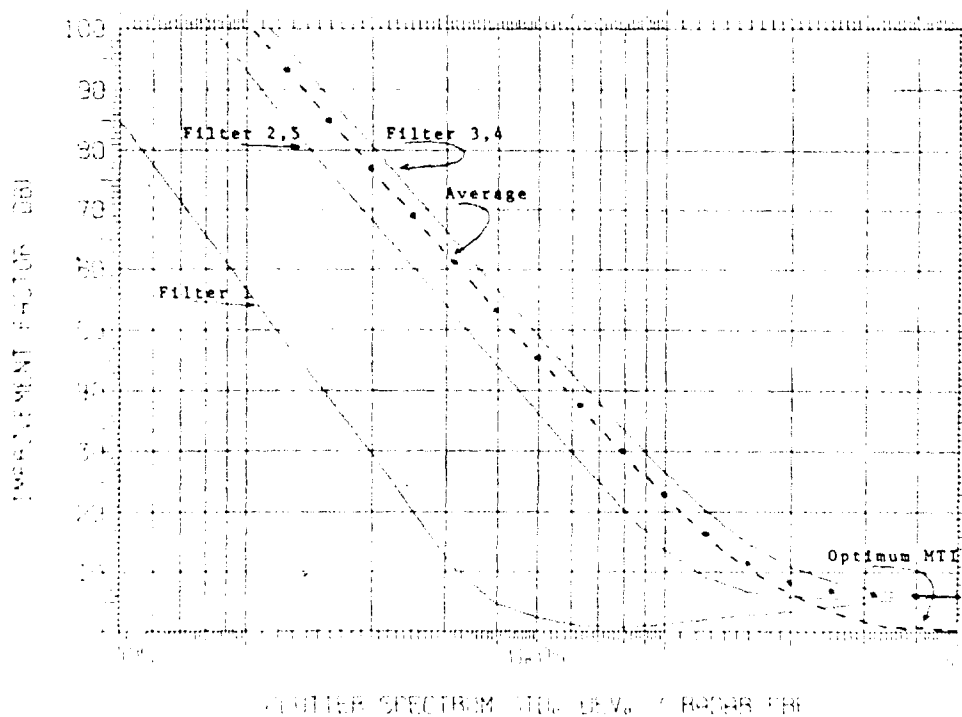
(a) Two-port processor

(b) Three-port processor

Fig. 11 — Improvement factor of an N-port doppler processor compared with that of an optimum N-pulse MTI.

(c) Four-port processor

(d) Five-port processor

Fig. 11 (Continued) — Improvement factor of an N-port doppler processor compared with that of an optimum N-pulse MTI.

21

For comparison, the improvement factors using the optimum weights derived for the MTI are shown by dotted curves in Fig. 11. The improvement factor for the optimal MTI and the average improvement factor for the N-port doppler processor coincide until the clutter spectrum becomes very wide. The reason for this can be understood by examining Fig. 12, which shows the optimum weights of each filter for a two-pulse processor ($N = 2$). The □ curves are the real parts of the weights and the X curves are the imaginary parts. Both filters have weights of $(1, -1)$ until the clutter spectrum becomes very wide ($\sigma_c T > 0.15$). Therefore, since both filters have the same weights, only one is needed for $\sigma_c T < 0.15$. That one filter has the same weights as the optimum MTI for $N = 2$. It follows that the improvement factor would be the same in each case.

When $\sigma_c T > 0.15$, the weights on filter 1 become $(1, 1)$. At this point the two filters are different, so that two filters are needed and the improvement factor is greater than for the optimum MTI, as was seen in Fig. 11. The transfer characteristics of the two filters are shown in Fig. 13. The □ curve represents the optimum 2-pulse MTI. The Δ and X curves represent the 2-port processor for $\sigma_c T > 0.15$.

The optimum weights for the four filters of a 4-port processor are shown in Figs. 14-17. When the clutter spectrum is narrow ($\sigma_c T < 0.05$), the optimum weights of all four filters are identical and they are the same as the optimal weights of the optimal 4-pulse MTI. Therefore, again, only one filter is needed for narrow clutter spectra, and that filter is the optimal MTI.

An N-point discrete Fourier transform (DFT) is given by

$$a_{kn} = \exp\left[-j2\pi \ \frac{(n-1)(k-1)}{N}\right], \quad n, k \ 1, 2, ..., N.$$

This operation corresponds to N contiguous filters. For $N = 2$, the DFT weights for the two filters f_1 and f_2 are

$$f_1 \rightarrow (1, 1)$$

and

$$f_2 \rightarrow (1, -1).$$

These weights correspond to those of the optimal 2-port processor for a wide clutter spectrum. For $N = 4$, the DFT weights for the four filters are

$$f_1 \rightarrow (1, 1, 1, 1)$$
$$f_2 \rightarrow (j, 1, -j, -1)$$
$$f_3 \rightarrow (-1, 1, -1, 1)$$
$$f_4 \rightarrow (-j, 1, j, -1).$$

These weights are similar to those of the optimal 4-port processor for a wide clutter spectrum. The optimal 4-port weights are modified by a "window" $(0.83, 1, 1, 0.83)$. It is well known that the optimal window is uniform $(1, 1, 1, 1)$ when the noise is white. When the clutter spectrum is very wide, the optimal N-port processor is very close to an N-point DFT.

In summary, the optimal N-port processor is a single filter (i.e., the optimal MTI) when the clutter spectrum is narrow and approaches an N-point DFT when it is wide. In the transition region, the improvement factor is very low (Fig. 11), and the weights may change drastically for small changes in the width of the clutter (Figs. 14-17). However, the filter gain changes very slowly in this region (Fig. 11), and this implies that the values of the weights are not critical in this region.

The filter transfer characteristics of three of the four filters of the 4-port processor are shown in Fig. 18. The □ curves represent the filters when the clutter is narrow $(\sigma_c T = 0.005)$. All four filters are the same for this condition and all four are also the same as the 4-pulse optimal MTI (Fig. 3). Not all of the filters have maxima in their detection regions when the clutter is narrow, as one might expect.

The X curves represent the optimal filters when the clutter is wide $(\sigma_c T > 0.5)$. Notice that each is very close to a $(\sin x)x$ shape, the shape a DFT would have. The peak of each filter is centered in the detection region for this case.

The Δ curves represent the filter shapes in transition region $(\sigma_c T = 0.1)$. The peaks are closer to the detection region than for narrow spectrum clutter, and the mainlobes of the filters are narrower and the sidelobes are higher than the $(\sin x)x$ shape. This corresponds to an inverse taper on the window function; i.e., the end samples are weighted heavier than the center samples.

Similar curves of the filter shapes for $N = 3$ and $N = 5$ are shown in Appendic C.

Performance Against Clutter Plus White Noise—It was shown above that the optimal MTI does not improve the signal-to-white-noise ratio. Thus, the MTI improvement factor becomes limited by the white noise (Fig. 10), and processing more pulses or reducing the clutter spectral width $\sigma_c T$ does not lead to a higher improvement factor. This difficulty is overcome by the N-port doppler processor.

If Eq. (25) is used to generate interference covariance matrix M_I and Eq. (17) to generate signal covariance matrix M_S, one can find the largest eigenvalues of M_S' which, along with the associated eigenvectors, give the improvement factor and the optimum weights for the N-port doppler processor. The results of this computation are shown in Figs. 19-22 for 2- through 5-port doppler processors. The improvement factors of the N ports are averaged and shown along with the improvement factor of the optimal N-pulse MTI for comparison.

Figure 19c shows that the average improvement factor for a 2-port doppler processor (dotted curves) and the improvement factor for a 2-pulse MTI (dashed curves) are identical unless the clutter spectrum is very wide. The reason for this is that the optimum weights for the 2-port processor are unaffected by the addition of white noise until the noise level becomes high enough to overcome the effects of the Gaussian clutter spectrum. This does not happen as long as the noise level is less than the clutter level $(E_W < 0.5)$.

Figures 20c, 21d, and 22d show that the N-port doppler processor for $N > 2$ gives a better average improvement factor than the N-pulse MTI improvement factor even when the clutter spectrum is narrow. As N is increased, this advantage of the N-port doppler processor becomes greater, so that the need for an optimal design becomes more important.
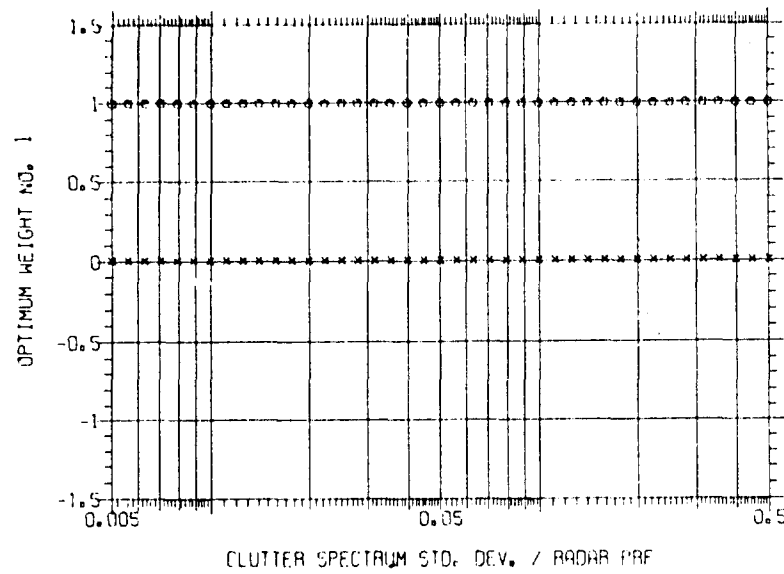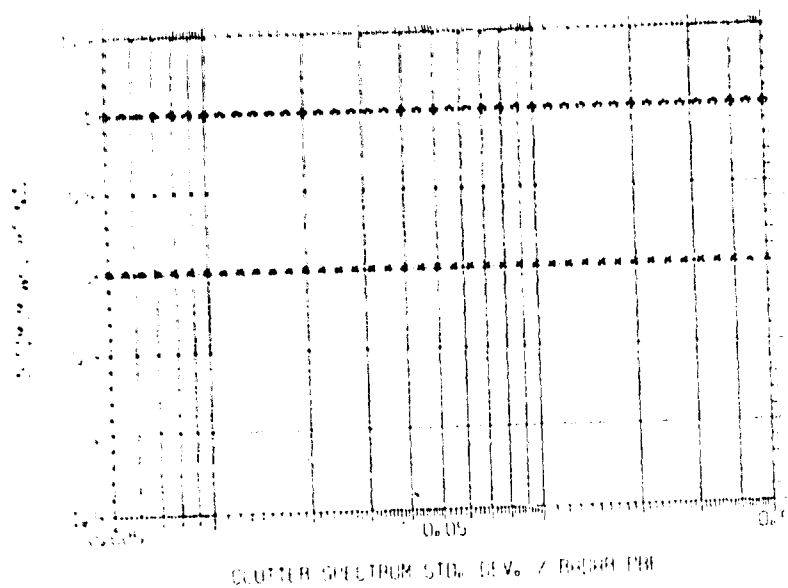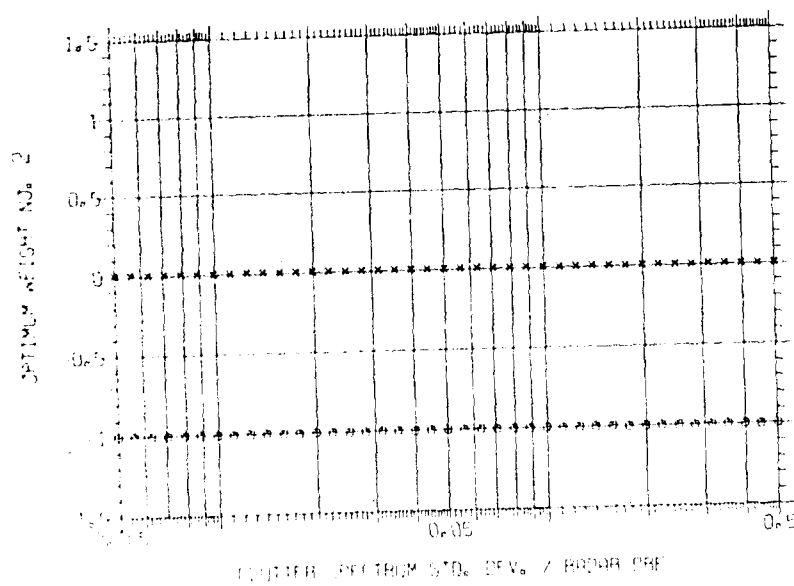
(a) Weight 1, Filter 1
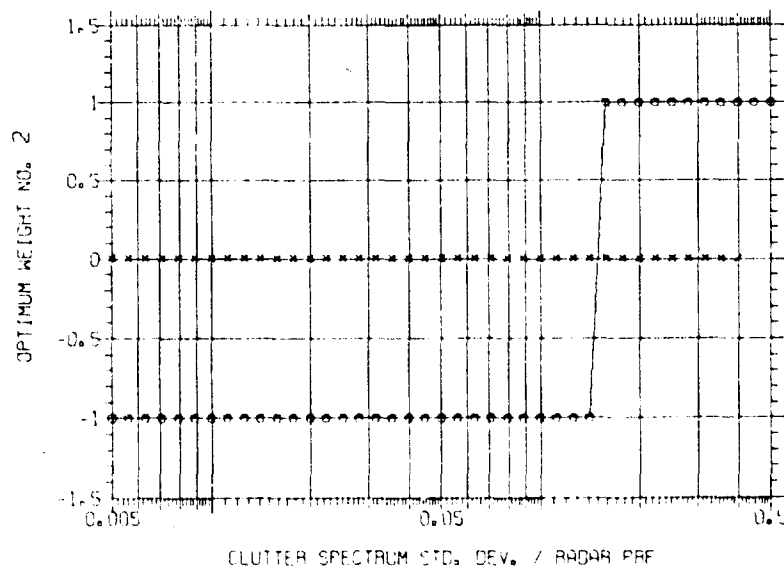
(b) Weight 2, Filter 1

Fig. 12 — Optimum weights for a 2-port processor. □ represents the real part of the complex weights. X represents the imaginary part.

(c) Weight 1, Filter 2

(d) Weight 2, Filter 2

Fig. 12 (Continued) — Optimum weights for a 2-port processor.
□ represents the real part of the complex weights. X represents
the imaginary part.

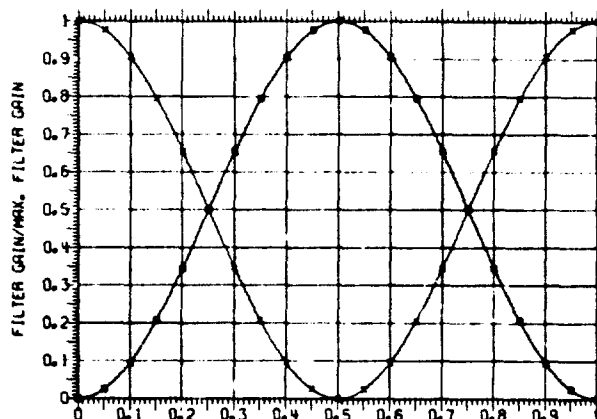Fig. 13 — Transfer characteristics of the 2-port doppler processor. ◻ represents both filters when the clutter spectrum is narrow ($\sigma_c T < 0.15$). X represents filter 1 and △ represents filter 2 when $\sigma_c T > 0.15$.

Figure 18 shows the four filter shapes of a 4-port doppler processor for three values of clutter spectral widths ($\sigma_c T = 0.005, 0.1, 0.5$). If the clutter is narrow, all four filters are the same and are also the same as in the 4-pulse optimal MTI. If the clutter is wide, all four filters approach a $(\sin x)/x$ shape centered at their respective detection regions.

The transition of these filter shapes from an optimal 4-pulse MTI to $(\sin x)/x$ filters centered at their detection regions is shown in Fig. 23. If white noise is 10^{-4} of the total interference, these filter shapes are altered appreciably, as shown in Fig. 24. The effect of white noise is much more severe for narrow clutter. For wide clutter all four filters again approach $(\sin x)/x$.

Comparing Fig. 24(a) with Fig. 23(a), we see that filter 1 is drastically affected by noise, especially for a narrow clutter spectrum. With the addition of noise the optimum filter is no longer a 4-pulse MTI; it is seen that the peak response is moved closer to the center of the detection region (zero doppler). If Fig. 24b, c, and d is compared with Fig. 23b, c, and d, similar effects can be seen for filters 2, 3, and 4. The peak response moves closer to the detection region and the sidelobe level increases (and the main lobe level narrows) for a narrow clutter spectrum. These effects become more pronounced as the fractional noise energy is increased, 0.01 for Fig. 25 and 0.5 for Fig. 26.

The results of this investigation show that the clutter-to-noise ratio is an important parameter for determining the optimal N-port doppler processor.

CONCLUSIONS

An optimization procedure has been developed for the transversal filter using the maximum-likelihood-ratio criterion. When the interference has Gaussian amplitude statistics, the likelihood ratio is maximized when the output signal-to-interference ratio is

maximized. Under these conditions, the optimum weights for the transversal filter can be derived from the covariance of the signal and the interference.

If M_I is the covariance matrix of the interference and M_S is that of the signal, the maximum improvement in signal-to-interference ratio (the improvement factor) is given by the largest eigenvalue of M'_S where M'_S is defined by Eq. (34). The set of optimum weights is given by the eigenvector M'_S that is associated with this largest eigenvalue. With the design procedure reduced to finding the eigenvalues and eigenvectors of a matrix, the filter for a given application can be designed using numerical techniques to compute the eigenvectors and eigenvalues. The optimal design can be computed with this procedure and the improvement factor can be obtained with no additional computing.

The covariance of a function of time is the Fourier transform of the power spectrum of the function. Therefore, the spectrums of the signal and the interference must be known prior to deriving the optimum weights. This optimization procedure has been applied to the detection of a signal with an unknown doppler shift. Three cases were considered in this research. These were defined in terms of the a priori knowledge of the doppler shift, as follows: (a) the doppler shift is completely unknown, (b) the doppler shift is known exactly, and (c) the doppler shift is known within a region.

It was shown that if the doppler shift is completely unknown this optimization procedure gives the same results as the procedure of Emerson (3), which is to maximize the rejection of interference. However, it has been shown in this research that his procedure is equivalent to one using the stronger criterion of maximizing the output signal-to-interference ratio.

The procedure developed in this research is equivalent to that of Applebaum (4) and Brennan (7) when the doppler shift is known exactly. For this condition a filter is optimized to detect a signal at a given doppler shift.

When the doppler shift is unknown, it must be assumed to have equal probability of occurring at any frequency within the analyzing bandwidth of the filter. However, this bandwidth can be covered by several contiguous filters instead of a single filter. This incurs no additional data storage when several independent sets of weights are applied to the data. In this way, each filter can be designed to detect a signal within a portion of the total bandwidth instead of the entire bandwidth. The doppler shift of the signal can be assumed to have equal probability of occurring anywhere within a region instead of the entire doppler domain. This additional information about the signal has been used to improve the output signal-to-interference ratio.

The results of this research were applied to a radar incorporating a single-port MTI processor. In this, a single-filter output is used to detect returns from moving targets which may have any doppler shift and to reject returns from fixed objects. These latter returns are referred to as clutter. A zero-mean Gaussian clutter spectrum was used to compare the improvement factor of the optimal MTI with that of the conventional MTI. The results are shown in Fig. 8, which shows that the increased improvement factor is affected only slightly by the width of the clutter spectrum or standard deviation of the Gaussian spectrum. Typical values for this increase are 0 dB for a 2-pulse MTI, 2 dB for a 3-pulse MTI, 3 dB for a 4-pulse MTI, and 5 dB for a 5-pulse MTI. The advantage of using optimum weights is modest when the returns from only a small number of pulses
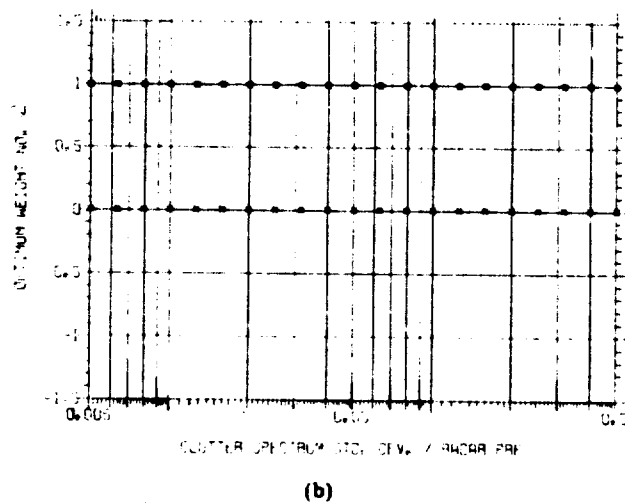
27

(a)

(b)
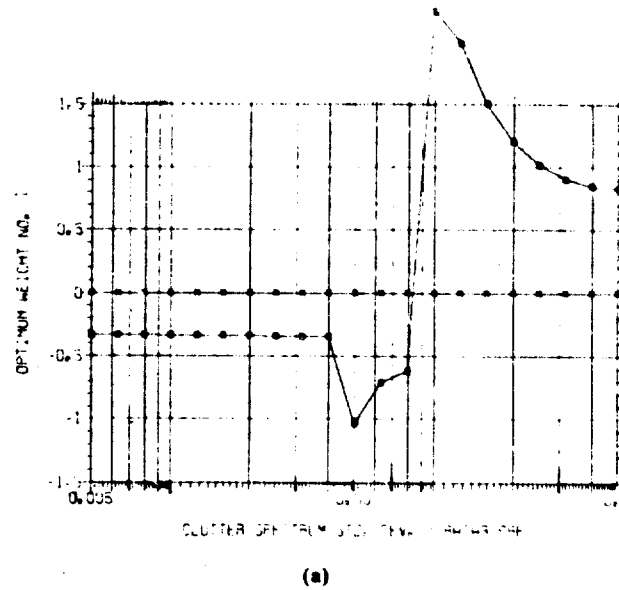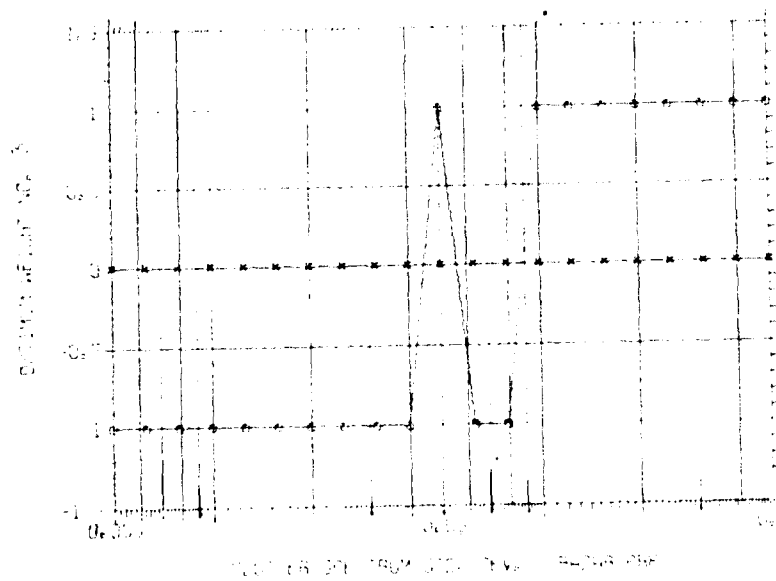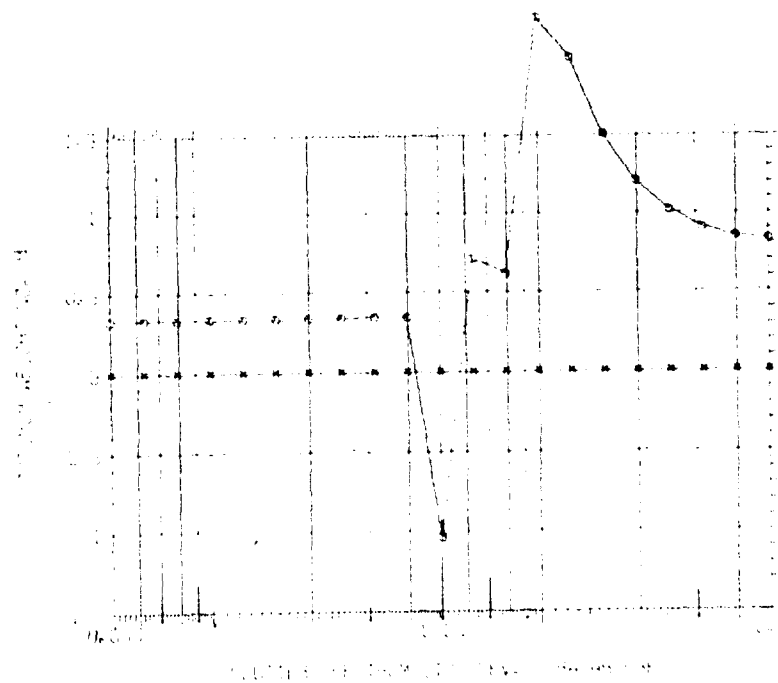
Fig. 14 — Optimum weights for filter 1 of a 4-port doppler processor. □ represents the real part of the complex weights. x represents the imaginary part.
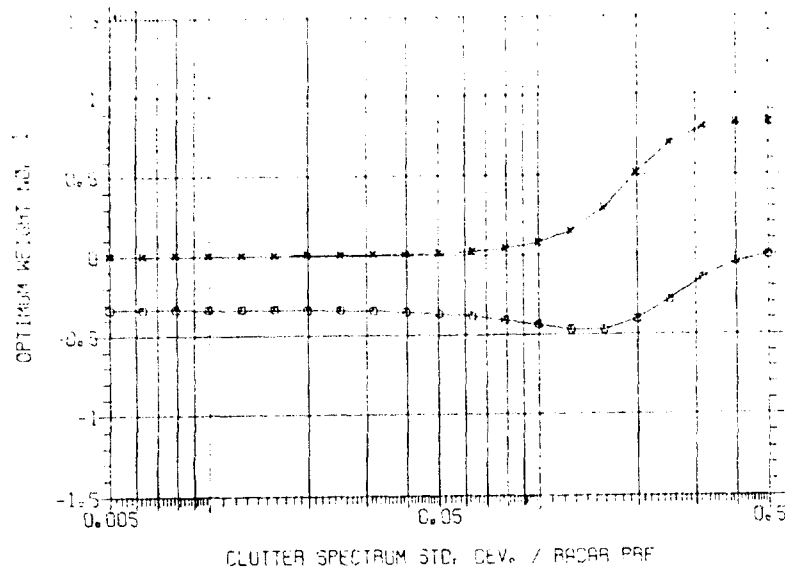
(c)
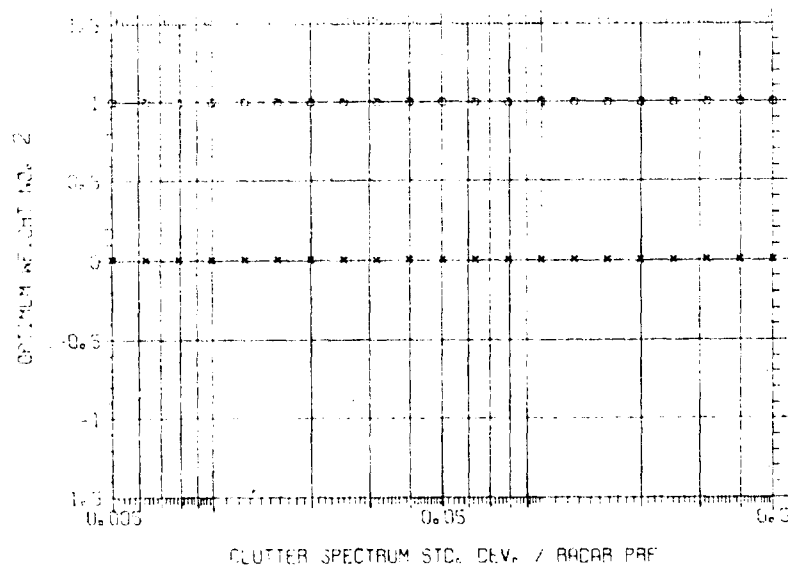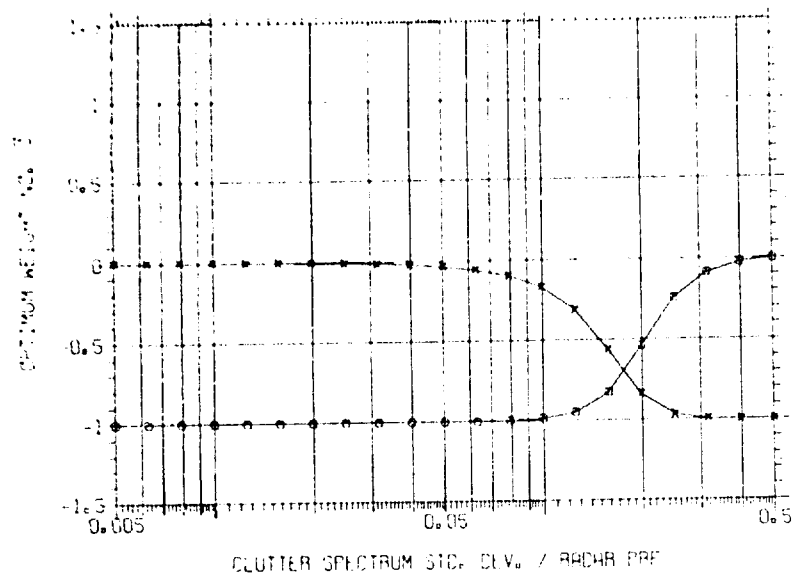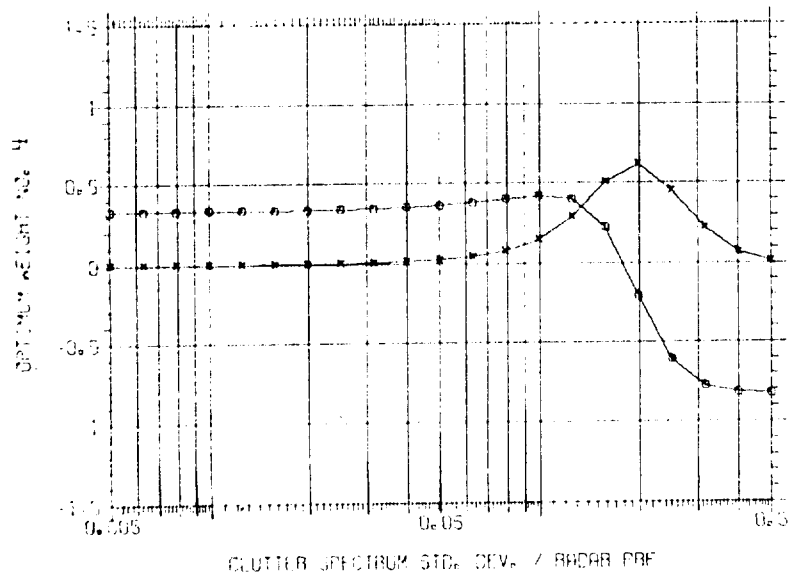

(d)

Fig. 14 (Continued) — Optimum weights for filter 1 of a 4-port doppler processor. □ represents the real part of the complex weights. X represents the imaginary part.

(a)

(b)

Fig. 15 — Optimum weights for filter 2 of a 4-port doppler processor. □ represents the real part of the complex weights. X represents the imaginary part.

30

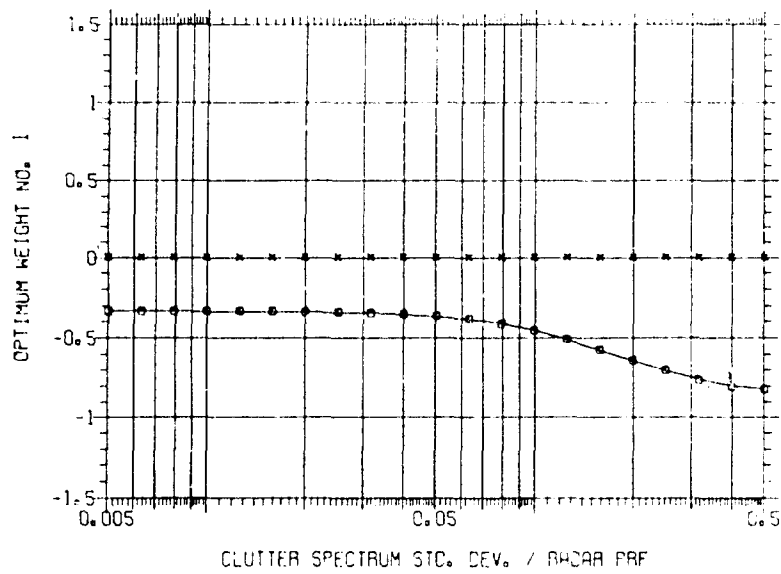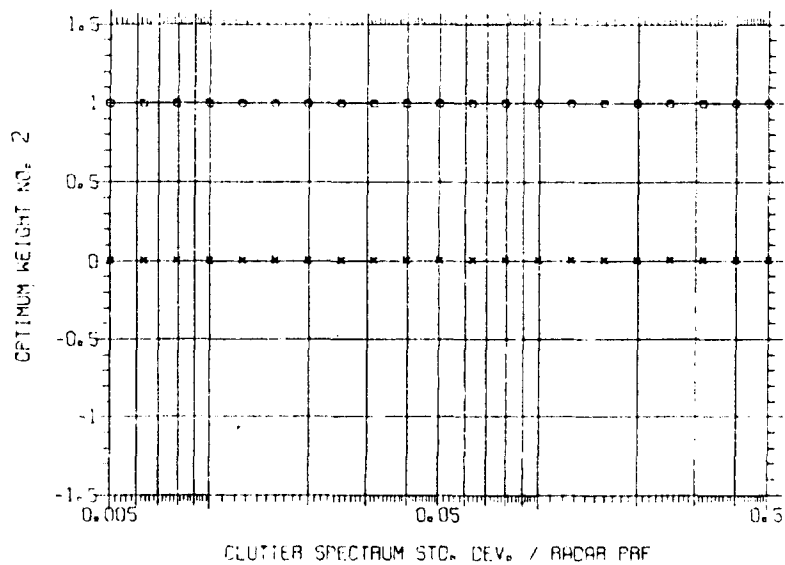(c)

(d)

Fig. 15 (Continued) — Optimum weights for filter 2 of a 4-port doppler processor. □ represents the real part of the complex weights. X represents the imaginary part.

31

(a)

(b)

Fig. 16 — Optimum weights for filter 3 of a 4-port doppler processor. □ represents the real part of the complex weights. x represents the imaginary part.

(c)

(d)

Fig. 16 (Continued) — Optimum weights for filter 3 of a 4-port doppler processor. □ represents the real part of the complex weights. X represents the imaginary part.

33

(a)

(b)

Fig. 17 — Optimum weights for filter 4 of a 4-port doppler processor. ☐ represents the real part of the complex weights. X represents the imaginary part.
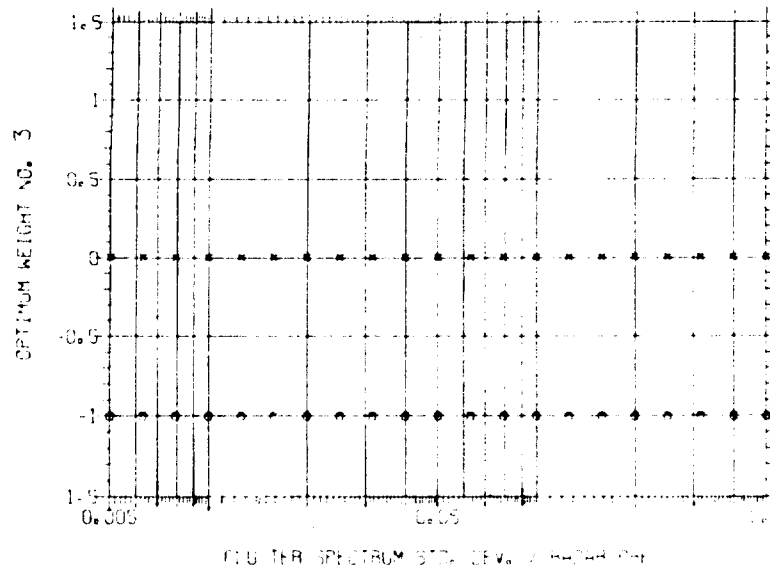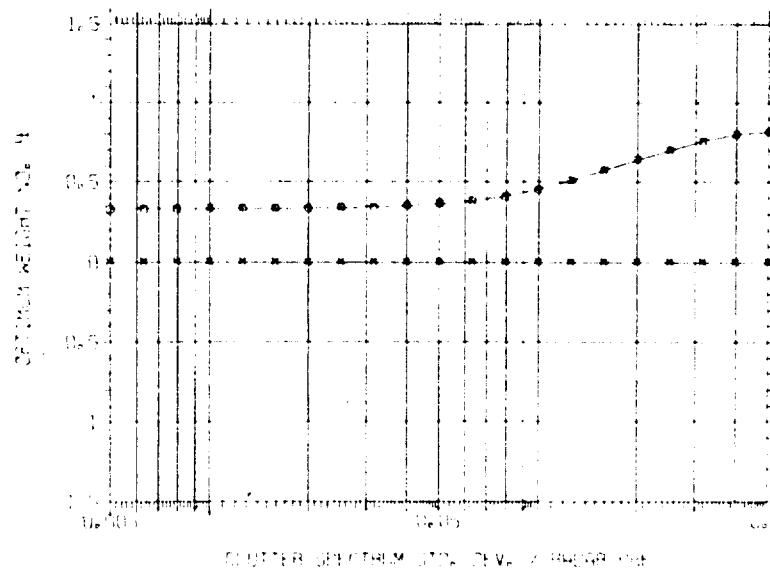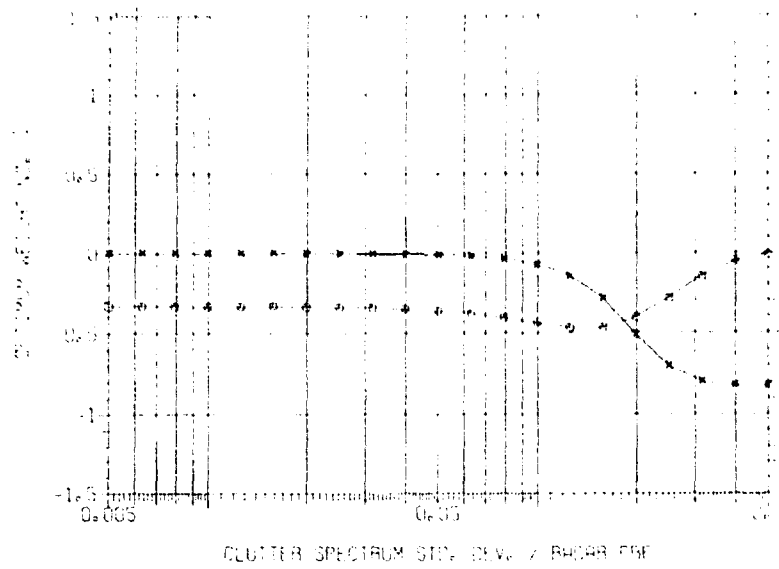
34
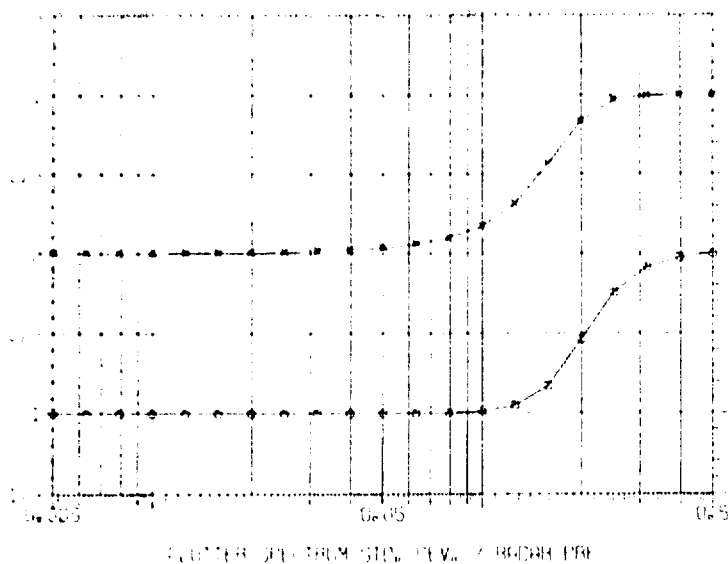
(c)
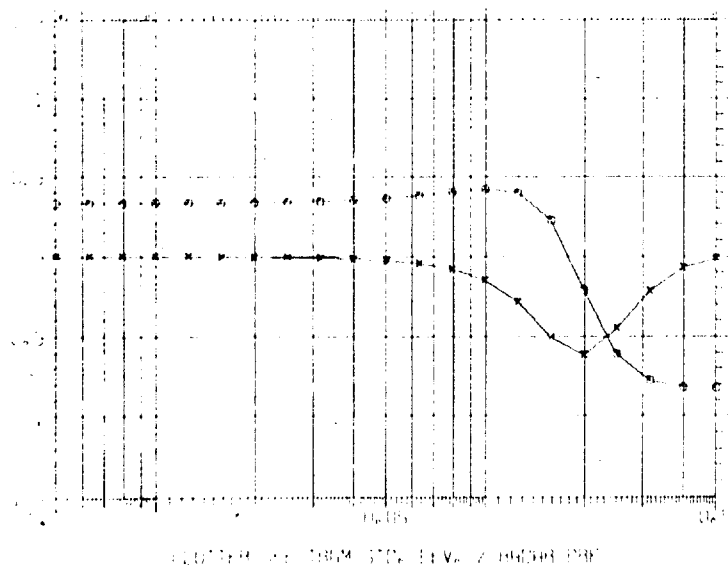
(d)

Fig. 17 (Continued) — Optimum weights for filter 4 of a 4-port
doppler processor. □ represents the real part of the complex
weights. X represents the imaginary part.

(b)

(a)
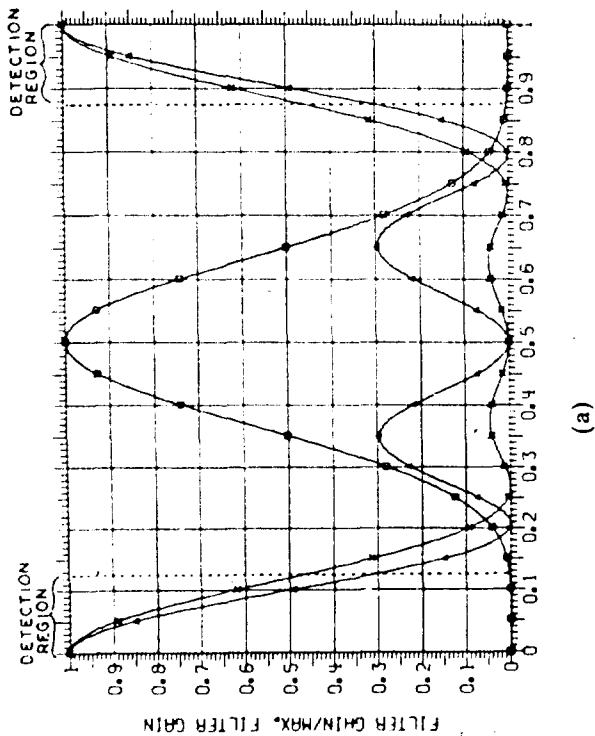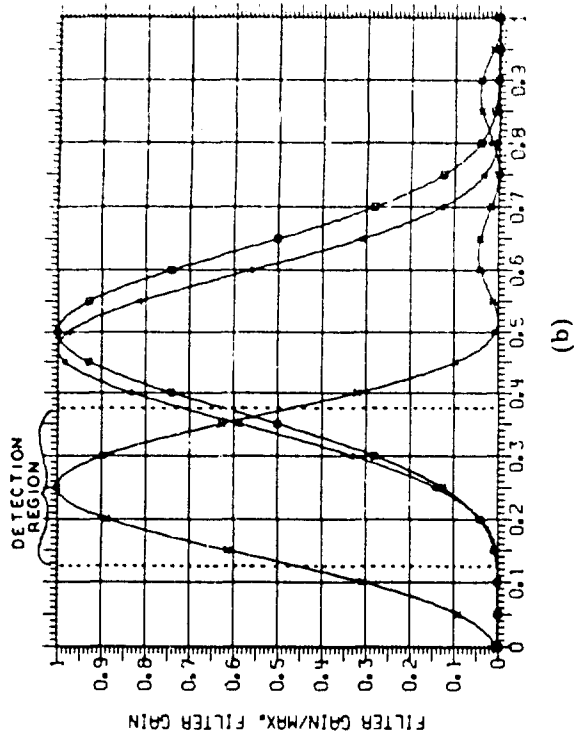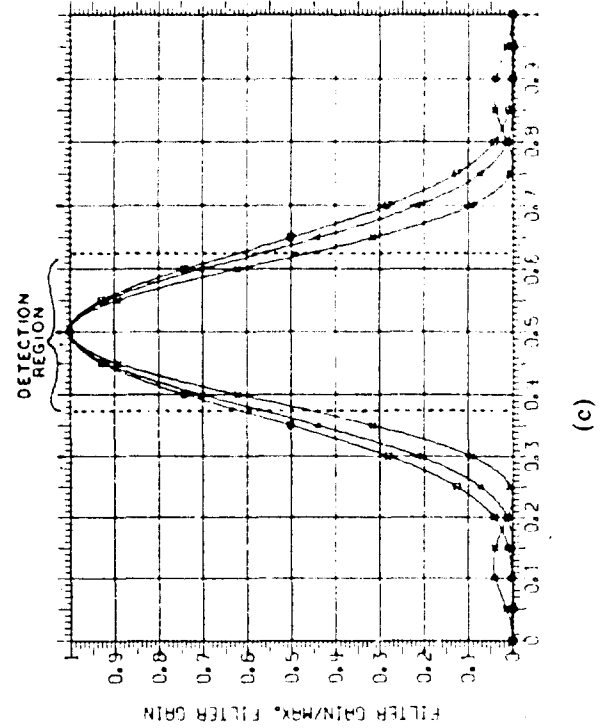
(c)
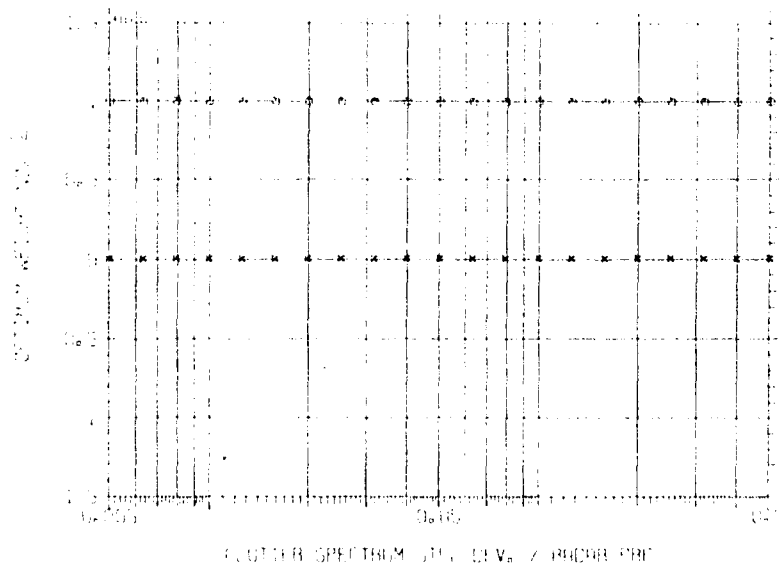
Fig. 18 — Filter transfer characteristics of a 4-port doppler processor. □ represents the filter shape when the width of the clutter spectrum is narrow ($\sigma_c T = 0.005$), $\triangle$ represents the filter shape for $\sigma_c T = 0.1$, and X represents the filter shape for $\sigma_c T = 0.5$.

(a) Filter one

(b) Filter two

(c) Average (dotted curves) and optimal 2-pulse
MTI (broken curve)
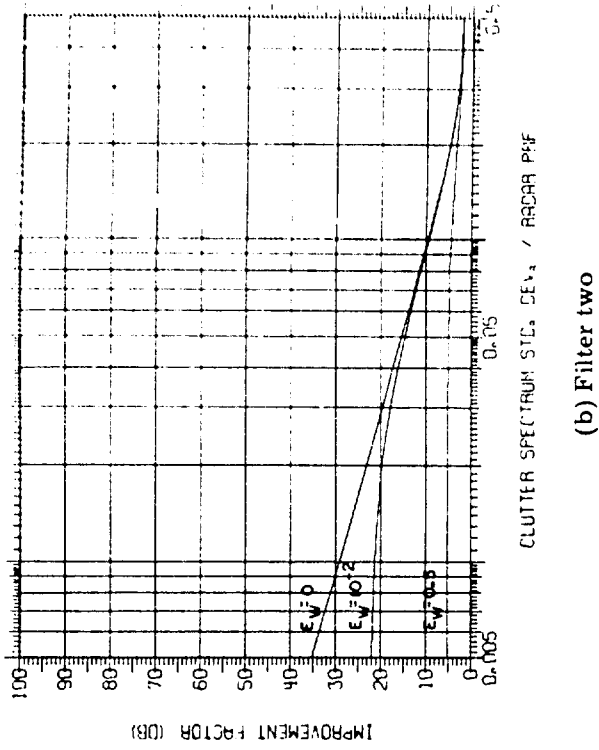
Fig. 19 — The effect of white noise on the improvement factor of a 2-port doppler processor. E_W is the fraction of the total interference energy that is white noise.

37
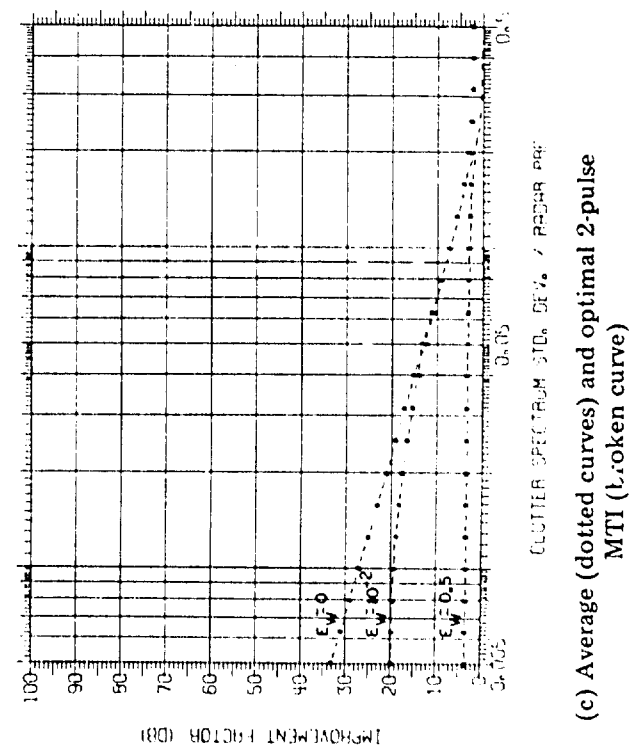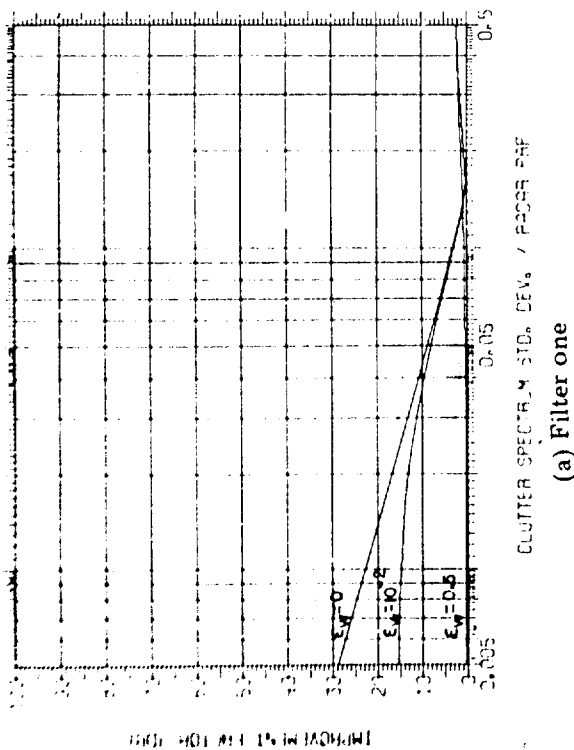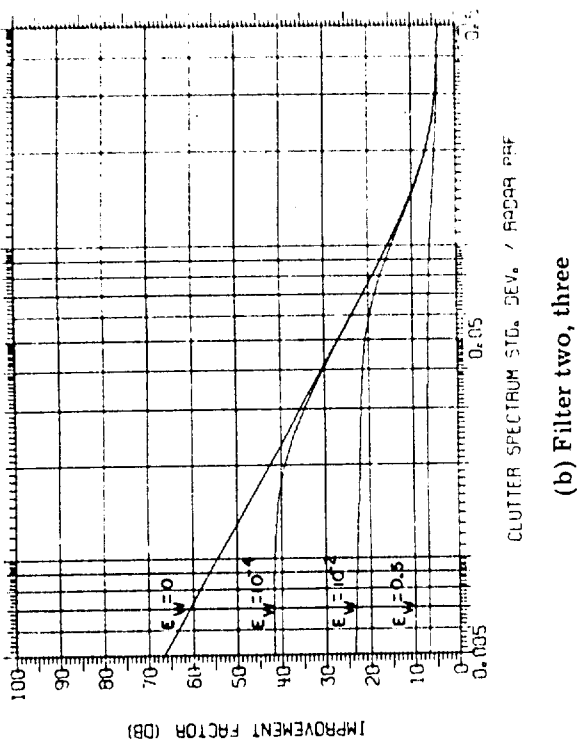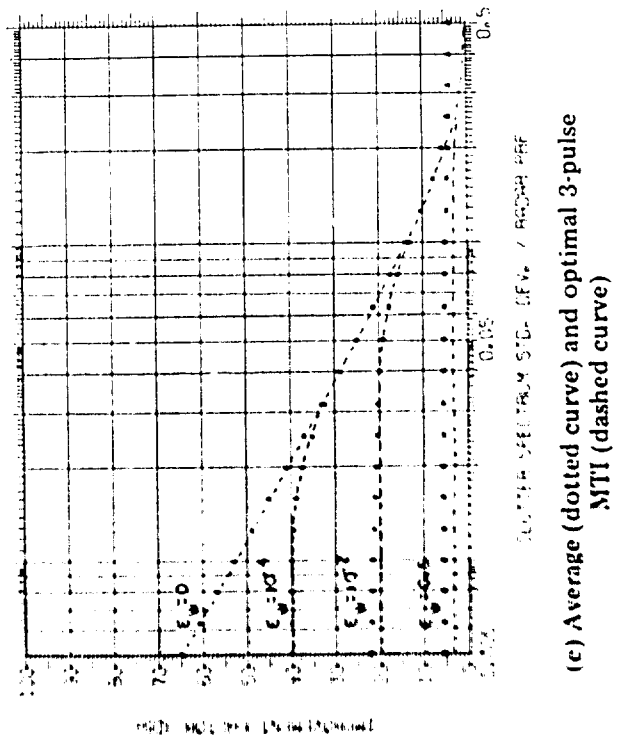
(b) Filter two, three

Fig. 20 — The effect of white noise on the improvement factor of a 3-port doppler processor. E_W is the fraction of the total interference energy that is white noise.

(a) Filter one

(c) Average (dotted curve) and optimal 3-pulse MTI (dashed curve)
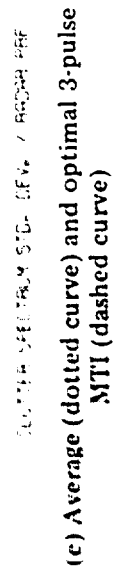
are processed at one time, but it quickly becomes significant as the number of pulses for which returns are processed is increased.

The techniques developed in research were also applied to a radar N-port doppler processor in which N independent sets of filter weights were used to design N filters. For this, the doppler domain was divided into N regions. Each filter was optimized for a target whose doppler shift has equal probability of occurring anywhere within one of the regions. These results are shown in Fig. 11. Comparing the average improvement factor of the N filters of an N-port processor with the improvement factor of the optimal MTI shows that the optimal MTI approaches a 0-dB improvement factor when the clutter spectrum is wide. The N-port processor provides an improvement in signal-to-clutter ratio even under this condition. The value of this improvement factor depends on the number of returns processed. Typical values are 2.5 dB for a 2-port processor, 4 dB for a 3-port processor, 5 dB for a 4-port processor, and 6 dB for a 5-port processor.

The optimum weights, or filter shapes, vary as the width of the clutter spectrum is changed. This is shown in Fig. 18 for a 4-port processor. When the width of the clutter spectrum is very small, all four filters are the same. Furthermore, they are the same as the optimal MTI with a single output. Therefore, when the width of the clutter spectrum is very small, only one output is needed, and that output is the optimal MTI. Unexpectedly, the peak response of the filters was sometimes found to occur outside the detection region for that particular filter. This implies that for clutter with a very narrow spectrum, maximization of the improvement factor results mainly from minimizing the output clutter.

For clutter with a large spectral width, the characteristic of each of the four filters identified by triangles on the curves is very close to a $(\sin x)/x$ function in shape, and the peak response is centered in the detection region of each filter. This implies that for clutter of large spectral width, the optimal processor is a discrete Fourier transform with no weighting of the input data.

In the transition region between small and large spectral widths of the clutter, the peaks of the filter responses are closer to the center of the detection regions. In this region, the sidelobes of the filter response are found to be very high, even higher than those of the $(\sin x)/x$ filter shape. The shapes of the filters are controlled by weighting the input data.

The optimum filter weights are easily computed when the clutter has either a very narrow or a very wide spectrum. In the transition region, it is necessary to go through the optimization procedure developed during this research. The design parameters of a radar system must be chosen with many factors in mind. In general, they cannot be selected in such a way that the ratio of the clutter spectrum and the PRF is either very small or very large. For most applications, the doppler processor must be designed to operate within this transition region. Furthermore, as the number of returns to be processed is increased, this transition region becomes wider. That is, the clutter spectrum must be much narrower before all the filters approach the optimal MTI, or the spectrum must be much wider before the N-port processor approaches the discrete Fourier transform. Therefore, for a radar system processing a large number of returns this optimization procedure is necessary to ensure the best performance in detecting moving targets.
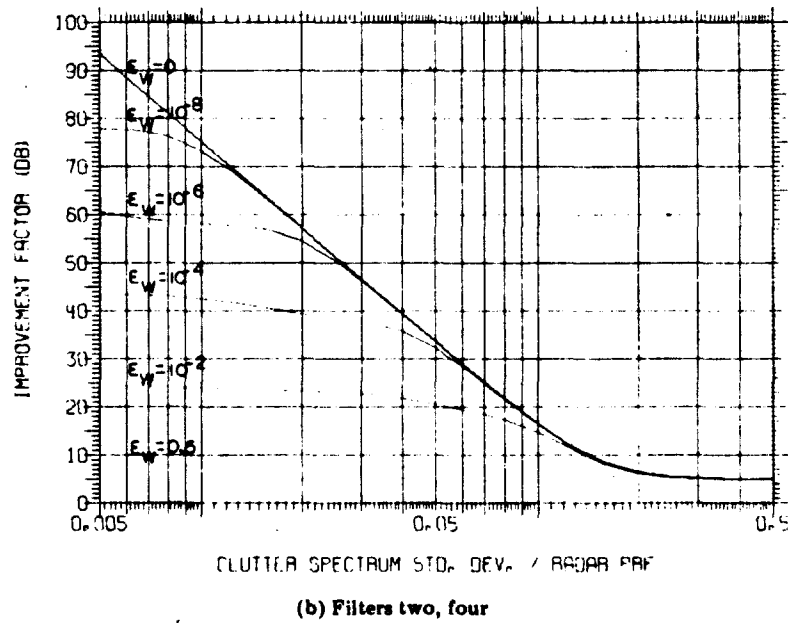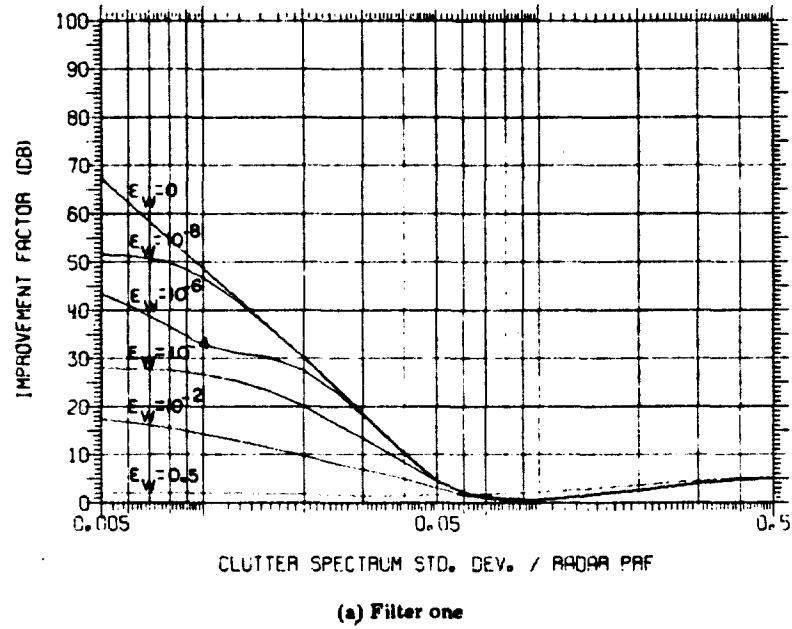
(a) Filter one

(b) Filters two, four

Fig. 21 — The effect of white noise on the improvement factor of a 4-port doppler processor. E_W is the fraction of the total interference energy that is white noise.

(c) Filter three

(d) Average (dotted curve) and optimal 4-pulse MTI (dashed curve)
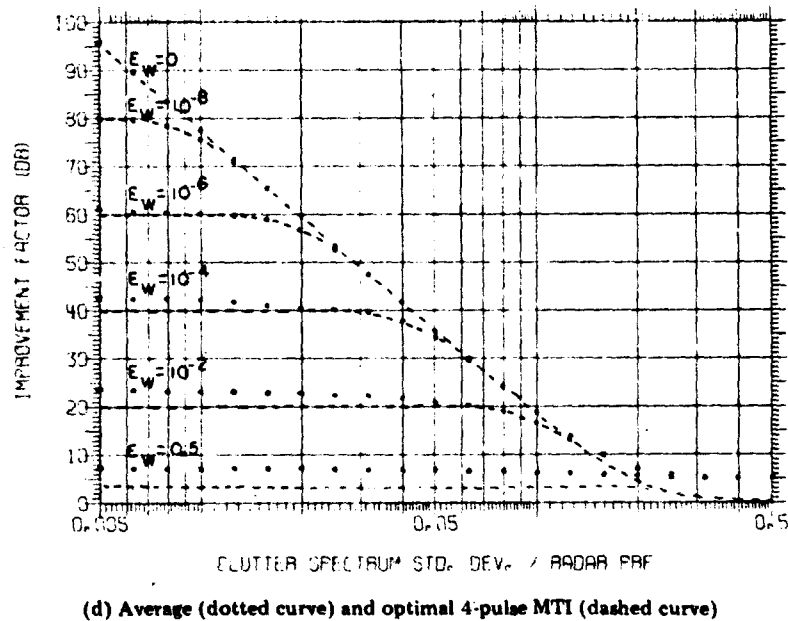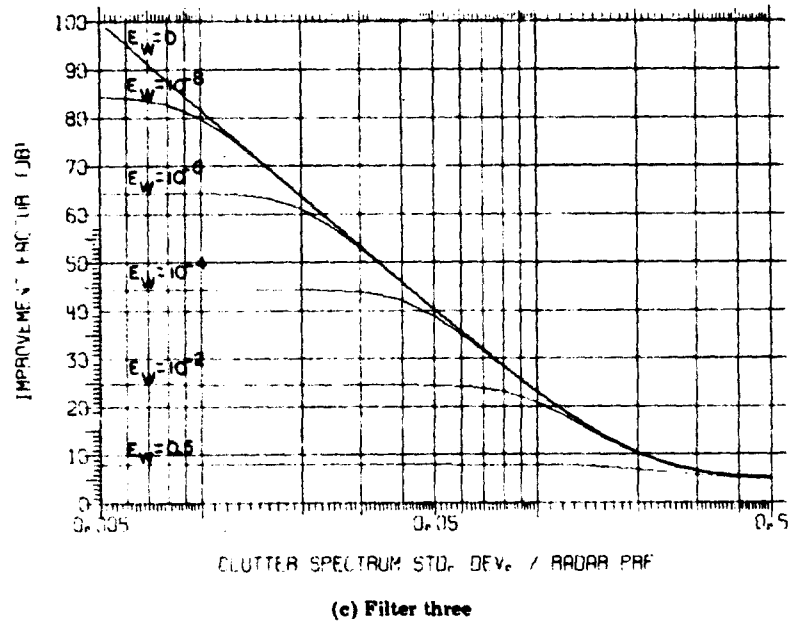
Fig. 21 (Continued) — The effect of white noise on the improvement factor of a 4-port doppler processor. E_W is the fraction of the total interference energy that is white noise.

(a) Filter one

(b) Filter two, five
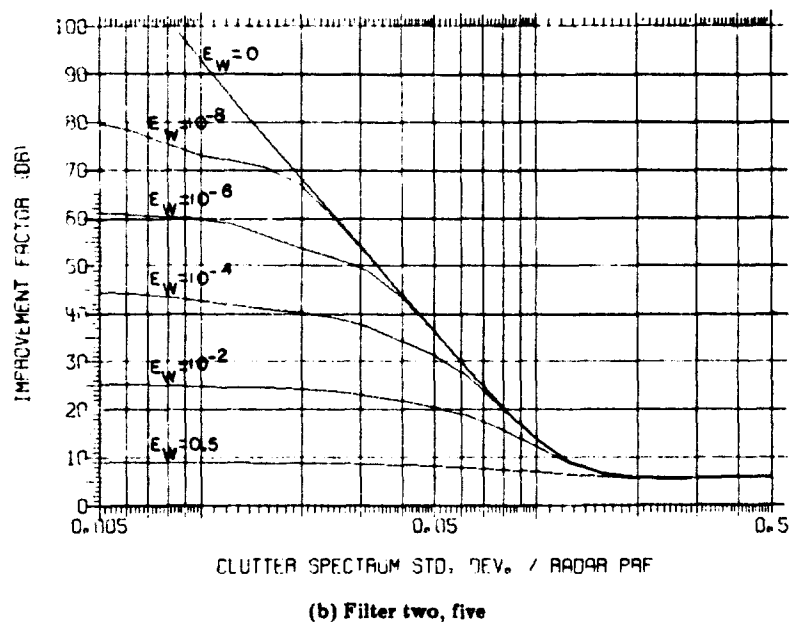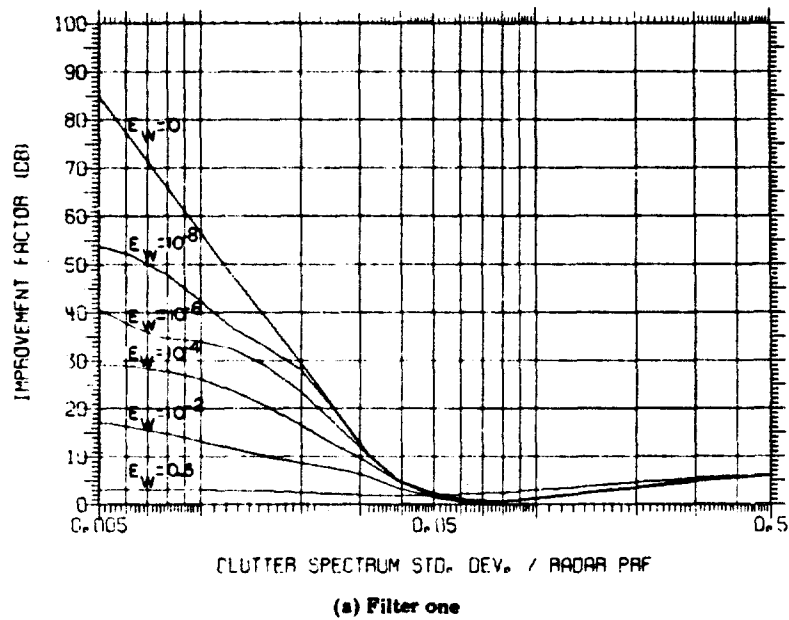
Fig. 22 — The effect of white noise on the improvement factor of a 5-port doppler processor. E_W is the fraction of the total interference energy that is white noise.
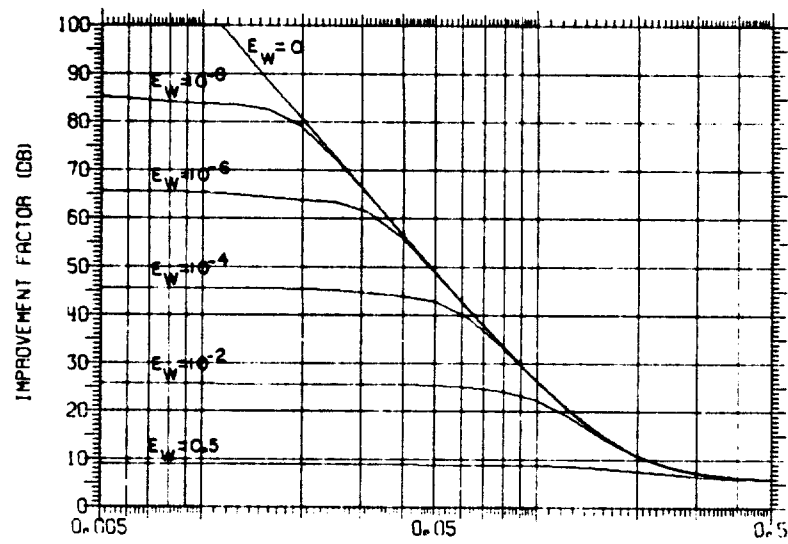
(c) Filters three, four
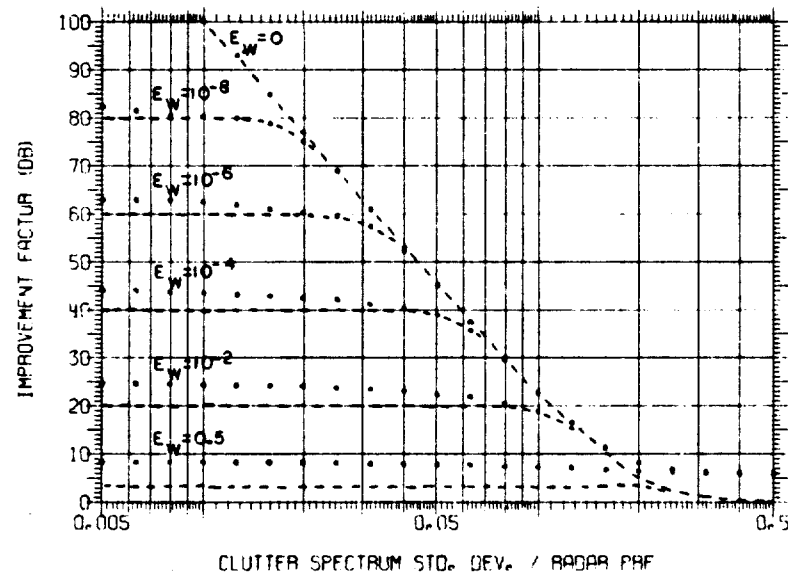
(d) Average (dotted curves) and optimal 5-pulse MTI (dashed curves)

Fig. 22 (Continued) — The effect of white noise on the improvement factor of a 5-port doppler processor. E_W is the fraction of the total interference energy that is white noise.

43
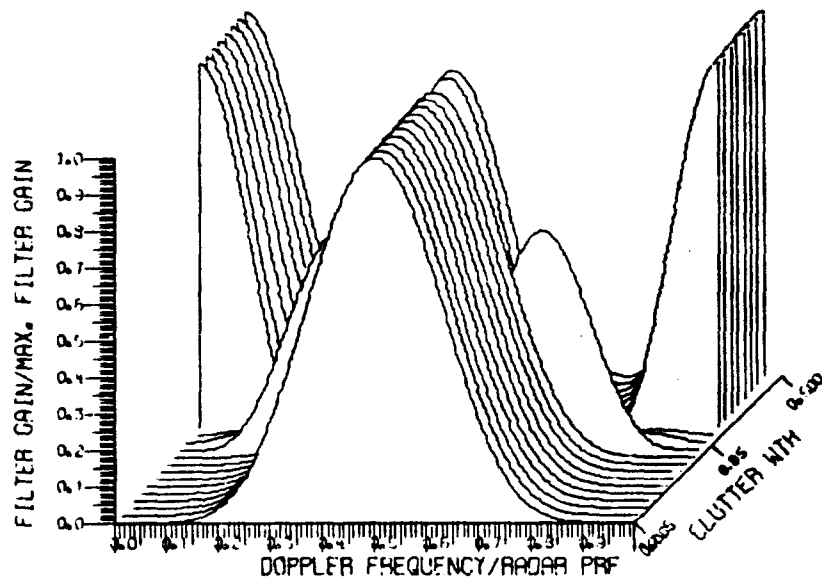
(a) Filter No. 1, centered at zero doppler
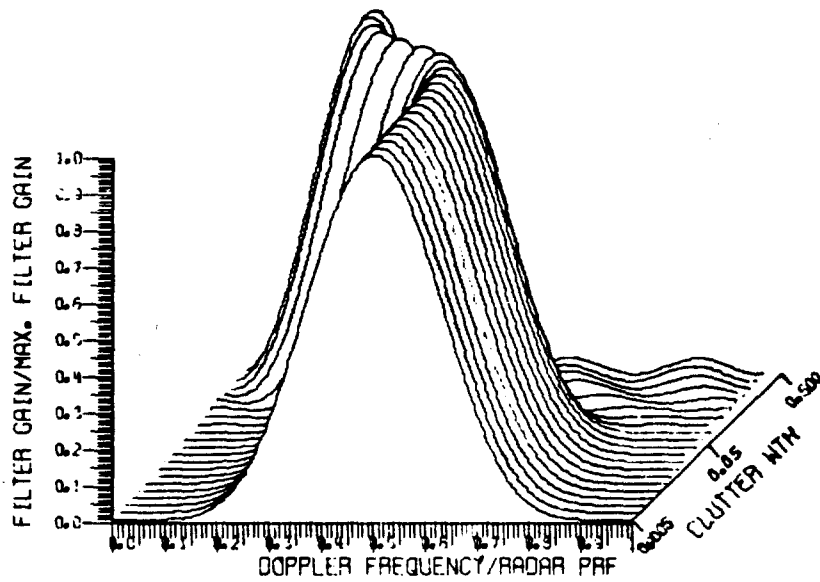
(b) Filter No. 2, centered at 1/4 PRF

Fig. 23 — The effect of the width of the clutter spectrum ($\sigma_c T$) on the filter shapes of a 4-port doppler processor. No white noise.
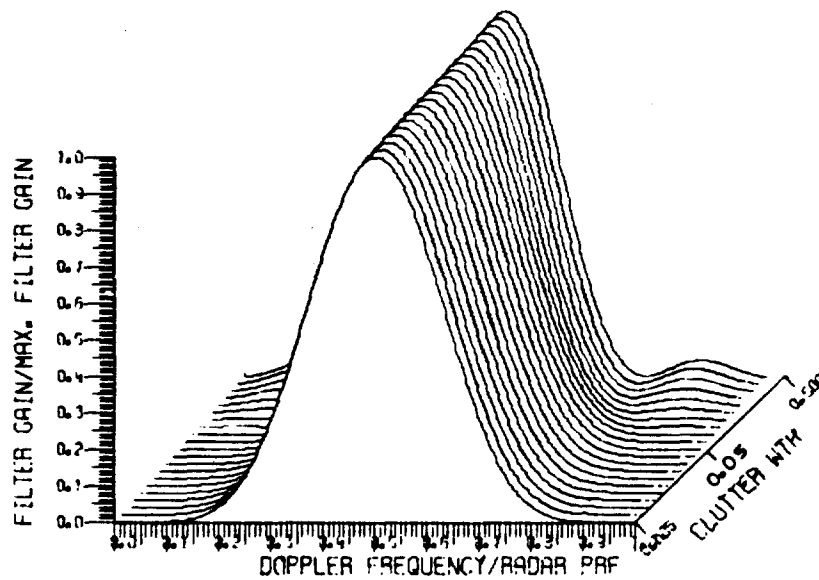
(c) Filter No. 3, centered at 1/2 PRF
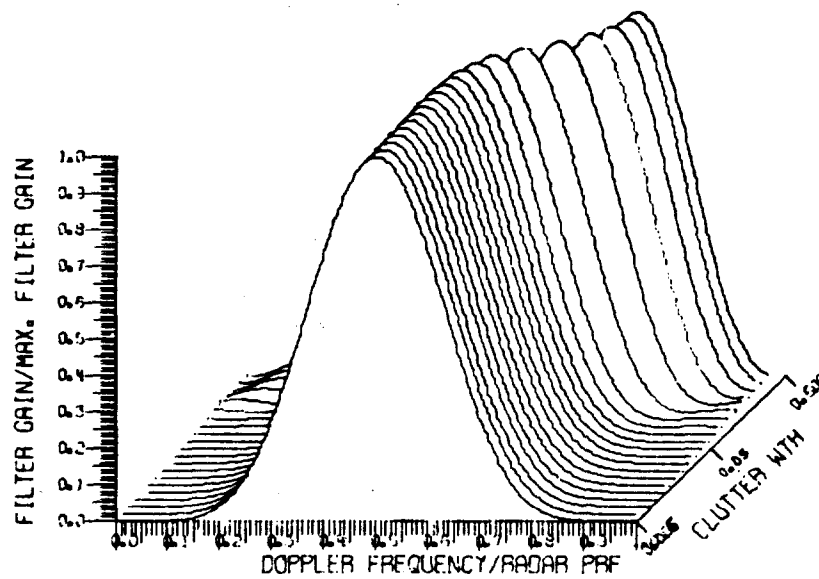
(d) Filter No. 4, centered at 3/4 PRF

Fig. 23 (Continued) — The effect of the width of the clutter spectrum ($\sigma_c T$) on the filter shapes of a 4-port doppler processor. No white noise.

45
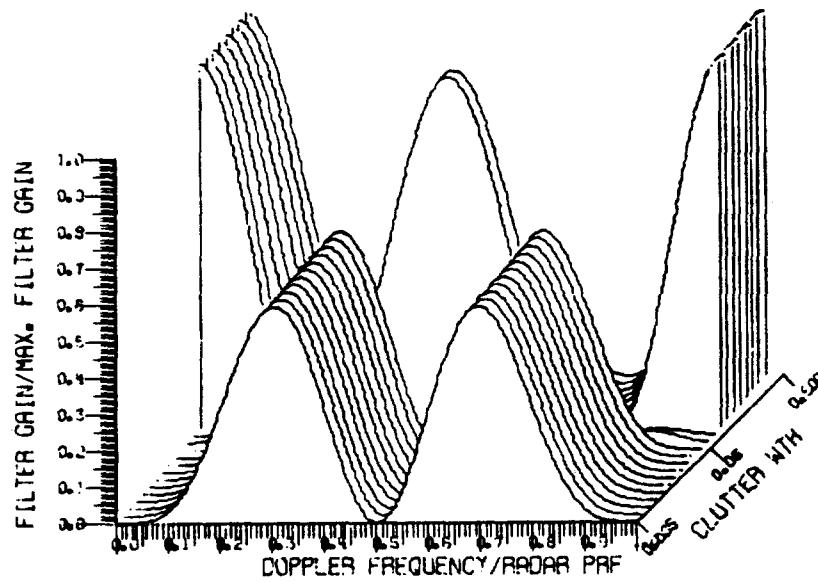
(a)
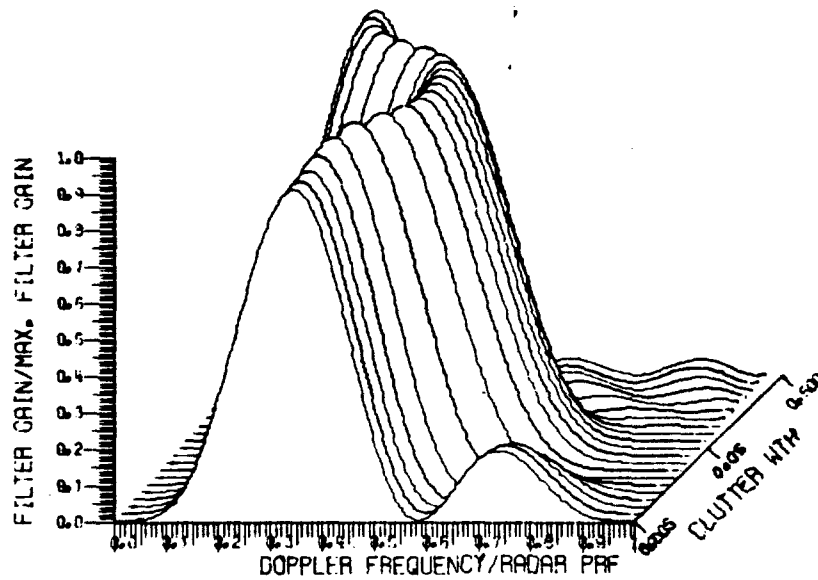
(b)

Fig. 24 — The effect of the width of the clutter spectrum ($\sigma_c T$) on the filter shapes of a 4-port doppler processor. The white noise input energy is 10^{-4} of the total input interference energy.

46

(c)

(d)
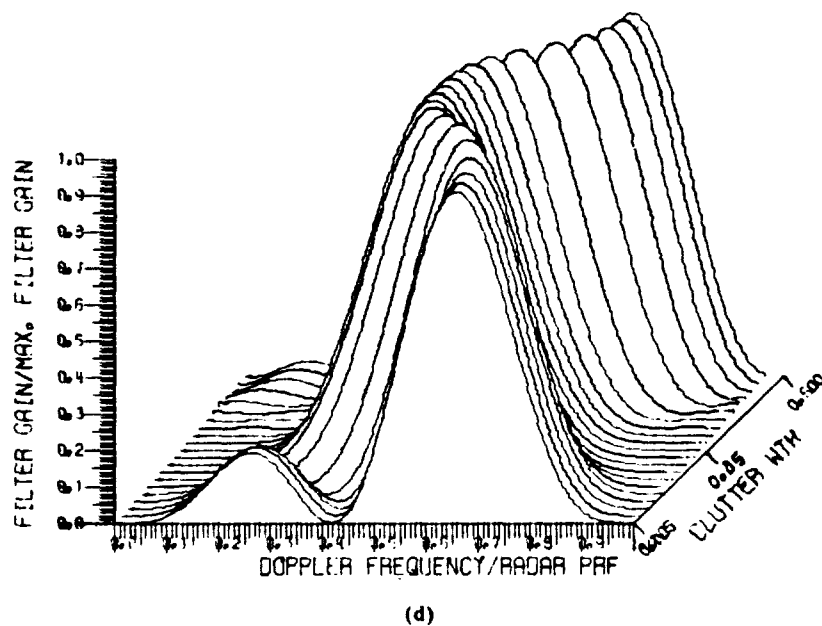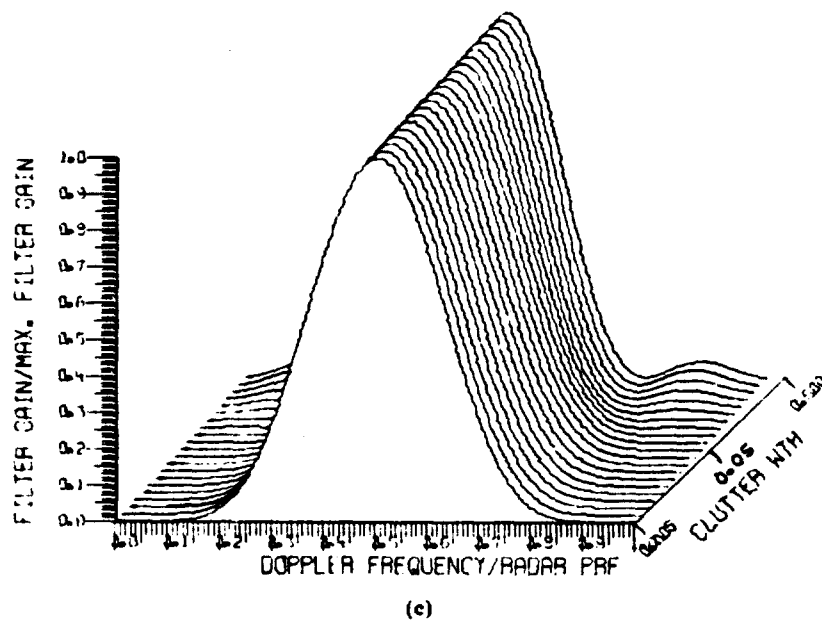
Fig. 24 (Continued) — The effect of the width of the clutter spectrum $(\sigma_c T)$ on the filter shapes of a 4-port doppler processor. The white noise input energy is 10^{-4} of the total input interference energy.

47

(a)

(b)
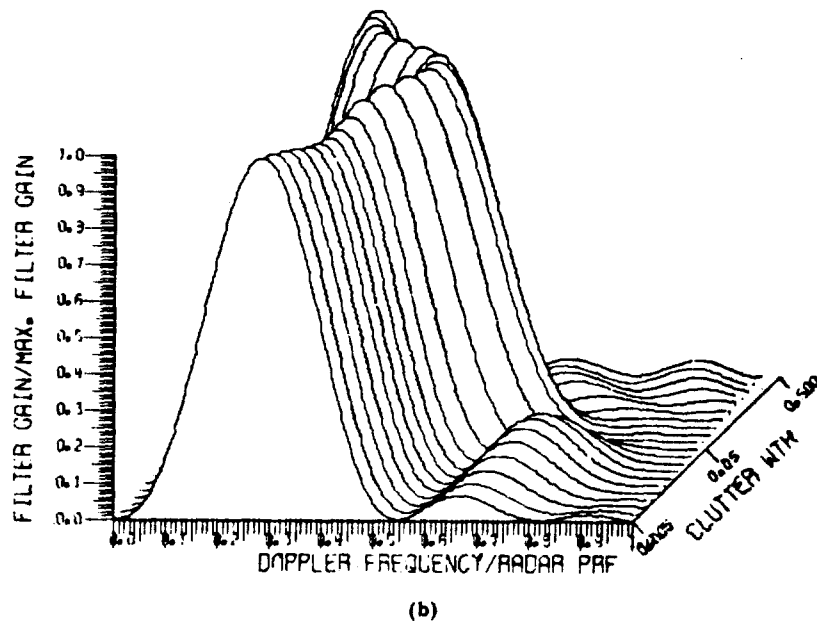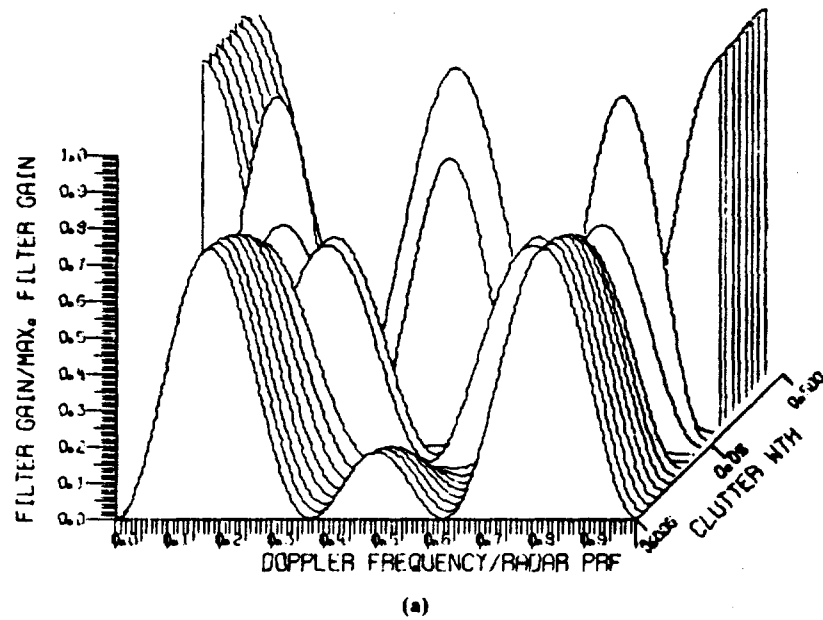
Fig. 25 — The effect of the width of the clutter spectrum ($\sigma_c T$) on the filter shapes of a 4-port doppler processor. The white noise input energy is 10^{-2} of the total input interference energy.

48
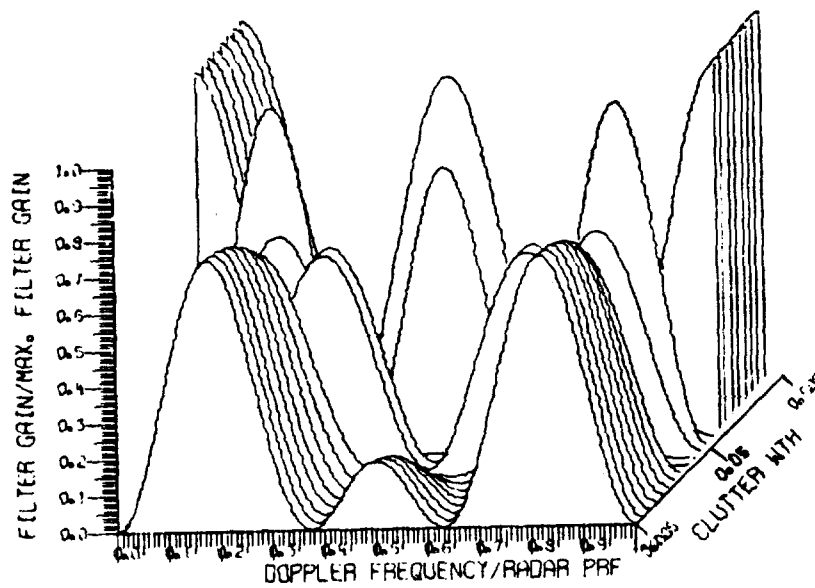
(c)
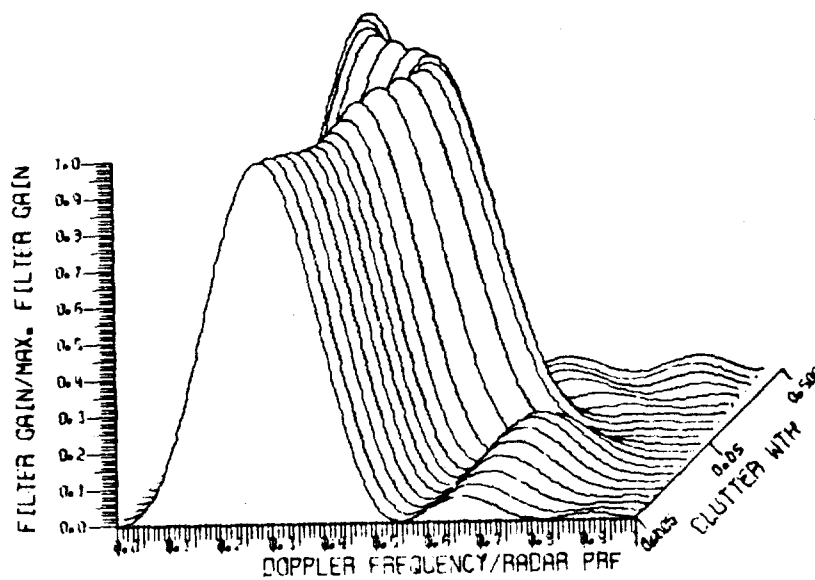
(d)

Fig. 25 (Continued) — The effect of the width of the clutter spectrum ($\sigma_c T$) on the filter shapes of a 4-port doppler processor. The white noise input energy is 10^{-2} of the total input interference energy.

49
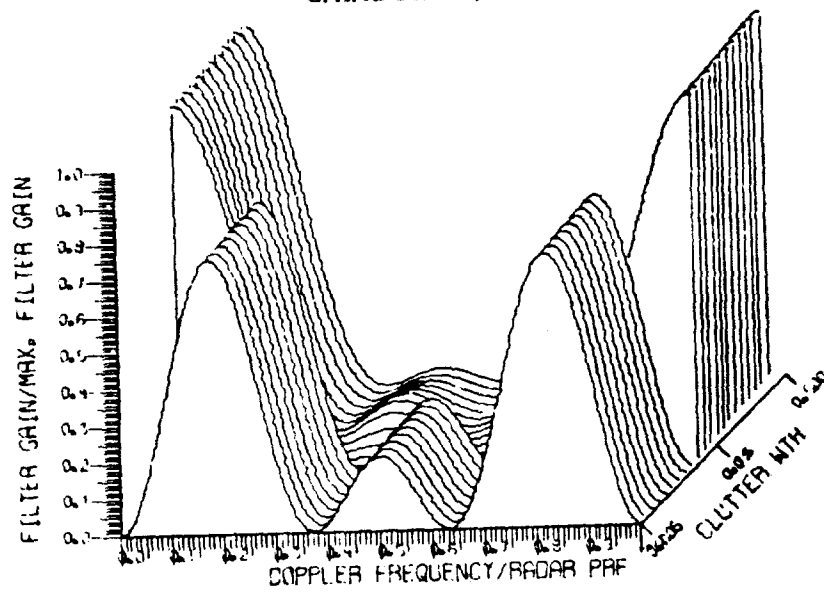
(a)
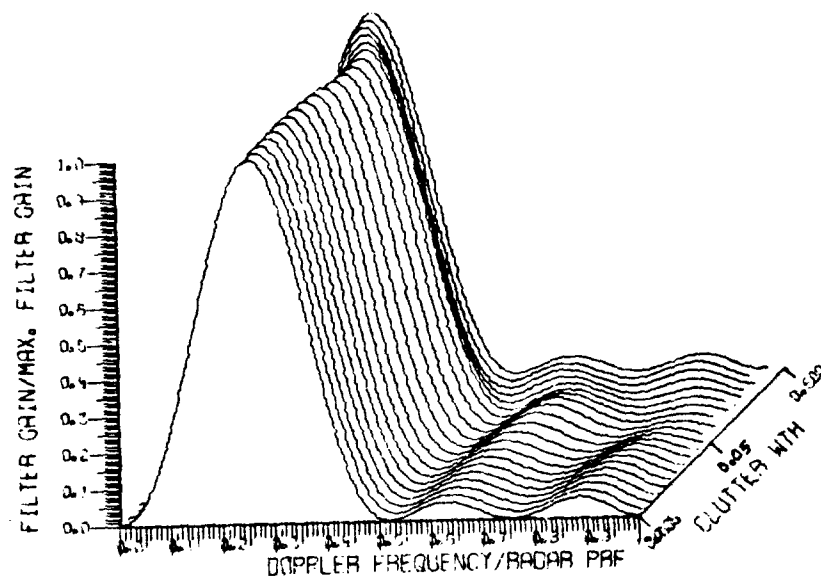
(b)

Fig. 26 — The effect of the width of the clutter spectrum ($\sigma_c T$) on the filter shapes of a 4-port doppler processor. The white noise input energy is 0.5 of the total input interference energy.

50
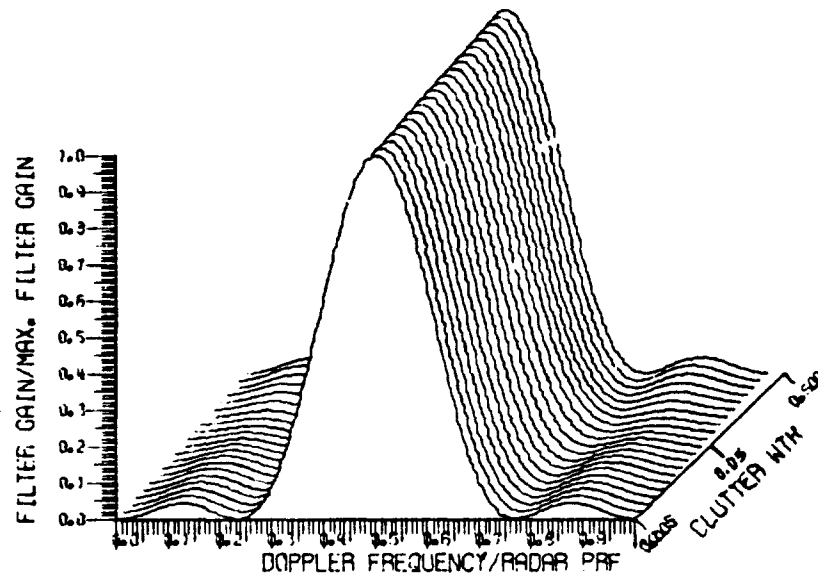
(c)
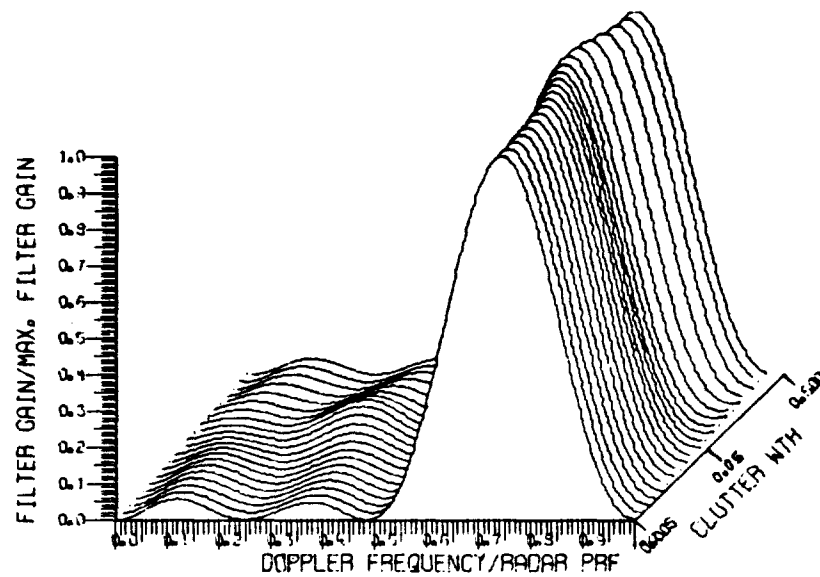
(d)

Fig. 26 (Continued) — The effect of the width of the clutter spectrum $(\sigma_c T)$ on the filter shapes of a 4-port doppler processor. The white noise input energy is 0.5 of the total input interference energy.

51

It has also been shown by this research that neither the conventional nor the optimal MTI provides any improvement factor when the interference corresponds to white noise. Therefore, when the total interference consists of both clutter and white noise, the improvement factor is reduced significantly (Figs. 9 and 10). The N-port processor provides a larger improvement factor against clutter plus white noise (Figs. 19-22). The shapes for the optimal filters of a 4-port processor are shown in Fig. 23-26 for noise levels constituting fractions (0, 0.0001, 0.01, and 0.5) of the total interference. As the noise level is increased, the optimal filter shapes never approach the optimal MTI for narrow clutter, even when the ratio of the standard deviation of the clutter to the PRF of the radar is as small as 0.005. However, the optimal shape approaches that of the (sin x)/x function when the spectral width of the clutter is smaller than necessary for interference consisting only of clutter. Therefore, the width of the transition region seems to be unaffected by the addition of white noise. The transition region as a whole, though, is shifted downward.

Since the shapes of the optimal filters are altered drastically by the addition of white noise, the clutter-to-noise ratio is an important parameter for determining the optimal N-port doppler processor. Therefore, the optimization procedure developed during this research will ensure the best performance in the most important and general case, in which a radar system must contend with both clutter and white noise.

ACKNOWLEDGMENTS

REFERENCES

1. R.S. Berkowitz, editor, "Modern Radar," Wiley, New York, 1965.

2. B. Gold, M.C. Rader, *Digital Processing of Signals*, McGraw-Hill, New York, 1969.

3. R.C. Emerson, "Some Pulsed Doppler MTI and AMTI Techniques," Report R-274, Rand Corporation, Mar. 1, 1954.

4. S.P. Applebaum, "Adaptive Arrays," Syracuse University Research Corp., SPL-769, June 1964.

5. G.A. Andrews, "Performance of Cascaded MTI and Coherent Integration Filters in a Clutter Environment," NRL Report 7533, March 1973.

6. F.E. Nathanson, and J.P. Reilly, "Clutter Statistics Which Affect Radar Performance Analysis," Supplement to IEEE Trans. Aerospace Electron. Sys. AES-3, No. 6, 386-398, (Nov. 1967).

Appendix A
THEORY OF TRANSVERSAL FILTERS

In many fields of science and technology, signals are detected or analyzed on the basis of their spectral content. In such fields as communications, radar, and sonar, the transmitted signal is designed to have special spectral characteristics. These characteristics are used at the receiver to detect and identify the signal. In such fields as medical technology, radiometry, and passive sonar, the receiver designer does not have control of the signal characteristics; however, particular spectral characteristics can be related to particular physical occurrences. The fundamental theory used in these and many other branches of science and technology is that associated with linear filtering and spectrum analysis. A review of digital filtering theory can be obtained from the work of Gold and Rader*. The most important difference between digital and analog filtering is that in the former the input signal must be sampled. Assuming a constant sampling rate, the sampling interval determines the highest frequency that can be analyzed. Frequency components higher than this maximum are "folded" back into the analyzing bandwidth and cause "aliasing."

The canonical form for a digital filter is defined as that form which requires the minimum storage, or memory, to perform a particular operation. From Gold and Rader (A1), the canonical form for an Nth-order filter is shown in Fig. A1. The output $y(t)$ for this filter can be described in terms of the input $x(t)$ by an Nth-order difference equation,

$$y(nT) = \sum_{i=0}^{N} a_i x(nT - iT) - \sum_{i=1}^{N} b_i y(nT - iT), \tag{A1}$$

where T is the sampling interval. The input and output are defined only at the particular times $t = nT$. The form of Eq. (A1) shows the recursive relationship needed to derive output $y(t)$ at time $t = nT$. The nonrecursive form of Eq. (A1) is obtained by setting $b_i = 0$, for all i. The canonical form for a nonrecursive digital filter is shown in Fig. A2. All digital filters can be classed as either recursive or nonrecursive.

Transversal Filters

A transversal filter is a nonrecursive filter as shown in Fig. A2. The input/output relationship for this filter is

$$y(nT) = \sum_{i=0}^{N} a_i x(nT - iT). \tag{A2}$$

---

*B. Gold and C. M. Rader, <u>Digital Processing of Signals</u>, McGraw-Hill, New York, 1969.
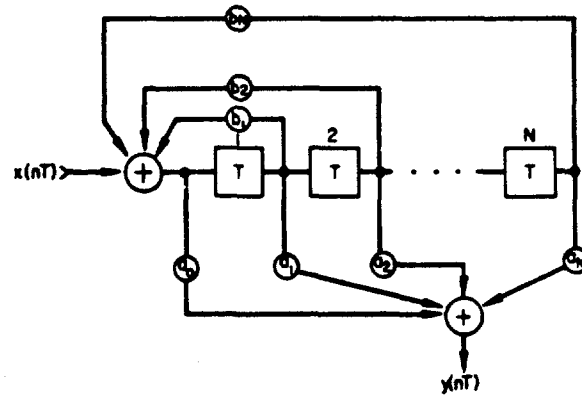
Fig. A1—Cannonical form for an nth-order digital filter
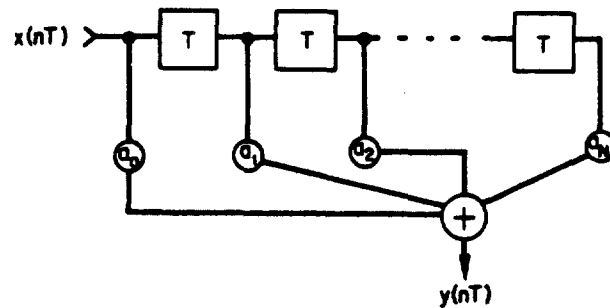
Fig. A2 — Canonical form for an nth-order nonrecursive digital filter

This equation can also be expressed as either of two matrix operations,

$$y(nT) = a_T x$$

or

$$y(nT) = x_T a,$$

where

$$a = \begin{bmatrix} a_1 \\ a_2 \\ \cdot \\ \cdot \\ \cdot \\ a_{N+1} \end{bmatrix} \quad \text{and } x = \begin{bmatrix} x(nT) \\ x(nT - T) \\ \cdot \\ \cdot \\ \cdot \\ x(nT - NT) \end{bmatrix} = \begin{bmatrix} x_1 \\ x_2 \\ \cdot \\ \cdot \\ \cdot \\ x_{N+1} \end{bmatrix} .$$

Subscript T represents the transpose of the matrix.

The output power, as shown by Applebaum[*]

$$p = |y(nT)|^2 = yy_T^*.$$

The asterisk represents the complex conjugate. If Eqs. (A3) and (A4) are used,

$$P = a_T xx_T^* a^*. \tag{A5}$$

Expected Output Power—The expected output power is found by taking the expected value of Eq. (A5):

$$\overline{P} = E\left\{a_T xx_T^* a^*\right\} = a_T \overline{xx_T^*} a^*.$$

If

$$M = \overline{xx_T^*},$$

then

$$\overline{P} = a_T M a^*, \tag{A6}$$

where M, the covariance matrix of the input, can be derived from the Fourier transform of the normalized input power density spectrum. The normalization is such that

$$\int_{-\infty}^{\infty} |x(t)|^2 dt = 1$$

or, using Parseval's theorem,

$$\int_{-\infty}^{\infty} p_c(f) df = 1,$$

where $p_c(f) = |X(f)|^2$ and $X(f)$ is the Fourier transform of $x(t)$.

Power Transfer Function—The power transfer function is usually found by taking the ratio of the output power to the input power as a function of the frequency of the input. With the normalization described above, the power of a single-frequency input is unity, and it is only necessary to compute the power at the output as a function of frequency. Also, since the filter characteristic repeats at multiples of the sampling frequency $(1/T)$, it is only necessary to compute the output power for frequencies between zero and $1/T$. Consider an input:

$$x(t) = \cos(2\pi f_0 t + \phi). \tag{A7}$$

---

[*]S. P. Applebaum, "Adaptive Arrays," Syracuse University Research Corp. SPL-769, June 1964.

If N is the number of delay lines (or memory elements) in the transversal filter and T is the time interval between samples, NT is the total processing time of the filter. $N + 1$ samples are taken during this time. When sampled at $t = iT$, Eq. (A7) becomes

$$x(t) = \sum_{i=0}^{N} \delta(t - iT) \cos(2\pi f_0 t + \phi).$$

The covariance of this input is found by

$$\psi(\tau) = \int_{-\infty}^{\infty} x(t)x(t - \tau)dt \tag{A8}$$

$$= \int_{-\infty}^{\infty} \left[\sum_{k=0}^{N} \delta(t - kT) \cos(2\pi f_0 t + \phi) \right] \left[\sum_{i=0}^{N} \delta(t - \tau - iT) \cos(2\pi f_0 (t - \tau) + \phi) \right] dt.$$

The integral is zero except when $t - kT = 0$ and $t - \tau - iT = 0$ or $\tau = (k - i)T$. Therefore the (i, k) term of the covariance matrix is

$$m_{i,k} = \cos(2\pi f_0 kT + \phi) \cos(2\pi f_0 iT + \phi), \tag{A9}$$

where $i = 0, 1, ..., N$ and $k = 0, 1, ..., N$. To normalize M, it is necessary for

$$\int_{-\infty}^{\infty} x(t)^2 dt = \int_{-\infty}^{\infty} x^2(t)dt = 1$$

When $\tau = 0$, Eq. (A8) becomes

$$\psi(0) = \int_{-\infty}^{\infty} x^2(t)dt.$$

But $\tau = 0$ implies $k = i$ in Eq. (A9), and therefore M is normalized if

$$\psi(0) = m_{ii} = \cos^2(2\pi f_0 iT + \phi) = 1.$$

Since phase ϕ is arbitrary it is chosen to be $\phi = -2\pi f_0 iT$. Then M is normalized and $m_{i,k}$ becomes

$$m_{i,k} = \cos 2\pi f_0 (k - i)T. \tag{A10}$$

In summary, the power transfer function of a transversal filter can be derived by using Eq. (A6) with a real input from Eq. (A7), which results in a covariance matrix defined by Eq. (A10).

Complex Filter Weights—For most applications of digital filters, it is desirable for the spectrum being filtered to be at "baseband."; that is, the bandwidth should span a region
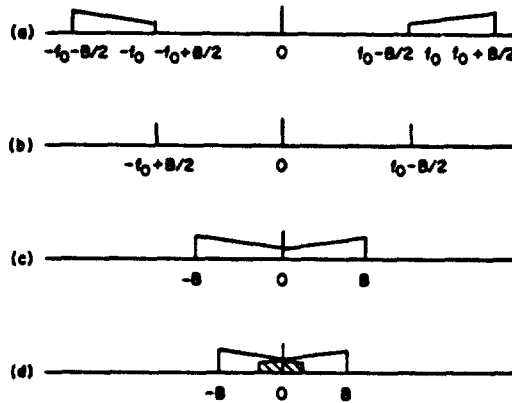
Fig. A3 — Translation of a real spectrum to baseband.
(a) Real signal to be analyzed. (b) Sinusoidal refer-
ence signal. (c) Spectrum (a) times spectrum (b).
(d) Aliasing caused by using a reference signal greater
than $f_0-B/2$.
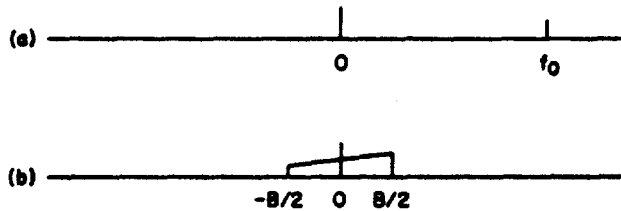
Fig. A4 — Complex translation of a real spectrum to baseband.
(a) Complex exponential reference signal. (b) Spectrum of Fig.
A3(a) times complex reference signal (a).

from zero to some maximum frequency. The maximum frequency determines the mini-
mum sampling frequency to meet the Nyquist sampling criterion. If the signal spectrum
of interest is not at baseband, it is usually multiplied by a sinusoidal signal of appropriate
frequency to translate the spectrum to baseband. This is shown in Fig. A3a, b, and c. If
the spectrum is translated more, then aliasing occurs as negative frequencies interfere with
positive frequencies, as shown in Fig. A3d.

This aliasing problem could be overcome by multiplying the signal of interest with a
complex exponential signal. The spectrum of this complex signal is not an even function,
and positive frequencies, therefore, can be distinquished from negative frequencies as
shown by Fig. A4.

A transversal filter can be designed to have a complex impulse response simply by
using complex weights a_j. In this way, a filter can be designed which discriminates be-
tween positive and negative frequencies. An example of this is the discrete Fourier trans-
form, which can be considered a contiguous bank of transversal filters. N filters are
formed when N samples are taken. The effective weights of the kth filter are

$$a_{kn} = e^{-j2\pi(n-1)(k-1)/N}, \qquad n = 1, 2, ..., N \qquad (A11)$$

where $k = 1, 2, ..., N$. Using the weights defined by Eq. (A11) and a complex signal input, we have

$$x(t) = e^{j2\pi f_0 t}, \tag{A12}$$

the power transfer function of a discrete Fourier transform can be derived using Eq. (A6). The autocorrelation of Eq. (A12) is

$$\psi(\tau) = e^{j2\pi f_0 \tau},$$

which results in a covariance matrix defined by

$$m_{i,k} = e^{j2\pi f_0 (i-k)T}.$$

The power transfer function for 9 of the 16 filters generated by a 16-sample discrete Fourier transform is shown in Fig. A5. The filter characteristics shown in Fig. A5 repeat with multiples of the sampling frequency f_s. Therefore the filter response to negative frequencies from zero to $-f_s$ is simply the shapes of these filters translated to the negative frequency region. In this way, an unambiguous analyzing frequency bandwidth can be defined either from $-f_s/2$ to $+f_s/2$ or from 0 to f_s. These filters can discriminate between positive and negative frequencies over the region from $-f_s/2$ to $+f_s/2$.

Complex transversal filters can be implemented with real operations. Consider real input signal $x(t)$ which has a spectrum and center frequency f_c, as shown in Fig. A4. The spectrum is translated to baseband, so that

$$x'(t) = x(t)e^{j2\pi f_0 t}.$$

When an input signal is sampled, a vector can be defined,

$$\mathbf{x} = \begin{bmatrix} x'_1 \\ x'_2 \\ x'_3 \\ . \\ . \\ . \\ x'_N \end{bmatrix}$$

where

$$x'_i = x[(i - 1)T]e^{j2\pi f_0 (i-1)T}$$

$$= x[(i - 1)T][\cos 2\pi f_0 (i - 1)T + j \sin 2\pi f_0 (i - 1)T]$$

$$= x_i^R + j x_i^I.$$

58

The real component of the input is

$$x_i^R = x[(i-1)T] \cos 2\pi f_0 (i-1)T.$$

The imaginary component is

$$x_i^I = x[(i-1)T] \sin 2\pi f_0 (i-1)T.$$

The complex transversal filter is formed by the matrix multiplication of this input vector by the transpose of the complex weight vector:

$$\mathbf{a} = \begin{bmatrix} a \\ a_2 \\ \cdot \\ \cdot \\ \cdot \\ a_N \end{bmatrix} = \begin{bmatrix} a^R + ja^I \\ a_2^R + ja_2^I \\ \cdot \\ \cdot \\ \cdot \\ a_N^R + ja_N^I \end{bmatrix} = \mathbf{a}^R + j\mathbf{a}^I.$$

The output is

$$y = \mathbf{a}_T \mathbf{x} = (\mathbf{a}_T^R + j\mathbf{a}_T^I)(\mathbf{x}^R + j\mathbf{x}^I)$$

where

$$\mathbf{x}^R = \begin{bmatrix} x_i^R \\ x_2^R \\ \cdot \\ \cdot \\ \cdot \\ x_N^R \end{bmatrix} \quad \text{and } \mathbf{x}^I = \begin{bmatrix} x_i^I \\ x_2^I \\ \cdot \\ \cdot \\ \cdot \\ x_N^I \end{bmatrix}$$

$$y = (\mathbf{a}_T^R \mathbf{x}^R - \mathbf{a}_T^I \mathbf{x}^I) + j(\mathbf{a}_T^I \mathbf{x}^R + \mathbf{a}_T^R \mathbf{x}^I) = y^R + jy^I. \tag{A13}$$

The complex transversal filter described by Eq. (A13) is shown in Fig. A6.

Doppler Filtering

It is well known in the fields of optics and acoustics as well as electromagnetics, that if there is relative motion between the source of oscillation and the observer, an apparent shift in frequency will result. This is the doppler effect that is put to use in many fields, such as radio astronomy, coherent communication, radar, and sonar. Each field has a need to measure accurately the doppler caused by relative motion. The doppler shift f_d of a frequency f_t is
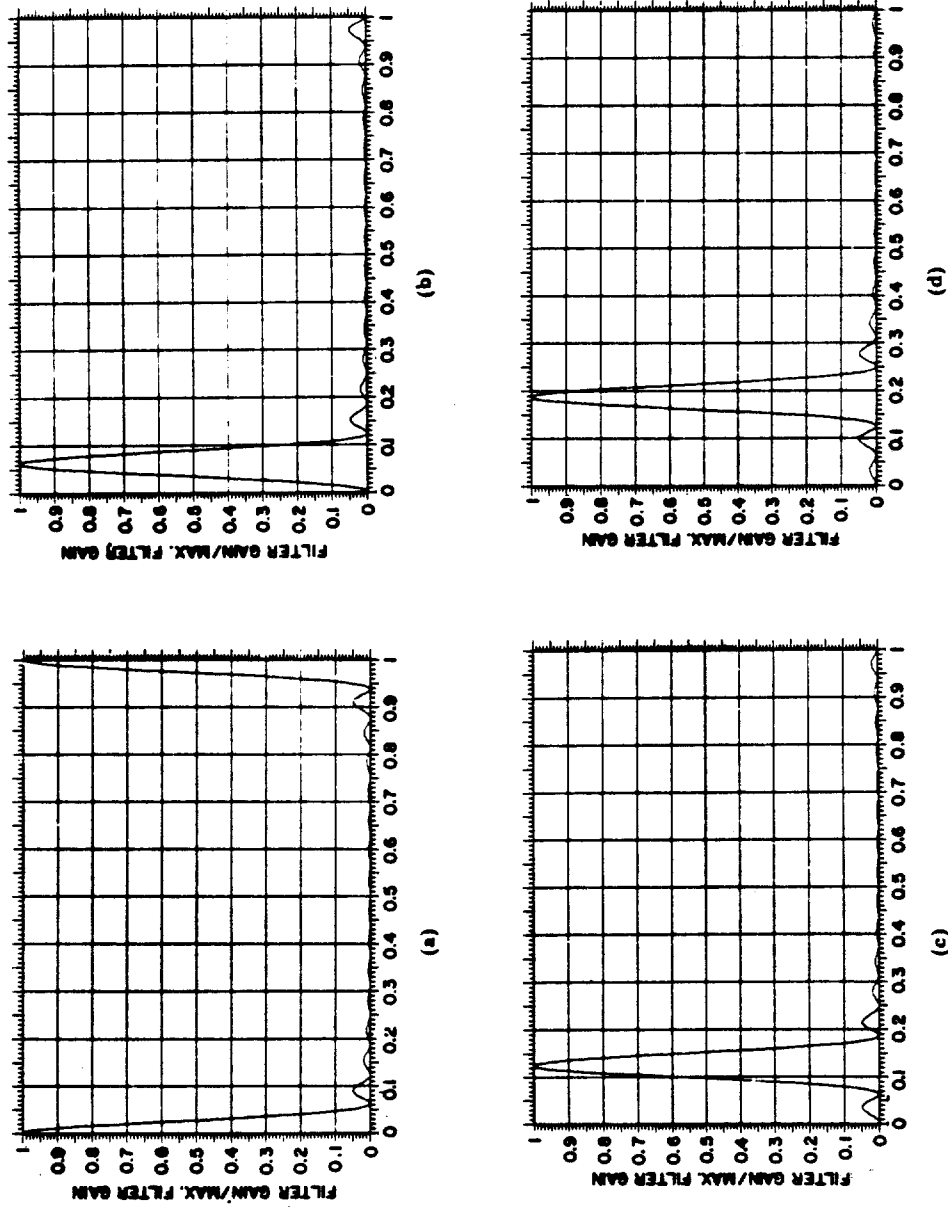
Fig. A5 — Transfer characteristics of a 16-sample discrete Fourier transform. Of the 16 filters, 9 are shown; the remaining 7 filters are the mirror images of filters 2 through 8.
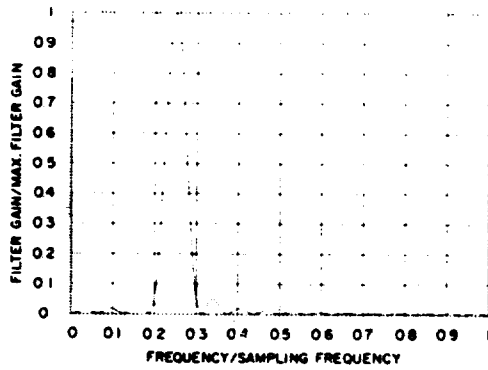
(e)
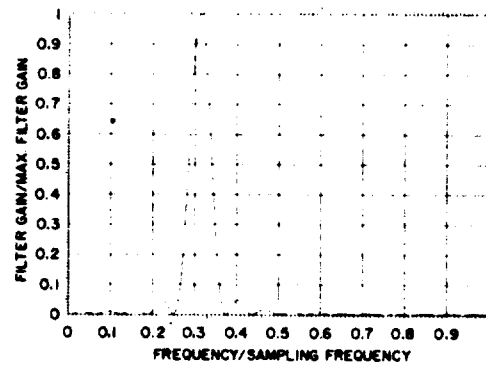
(f)
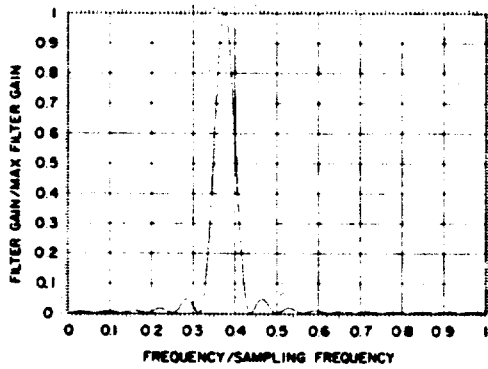
(g)
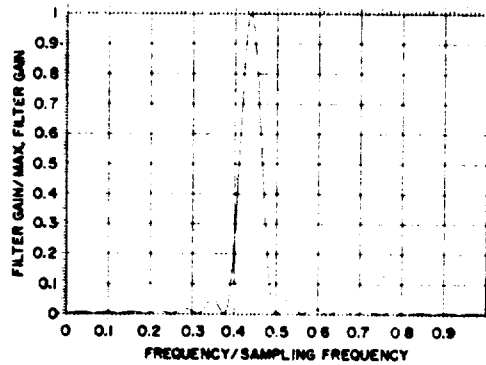
(h)
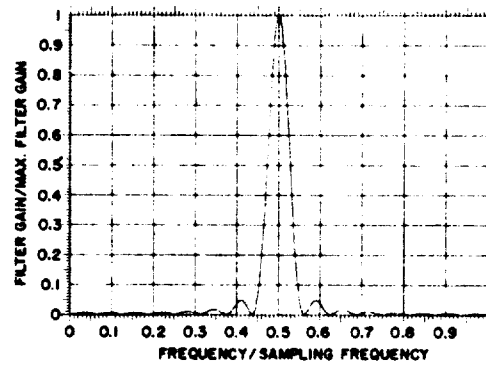
(i)

Fig. A5 (Continued) — Transfer characteristics of
a 16-sample discrete Fourier transform. Of the
16 filters, 9 are shown; the remaining 7 filters are
the mirror images of filters 2 through 8.

61
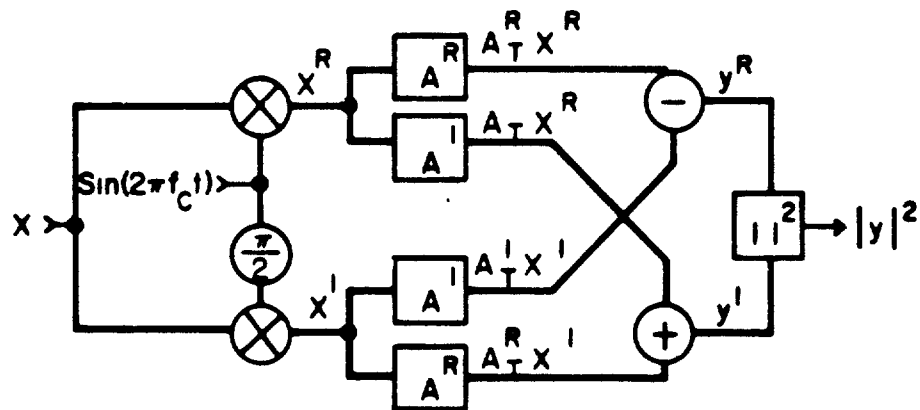
Fig. A6 — Model for a complex transversal filter.

$$f_d = \frac{f_t}{2} \left(\frac{c+v}{c-v}\right) - 1$$

where c is the speed of propagation and v is the relative velocity between source and observer.

Complex Demodulation—Consider a signal at the source,

$$v(t) = m(t) \cos 2\pi f_t t, \tag{A14}$$

where $m(t)$ is the modulation and f_t is the carrier frequency. With relative velocity v between source and observer, this signal appears to the observer to be

$$v(t) = m(t + t_d) \left[\cos 2\pi (f_t + f_d)(t + t_d)\right]$$

where t_d is the propagation time.

For many applications of this waveform, such as in radar, sonar, and communications, the modulation bandwidth is small as compared with the carrier frequency. In this case, the modulation spectrum is altered very little as compared with the shift in frequency of the carrier, so that the receiver spectrum can be considered to be the same shape as that of the transmitted spectrum but translated by the carrier doppler shift. The received spectrum is approximately

$$v'(t) = m(t + t_d) \cos \left[2\pi (f_t + f_d)t + \phi\right]$$

where $\phi = 2\pi (f_t + f_d)t_d$.

The attenuation due to propagation loss has been ignored since it does not affect the design of the optimum receiver for detecting this signal. As described above, this signal can be translated to baseband by forming the product $x(t) = v'(t)e^{j2\pi f_t t}$ and filtering out the difference frequency,

$$x(t) = m(t + t_d) \left[\cos (2\pi (f_t + f_d)t + \phi) \cos 2\pi f_t t + j \cos (2\pi (f_t + f_d)t + \phi) \sin 2\pi f_t t\right].$$

After filtering, we have

$$x(t) = \frac{1}{2} m(t + t_d) \left[\cos (2\pi f_d t + \phi) - j \sin (2\pi f_d t + \phi)\right]$$

$$= \frac{1}{2} m(t + t_d)e^{-j(2\pi f_d t + \phi)}. \tag{A15}$$

The demodulated complex signal, Eq. (A15), has been translated to baseband and is now of a form to be processed by a digital doppler filter.

Pulse Doppler Radar—The doppler shift created by a moving target can be measured with a pulse doppler radar. Although many transmitted waveforms are used for this purpose in radar, most of them can be related to conventional scanning pulsed radars. These

63

radars transmit a carrier frequency that is gated on and off by a sequence of pulses. The envelope of the basic pulse is

$$p(t) = \begin{cases} \dfrac{\sqrt{E_p}}{\Delta T}, & 0 \leq t < \Delta T \\ \\ 0, & \text{otherwise,} \end{cases}$$

where E_p is the energy per pulse and ΔT is the pulse width. The transmitted waveform is therefore

$$v(t) = e^{j2\pi f_c t} \sum_{n=-\infty}^{\infty} p(t - nT),$$

where f_c is the carrier frequency and T is the interpulse period. The composite returns from these transmitted pulses are made up of moving target returns and usually much larger returns from fixed objects (clutter). The objective is to design a processor that can pass the moving targets and reject the clutter by processing the returns from a fixed number N of pulses.

If a moving target is at azimuth α with respect to the axis of the antenna pattern $G(\theta)$ and if the antenna scans at a rate of ω_s rad/s, the detailed model of the signal return for the conventional scanning pulsed radar is

$$x(t) = a G^2(\omega_s t - \alpha) e^{j2\pi f_d(t-t_d)} \sum_{n=0}^{N} p(t - nT - t_d).$$

The carrier frequency has been removed at the receiver. The term $a = A e^{j\phi}$ represents the unknown amplitude and phase of the carrier signal return; $(j2\pi f_d t)$ is the doppler modulation due to the target motion. The delay t_d corresponds to the distance from the radar to the target. Signal parameters a, α, f_d, and t_d are not known a priori.

If it is assumed that the modulation of the returned signal by the antenna pattern $G(\theta)$ is small and that the received complex amplitude a is not significant to the receiver design, then the signal to be processed by the doppler filters becomes

$$x(t) = e^{j2\pi f_d(t-t_d)} \sum_{n=0}^{N} p(t - nT - t_d), \tag{A16}$$

which is of the same form as Eq. (A15).

The time duration ΔT of the modulating pulse is usually very short as compared with the period of the doppler frequency. Therefore, the demodulated signal is essentially a sampled version of the doppler-shifted signal where the sampling rate is the radar PRF. Thus, digital filtering technology is directly applicable to radar doppler processing. For analysis, the pulse duration can be considered to be zero, and the input signal to the doppler filter becomes

$$x(t) = e^{j2\pi f_d(t-t_d)} \sum_{n=0}^{N} \delta(t - nT - t_d). \tag{A17}$$

With Eq. (A17) as an input, a transversal filter can be designed to detect moving targets and reject returns from fixed objects (clutter).

Appendix B
OPTIMUM WEIGHTS FOR MTI RADAR PROCESSORS

Table B1
Two Cancelers (Three Pulses)

$\sigma_c T$	Improvement Factor (dB)	Optimum Weights	
		Real	Imagining
0.0050	64.8868	▪0.5002	-0.0000
		1.0000	0.0000
		▪0.5002	0.0000
0.0056	62.8868	-0.5003	-0.0000
		1.0000	0.0000
		-0.5003	0.0000
0.0063	60.8876	-0.5004	-0.0000
		1.0000	0.0000
		-0.5004	0.0000
0.0071	58.8881	▪0.5005	-0.0000
		1.0000	0.0000
		-0.5005	0.0000
0.0079	56.8888	-0.5006	-0.0000
		1.0000	0.0000
		-0.5006	0.0000
0.0089	54.8897	-0.5008	-0.0000
		1.0000	0.0000
		▪0.5008	0.0000
0.0100	52.8909	▪0.5010	-0.0000
		1.0000	0.0000
		▪0.5010	0.0000
0.0112	50.8924	▪0.5012	-0.0000
		1.0000	0.0000
		-0.5012	0.0000
0.0126	48.8943	▪0.5016	-0.0000
		1.0000	0.0000
		▪0.5016	0.0000
0.0141	46.8966	-0.5020	-0.0000
		1.0000	0.0000
		-0.5020	0.0000
0.0158	44.8996	▪0.5025	-0.0000
		1.0000	0.0000
		-0.5025	0.0000
0.0177	42.9034	▪0.5031	-0.0000

67

Table B1—Continued

$\sigma_c T$	Improvement Factor (dB)	Optimum Weights	
		Real	Imagining
0.0199	40.9081	1.0000 -0.5031 -0.5039	0.0000 0.0000 -0.0000
0.0223	38.9141	1.0000 -0.5039 -0.5049	0.0000 0.0000 -0.0000
0.0251	36.9218	1.0000 -0.5049 -0.5061	0.0000 0.0000 0.0000
0.0281	34.9314	1.0000 -0.5061 -0.5077	0.0000 -0.0000 0.0000
0.0315	32.9437	1.0000 -0.5077 -0.5097	0.0000 0.0000 0.0000
0.0354	30.9594	1.0000 -0.5097 -0.5121	0.0000 0.0000 0.0000
0.0397	28.9794	1.0000 -0.5121 -0.5152	0.0000 0.0000 -0.0000
0.0446	27.0051	1.0000 -0.5152 -0.5190	0.0000 0.0000 0.0000
0.0500	25.0381	1.0000 -0.5190 -0.5236	0.0000 0.0000 0.0000
0.0561	23.0807	1.0000 -0.5236 -0.5294	0.0000 0.0000 -0.0000
0.0629	21.1360	1.0000 -0.5294 -0.5365	0.0000 0.0000 -0.0000
0.0706	19.2080	1.0000 -0.5365 -0.5451	0.0000 0.0000 0.0000
0.0792	17.3022	1.0000 -0.5451 -0.5554	0.0000 0.0000 0.0000
0.0889	15.4258	1.0000 -0.5554 -0.5677	0.0000 -0.0000 0.0000
		1.0000 -0.5677	0.0000 0.0000

Table B1—Continued

$\sigma_c T$	Improvement Factor (dB)	Optimum Weights	
		Real	Imagining
0.0998	13.5883	-0.5819	-0.0000
		1.0000	0.0000
		-0.5819	0.0000
0.1119	11.8021	-0.5980	-0.0000
		1.0000	0.0000
		-0.5980	0.0000
0.1256	10.0824	-0.6157	-0.0000
		1.0000	0.0000
		-0.6157	0.0000
0.1409	8.4477	-0.6342	-0.0000
		1.0000	0.0000
		-0.6342	0.0000
0.1581	6.9188	-0.6525	-0.0000
		1.0000	0.0000
		-0.6525	0.0000
0.1774	5.5175	-0.6694	-0.0000
		1.0000	0.0000
		-0.6694	0.0000
0.1991	4.2642	-0.6836	-0.0000
		1.0000	0.0000
		-0.6836	0.0000
0.2233	3.1756	-0.6942	-0.0000
		1.0000	0.0000
		-0.6942	0.0000
0.2506	2.2616	-0.7011	-0.0000
		1.0000	0.0000
		-0.7011	0.0000
0.2812	1.5246	-0.7048	-0.0000
		1.0000	0.0000
		-0.7048	0.0000
0.3155	0.9588	-0.7064	-0.0000
		1.0000	0.0000
		-0.7064	0.0000
0.3540	0.5513	-0.7070	-0.0000
		1.0000	0.0000
		-0.7070	0.0000
0.3972	0.2819	-0.7071	-0.0000
		1.0000	0.0000
		-0.7071	0.0000
0.4456	0.1236	-0.7071	-0.0000
		1.0000	0.0000
		-0.7071	0.0000
0.5000	0.0444	-0.7071	-0.0000
		1.0000	0.0000
		-0.7071	0.0000

Table B2
Three Cancelers (Four Pulses)

$\sigma_c T$	Improvement Factor (dB)	Optimum Weights	
		Real	Imagining
0.0050	95.6728	-0.3337	0.0000
		1.0000	0.0000
		-1.0000	-0.0000
		0.3337	0.0000
0.0056	92.1967	-0.3337	-0.0000
		1.0000	0.0000
		-1.0000	0.0000
		0.3337	0.0000
0.0063	89.4701	-0.3339	0.0000
		1.0000	0.0000
		-1.0000	0.0000
		0.3339	0.0000
0.0071	86.4063	0.3340	0.0000
		-1.0000	0.0000
		1.0000	0.0000
		-0.3340	-0.0000
0.0079	83.4174	-0.3342	-0.0000
		1.0000	0.0000
		-1.0000	0.0000
		0.3342	0.0000
0.0089	80.4001	0.3344	-0.0000
		-1.0000	0.0000
		1.0000	0.0000
		-0.3344	-0.0000
0.0100	77.4124	0.3346	-0.0000
		-1.0000	0.0000
		1.0000	0.0000
		-0.3346	-0.0000
0.0112	74.4093	-0.3350	0.0000
		1.0000	0.0000
		-1.0000	-0.0000
		0.3350	0.0000
0.0126	71.4135	0.3354	-0.0000
		-1.0000	0.0000
		1.0000	0.0000
		-0.3354	-0.0000
0.0141	68.4156	0.3359	-0.0000
		-1.0000	0.0000
		1.0000	0.0000
		-0.3359	-0.0000
0.0158	65.4193	0.3366	-0.0000
		-1.0000	0.0000
		1.0000	0.0000
		-0.3366	-0.0000

Table B2—Continued

$\sigma_c T$	Improvement Factor (dB)	Optimum Weights	
		Real	Imagining
0.0177	62,4244	0.3375	-0.0000
		-1.0000	0.0000
		1.000u	0.00C0
		-0.3375	-0.0000
0.0199	59,4311	0.3385	-0.0000
		-1.0000	0.0000
		1.0000	0.0000
		-0.3385	-0.0000
0.0223	56,4392	-0.3399	0.0000
		1.0000	0.0000
		-1.0000	-0.0000
		0.3399	0.0000
0.0251	53,4498	-0.3416	0.0000
		1.0000	0.0000
		-1.0000	-0.0000
		0.3416	0.0000
0.0281	50,4632	-0.3437	0.0000
		1.0000	0.0000
		-1.0000	-0.0000
		0.3437	0.0000
0.0315	47,4804	0.3463	-0.0000
		-1.0000	0.0000
		1.0000	0.0000
		-0.3463	-0.0000
0.0354	44,5024	-0.3497	0.0000
		1.0000	0.0000
		-1.0000	-0.0000
		0.3497	0.0000
0.0397	41,5309	-0.3538	0.0000
		1.0000	0.0000
		-1.0000	-0.0000
		0.3538	0.0000
0.0446	38,5678	-0.3590	0.0000
		1.0000	0.0000
		-1.0000	-0.0000
		0.3590	0.0000
0.0500	35,6160	0.3655	-0.0000
		-1.0000	0.0000
		1.0000	0.0000
		-0.3655	-0.0000
0.0561	32,6793	0.3736	-0.0000
		-1.0000	0.0000
		1.0000	0.0000
		-0.3736	-0.0000

Table B2—Continued

$\sigma_c T$	Improvement Factor (dB)	Optimum Weights	
		Real	Imagining
0.0629	29.7630	0.3835	-0.0000
		-1.0000	0.0000
		1.0000	0.0000
		-0.3835	-0.0000
0.0706	26.8744	0.3957	-0.0000
		-1.0000	0.0000
		1.0000	0.0000
		-0.3957	-0.0000
0.0792	24.0237	0.4105	-0.0000
		-1.0000	0.0000
		1.0000	0.0000
		-0.4105	-0.0000
0.0889	21.2248	-0.4282	0.0000
		1.0000	0.0000
		-1.0000	-0.0000
		0.4282	0.0000
0.0998	18.4964	-0.4488	0.0000
		1.0000	0.0000
		-1.0000	-0.0000
		0.4488	0.0000
0.1119	15.8628	-0.4723	0.0000
		1.0000	0.0000
		-1.0000	-0.0000
		0.4723	0.0000
0.1256	13.3541	-0.4978	0.0000
		1.0000	0.0000
		-1.0000	-0.0000
		0.4978	0.0000
0.1409	11.0048	0.5242	0.0000
		-1.0000	0.0000
		1.0000	0.0000
		-0.5242	0.0000
0.1581	8.8511	-0.5497	0.0000
		1.0000	0.0000
		-1.0000	-0.0000
		0.5497	0.0000
0.1774	6.9257	-0.5722	0.0000
		1.0000	0.0000
		-1.0000	-0.0000
		0.5722	0.0000
0.1991	5.2523	-0.5903	0.0000
		1.0000	0.0000
		-1.0000	-0.0000
		0.5903	0.0000

Table B2—Continued

$\sigma_c T$	Improvement Factor (dB)	Optimum Weights	
		Real	Imagining
0.2233	3.8424	0.6032	-0.0000
		-1.0000	0.0000
		1.0000	0.0000
		-0.6032	-0.0000
0.2506	2.6936	0.6112	-0.0000
		-1.0000	0.0000
		1.0000	0.0000
		-0.6112	-0.0000
0.2812	1.7920	0.6155	-0.0000
		-1.0000	0.0000
		1.0000	0.0000
		-0.6155	-0.0000
0.3155	1.1155	0.6173	-0.0000
		-1.0000	0.0000
		1.0000	0.0000
		-0.6173	-0.0000
0.3540	0.6367	-0.6179	0.0000
		1.0000	0.0000
		-1.0000	-0.0000
		0.6179	0.0000
0.3972	0.3240	0.6180	-0.0000
		-1.0000	0.0000
		1.0000	0.0000
		-0.6180	-0.0000
0.4456	0.1417	0.6180	-0.0000
		-1.0000	0.0000
		1.0000	0.0000
		-0.6180	-0.0000
0.5000	0.0508	-0.6180	0.0000
		1.0000	0.0000
		-1.0000	-0.0000
		0.6180	0.0000

Table B3
Four Cancelers (Five Pulses)

$\sigma_c T$	Improvement Factor (dB)	Optimum Weights	
		Real	Imagining
0.0100	102.7361	0.1680	0.0000
		=0.6680	0.0000
		1.0000	0.0000
		=0.6680	0.0000
		0.1680	0.0000
0.0112	96.8687	0.1683	0.0000
		=0.6683	-0.0000
		1.0000	0.0000
		=0.6683	-0.0000
		0.1683	0.0000
0.0126	93.0812	0.1687	-0.0000
		=0.6687	0.0000
		1.0000	0.0000
		=0.6687	0.0000
		0.1687	0.0000
0.0141	88.9450	0.1693	0.0000
		=0.6693	0.0000
		1.0000	0.0000
		=0.6693	0.0000
		0.1693	-0.0000
0.0158	84.3900	0.1700	-0.0000
		=0.6699	0.0000
		1.0000	0.0000
		=0.6699	-0.0000
		0.1700	0.0000
0.0177	80.9018	0.1708	-0.0000
		=0.6708	0.0000
		1.0003	0.0000
		=0.6708	-0.0000
		0.1708	0.0000
0.0199	76.9232	0.1719	-0.0000
		=0.6718	0.0000
		1.0000	0.0000
		=0.6718	0.0000
		0.1719	0.0000
0.0223	72.9281	0.1733	0.0000
		=0.6732	-0.0000
		1.0000	0.0000
		=0.6732	-0.0000
		0.1733	0.0000

74

Table B3—Continued

$\sigma_c T$	Improvement Factor (dB)	Optimum Weights	
		Real	Imagining
0.0251	68,9416	0.1750	0.0000
		-0.6748	0.0000
		1.0000	0.0000
		-0.6748	0.0000
		0.1750	0.0000
0.0281	64,9587	0.1771	-0.0000
		-0.6769	0.0000
		1.0000	0.0000
		-0.6769	-0.0000
		0.1771	0.0000
0.0315	60,9817	0.1799	-0.0000
		-0.6795	0.0000
		1.0000	0.0000
		-0.6795	-0.0000
		0.1799	0.0000
0.0354	57,0111	0.1833	-0.0000
		-0.6827	0.0000
		1.0000	0.0000
		-0.6827	-0.0000
		0.1833	0.0000
0.0397	53,0496	0.1877	-0.0000
		-0.6868	0.0000
		1.0000	0.0000
		-0.6868	-0.0000
		0.1877	0.0000
0.0446	49,1001	0.1932	-0.0000
		-0.6918	0.0000
		1.0000	0.0000
		-0.6918	-0.0000
		0.1932	0.0000
0.0500	45,1669	0.2002	-0.0000
		-0.6979	0.0000
		1.0000	0.0000
		-0.6979	-0.0000
		0.2002	0.0000
0.0561	41,2562	0.2090	-0.0000
		-0.7054	0.0000
		1.0000	0.0000
		-0.7054	-0.0000
		0.2090	0.0000

Table B3—Continued

$\sigma_c T$	Improvement Factor (dB)	Optimum Weights	
		Real	Imagining
0.0629	37,3763	0.2200	-0.0000
		•0.7146	0.0000
		1.0000	0.0000
		•0.7146	-0.0000
		0.2200	0.0000
0.0706	33,5394	0.2338	-0.0000
		•0.7255	0.0000
		1.0000	0.0000
		•0.7255	-0.0000
		0.2338	0.0000
0.0792	29,7622	0.2510	-0.0000
		•0.7384	0.0000
		1.0000	0.0000
		•0.7384	-0.0000
		0.2510	0.0000
0.0889	26,0680	0.2720	-0.0000
		•0.7533	0.0000
		1.0000	0.0000
		•0.7533	-0.0000
		0.2720	0.0000
0.0998	22,4881	0.2971	-0.0000
		•0.7699	0.0000
		1.0000	0.0000
		•0.7699	-0.0000
		0.2971	0.0000
0.1119	19,0624	0.3260	-0.0000
		•0.7876	0.0000
		1.0000	0.0000
		•0.7876	-0.0000
		0.3260	0.0000
0.1256	15,8386	0.3579	-0.0000
		•0.8055	0.0000
		1.0000	0.0000
		•0.8055	-0.0000
		0.3579	0.0000
0.1409	12,8681	0.3908	-0.0000
		•0.8223	0.0000
		1.0000	0.0000
		•0.8223	-0.0000
		0.3908	0.0000

Table B3—Continued

$\sigma_c T$	Improvement Factor (dB)	Optimum Weights	
		Real	Imagining
0.1581	10.1984	0.4219	-0.0000
		-0.8368	0.0000
		1.0000	0.0000
		-0.8368	-0.0000
		0.4219	0.0000
0.1774	7.8650	0.4489	-0.0000
		-0.8481	0.0000
		1.0000	0.0000
		-0.8481	-0.0000
		0.4489	0.0000
0.1991	5.8846	0.4697	-0.0000
		-0.8561	0.0000
		1.0000	0.0000
		-0.8561	-0.0000
		0.4697	0.0000
0.2233	4.2538	0.4841	-0.0000
		-0.8611	0.0000
		1.0000	0.0000
		-0.8611	-0.0000
		0.4841	0.0000
0.2506	2.9522	0.4928	-0.0000
		-0.8639	0.0000
		1.0000	0.0000
		-0.8639	-0.0000
		0.4928	0.0000
0.2812	1.9484	0.4973	-0.0000
		-0.8652	0.0000
		1.0000	0.0000
		-0.8652	-0.0000
		0.4973	0.0000
0.3155	1.2056	0.4992	-0.0000
		-0.8658	0.0000
		1.0000	0.0000
		-0.8658	-0.0000
		0.4992	0.0000
0.3540	0.6853	0.4998	-0.0000
		-0.8660	0.0000
		1.0000	0.0000
		-0.8660	-0.0000
		0.4998	0.0000
0.3972	0.3478	0.5000	-0.0000
		-0.8660	0.0000
		1.0000	0.0000
		-0.8660	-0.0000
		0.5000	0.0000

Table B3—Continued

| $\sigma_c T$	Improvement Factor (dB)	Optimum Weights	
		Real	Imagining
0.4456	0.1519	0.5000	-0.0000
		-0.8660	0.0000
		1.0000	0.0000
		-0.8660	-0.0000
		0.5000	0.0000
0.5000	0.0544	0.5000	-0.0000
		-0.8660	0.0000
		1.0000	0.0000
		-0.8660	-0.0000
		0.5000	0.0000

Appendix C
FILTER CHARACTERISTICS OF N-PORT PROCESSORS
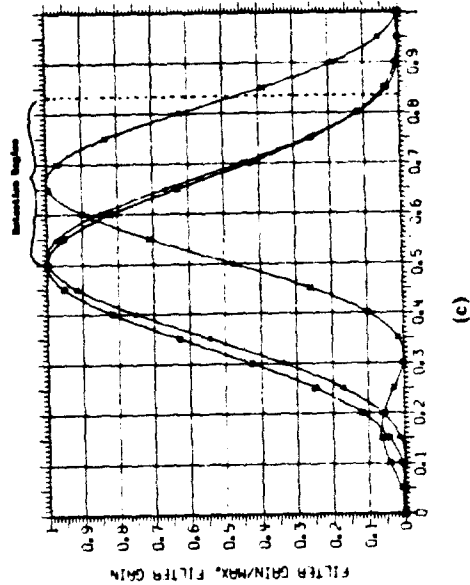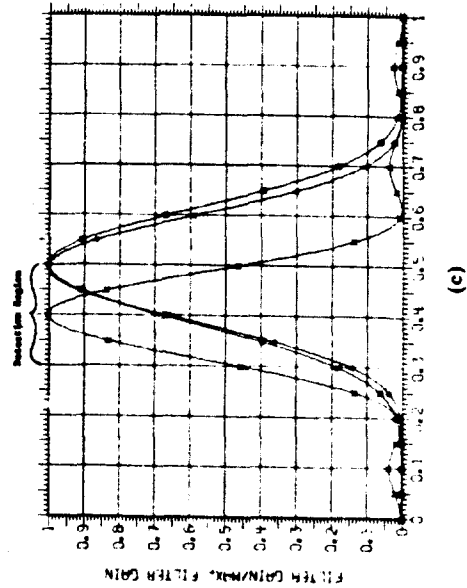

Fig. C1 — Filter transfer characteristics of a 3-port doppler processor. □ represents the filter shape when the width of the clutter spectrum is narrow ($\sigma_c T = 0.005$), Δ represents the filter shape for $\sigma_c T = 0.1$, and X represents the filter shape for $\sigma_c T = 0.5$.

79
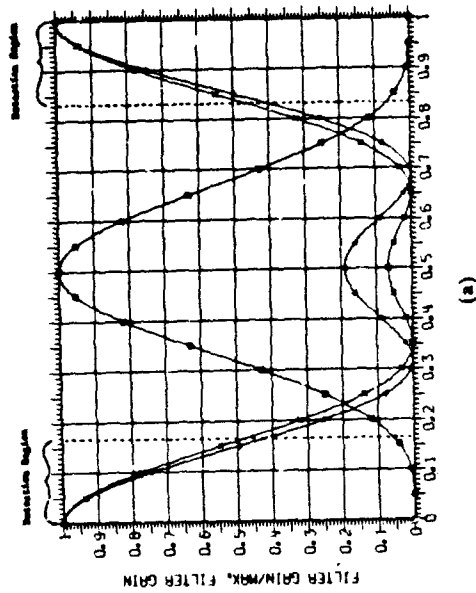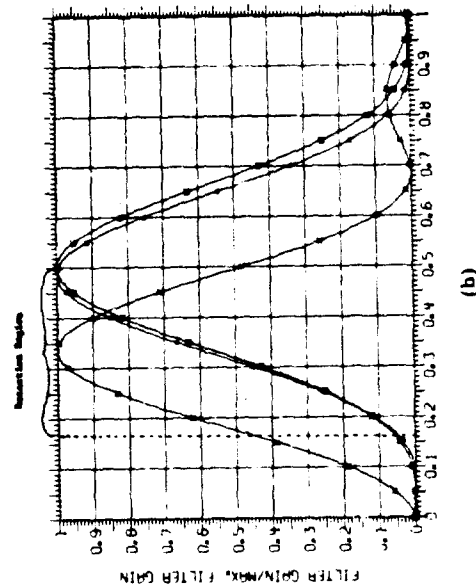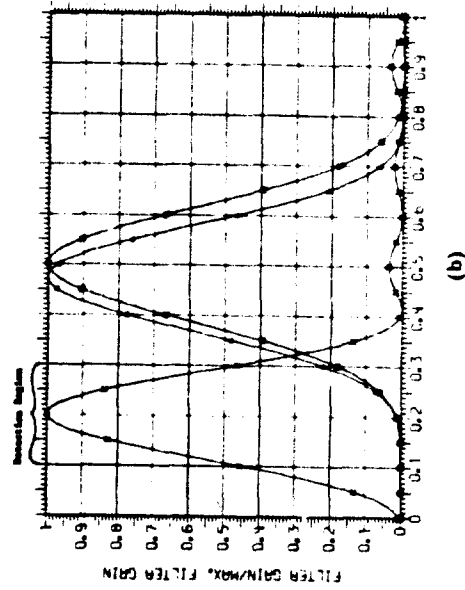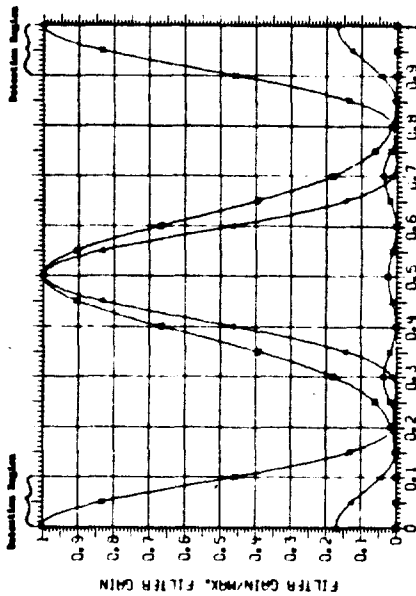
Fig. C2 — Filter transfer characteristics of a 5-port doppler processor. □ represents the filter shape when the width of the clutter spectrum is narrow ($\sigma_c T = 0.016$), △ represents the filter shape for $\sigma_c T = 0.08$, and X represents the filter shape for $\sigma_c T = 0.5$.

80

Naval Research Laboratory
Technical Library
Research Reports Section

DATE: March 03, 2004

FROM: **Mary Templeman**, Code 5596.3

TO: **Code 5300 Paul Hughes**

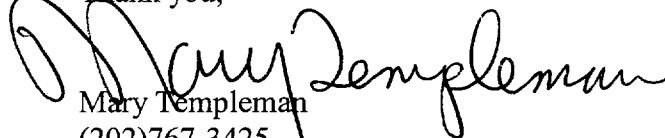C: Tina Smallwood, Code 1221.1 _to 3/3/04_

SUBJ: Review of NRL Report

Dear Sir/Madam:

Please review NRL Report 7727 for:

☑   Possible Distribution Statement _Change_
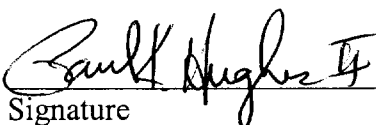☐   Possible Change in Classification

Thank you,

Mary Templeman
Mary Templeman
(202)767-3425
maryt@library.nrl.navy.mil

The subject report can be:

☑   Changed to Distribution A (Unlimited)
☐   Changed to Classification _____
☐   Other:

Paul Hughes II   3/3/2004
Signature   Date